DECOMPOSING ATMOSPHERIC VERSUS OCEANIC CONTRIBUTIONS TO THE HIGH-TO-LOW LATITUDE TELECONNECTION DURING A FRESHWATER TRIGGERED ABRUPT CLIMATE CHANGE

A Dissertation

by

GUANGLIN TANG

Submitted to the Office of Graduate and Professional Studies of
Texas A&M University
in partial fulfillment of the requirements for the degree of

DOCTOR OF PHILOSOPHY

Chair of Committee,	Richard Lee Panetta
Co-Chair of Committee,	Ping Chang
Committee Members,	Ramalingam Saravanan
	Achim Stössel
Head of Department,	Ping Yang

August 2015

Major Subject: Atmospheric Sciences

ABSTRACT

In this dissertation we study the high-to-low latitude teleconnection during Younger Dryas-like abrupt climate events using models. The teleconnection considered here is between climate change induced by a freshwater input in high-latitude North Atlantic and global response over the Northern Hemisphere and in the tropics. We focus on three primary questions: (1) What is the relative importance of oceanic vs. atmospheric processes in the teleconnection? (2) What are the respective mechanisms of the atmospheric and oceanic controlled teleconnection? (3) How important is sea surface temperature to the teleconnection, particularly in tropical climate responses.

To answer these questions we performed a series of model experiments using an Atmospheric General Circulation Model coupled to a thermodynamic slab ocean model. Previous studies identified a teleconnection between the high-latitude freshwater forced abrupt climate change and the low-latitude climate response during a Younger Dryas-like abrupt climate change using coupled Atmosphere-Ocean General Circulation Models. In this study we attempt to separate and compare the atmospheric and oceanic contributions to this teleconnection. The results show that these contributions have comparable climate response magnitudes, but different spatial characteristics with the atmospheric contribution being more zonally symmetric than the oceanic conterpart.

Physical atmospheric and oceanic processes are also analyzed to address the second question. It is found that the equatorward propagation of the high-latitude surface cooling is induced by increasing surface sensible heat flux in northern mid-latitudes and subtropics and surface latent heat flux in northern equatorial region. The increase in sensible heat flux is due to cooling of near surface air temperatures,

whereas latent heat response is caused by strengthening of the surface trade winds linked to an increase in meridional surface temperature gradient. The oceanic contribution in the North Atlantic is through changes in the oceanic circulation caused by freshwater forcing.

To address the third question, we performed additional modelling experiments with same high-latitude forcing but different oceanic mixed layer depths. It is found that change in sea surface temperature is necessary for the high-to-low latitude teleconnection and the tropical precipitation response. To determine the importance of sea surface temperature in Intertropical Convergence Zone (ITCZ) response, we further performed an experiment using a simple model developed by Lindzen and Nigam (1987) and found that the change in sea surface temperature, in concert with lower-tropospheric vertical mixing and surface drag, largely contributes to the simulated ITCZ shift.

ACKNOWLEDGEMENTS

NOMENCLATURE

AOGCM   Atmosphere-Ocean General Circulation Model

AGCM   Atmospheric General Circulation Model

SOM   Slab Ocean Model

CAM3   Community Atmosphere Model version 3

CCSM3   Community Climate System Model version 3

SST   Sea surface temperature

PRECT   precipitation

ITCZ   Intertropical Convergence Zone

YD   Younger Dryas

PW   PetaWatts

msu   model salinity unit

psu   practical salinity unit

Sv   sverdrup or $10^6 \mathrm{m}^3/\mathrm{s}$

TABLE OF CONTENTS

LIST OF FIGURES

LIST OF TABLES

1. INTRODUCTION

1.1 Identifying and comparing atmospheric versus oceanic contributions to the high-to-low latitude teleconnection during abrupt climate changes

1.1.1 Abrupt climate changes: observation and simulation

Abrupt climate changes that are more intense and rapid than the 1950-present global climate change occurred during past climate, a good example of which is the onset of the Younger Dryas (YD) Event around 11,000 years ago (Council, 2002). Greenland ice core records indicate that the Central Greenland temperature experienced sharp changes in the beginning of the YD Event (Alley, 2000). Annual mean temperature in the central Greenland dropped over 10°C within approximately a decade (Alley et al., 1993). Near-simultaneous abrupt climate changes appeared to occur over much of the globe, as indicated by various paleo proxy records (Augustin et al., 2004; Friele and Clague, 2002; Lea et al., 2003; Peterson et al., 2000; Voelker et al., 2002; Wang et al., 2001). A global picture emerged from these paleo proxy reconstructions includes a broad cooling over much of the Northern Hemisphere and a southward displacement of the Atlantic Intertropical Convergence Zone (ITCZ) (see Chiang and Friedman (2012) for a review), as well as a slowdown (or possibly a shutdown) of the Atlantic Meridional Overturn Circulation (AMOC) (Ritz et al., 2013). An important question pertinent to the current global climate change debate is whether such an abrupt climate change will occur as global warming continues. An understanding of this important issue requires an understanding of underlying dynamics governing abrupt climate changes, which is the primary focus of this dissertation research.

Sudden freshwater flux into the subpolar North Atlantic is widely speculated to

cause the YD cooling event (Broecker, 2006; Eisenman et al., 2009), in spite of lack of direct evidences. The freshwater flux in the Saint Lawrence River reconstructed from meltwater and precipitation runoff from North America to the North Atlantic and Arctic Oceans during the last deglaciation (Licciardi et al., 1999), along with the temperature drop in central Greenland derived from Greenland ice core records (Alley, 2000) laid strong scientific foundation for the freshwater flux hypothesis above. However, direct geological evidence of the sudden freshwater flux into the North Atlantic is still lacking (Broecker, 2006). Nevertheless, General Circulation Models (GCMs) have been used to study climate responses to such freshwater flux. For example, Wan et al. (2011) performed a freshwater hosing experiment by adding a freshwater source to the subpolar North Atlantic ocean using the Community Climate System Model Version 3 (CCSM3). The resultant climate responses include a weakening of the AMOC, a widespread cooling over the Northern Hemisphere and a southward dispalcement of the ITCZ, which are broadly consistent with paleo-records. Particularly, the magnitude and time-scale of these climate adjustments are comparable to paleo-records. For instance, the simulated surface temperature over the subpolar North Atlantic dropped around $10°C$ within approximately a decade. Cheng et al. (2007) and Stouffer et al. (2006) performed similar modeling experiments, which resulted in similar climate responses. Hence, a sudden freshwater flux into the subpolar North Atlantic can trigger a YD-like abrupt climate change in the modeling world.

1.1.2   Motivation

In the framework of freshwater fluxes triggering YD-like abrupt climate changes, investigations have been focused on the teleconnection linking the above mentioned remote climate responses to the high-latitude abrupt climate change. A prevailing

mechanism is that the freshening of the northern North Atlantic Ocean surface can increase the upper ocean stratification, which leads to a reduction in deep ocean convections, resulting in a cooling near the surface and a warming in the deep ocean, and a weakening in the AMOC. The broad Northern Hemispheric cooling in response to the freshwater forcing is generally thought to be through the change in oceanic heat transport associated with the weakening or shutdown of the AMOC (Eisenman et al., 2009; Stouffer et al., 2006), which carries vast amount of heat from the tropical to the high-latitude North Atlantic. However, Chiang and Bitz (2005) demonstrated that an abrupt cooling in the high-latitude North Atlantic can result in a wide spread Northern Hemispheric cooling in the absence of oceanic dynamics, raising the possibility that the oceanic heat transport change is not a necessity for the teleconnection. On the other hand, Chang et al. (2008), Wen (2009) and Wan et al. (2011) showed that freshwater-induced ocean circulation change does contribute to tropical sea surface temperature (SST) changes, which in turn affect the Atlantic ITCZ and African Monsoon. Clearly, further studies are required to understand the relative contributions from the atmosphere and the ocean to the high latitude-to-tropics teleconnection.

As discussed above, previous studies proposed that both atmospheric and oceanic processes contribute to the teleconnection during YD-like abrupt climate changes. However, their relative importance has not yet been quantified, because both atmospheric and oceanic processes are interactive in response to a freshwater "hosing". This is partly because quantifying their relative contributions in a fully coupled Atmosphere-Ocean General Circulation Model (AOGCM) hosing simulation can be a challenge. For example, when arguing that the AMOC weakening dominates Northern Hemispheric cooling, feedbacks from the atmosphere are often ignored. That is, surface temperature changes result in surface wind changes, which in turn affect the

3

AMOC through modifying the wind driven ocean circulation. On the other hand, because oceanic dynamics and its interaction with atmospheric processes are missing in a coupled Atmosphere General Circulation Model - Slab Ocean Model (AGCM-SOM) simulation (Chiang and Bitz, 2005), only the atmospheric contribution can be quantified. Hence, in such a modeling approach, these simulations are not suited to quantify the relative contributions from the atmosphere and ocean. A different modeling approach is needed.

1.1.3   A new modeling approach

A straightforward way is to perform two freshwater hosing simulations, in one of which the oceanic dynamics is turned off, and in the other of which it is on. In this way the climate response in the simulation where the oceanic dynamics is turned off quantifies the atmospheric contribution, and that in the simulation where the oceanic dynamics is turned on quantifies the total contribution. Supposing that the atmospheric and oceanic contributions add up linearly to the total, then the difference of the climate responses between the two simulations should quantify the oceanic contribution. However, it is difficult to turn *off* oceanic dynamics in AOGCMs because it will require a major undertaking to modify a highly complex AOGCM code, and it is difficult to turn *on* oceanic dynamics in AGCM-SOMs because it is absent. Thus, we cannot perform such simulations directly using AOGCMs or AGCM-SOMs. Fortunately, the oceanic dynamics can be *virtually* turned on in AGCM-SOMs using a specific technique. The "virtually" here means that the turned on oceanic dynamics is not a real one as that in AOGCMs, but a virtual one representing its energy effect so that the AGCM-SOMs can simulate the same climate as the corresponding AOGCM (whose AGCM is the same as the AGCM-SOM's) does. Turning off oceanic dynamics in AGCM-SOMs is straightforward. Hence we will perform such

freshwater hosing simulations using AGCM-SOMs in this study.

We will perform two such AGCM-SOM simulations where freshwater is hosed into the subpolar North Atlantic (this freshwater hosing is also represented by the virtual oceanic dynamics). The results show that the atmosphere along with the ocean mixed layer plays a role in propagating the surface cooling induced by the freshwater input from the Northern high-latitudes to the tropics in a nearly zonally symmetric manner, resulting in a southward shift of the ITCZ, which is consistent with Chiang and Bitz's (2005) results. The oceanic contribution is comparable to the atmospheric contribution but more zonally asymmetric, suggesting that neither of them is negligible. In a zonal mean view, the role of the AMOC slowdown is mainly cooling the northern mid-latitudes and warming the northern tropics, which leads to stronger atmospheric heat transport across subtropics. This adds more details to the results of Stouffer et al. (2006) and Eisenman et al. (2009), who proposed that the AMOC slowdown warms the Northern Hemisphere and cools the Southern Hemisphere. The ocean dynamics also does play a role in tropical SST responses. However, it does not simply result in a dipole-like pattern of anomalous SST as Dong and Sutton (2002) proposed, but forms a complicated and zonally asymmetric pattern. The oceanic contribution is partly through the surface geostrophic current change induced by the freshwater flux and partly as a feedback to the atmospheric processes.

1.2   SST's effect on ITCZ response

The mechanism of the ITCZ shift in response to extratropical forcings (i.e., freshwater flux forcing) is currently under dispute. Many studies (Dong and Sutton, 2002) attributed the ITCZ shift to the anomalous cross-equatorial SST gradient. Kang et al. (2008) and Kang and Held (2012) proposed that the cross-equatorial moisture

transport change associated with the Hadley Circulation change is responsible for the ITCZ shift: the anomalous moisture transport carried by the lower branch of the Hadley Circulation from the Northern tropics to the Southern tropics feeds the convection and rain in the Southern tropics, while the anomalous SST does not directly affect the ITCZ shift ("directly" means that the anomalous SST affects ITCZ position through manipulating local lower-tropospheric pressure gradient and thus the local lower-tropospheric convergence). Additionally, they argued that the Hadley circulation change results from the requirement that more energy should be transported from the relatively warmer hemisphere (Southern) to the relatively cooler hemisphere (Northern). However, this energetics mechanism is not complete since the "requirement" is not necessary to be met considering that the Top of Atmosphere (TOA) energy flux change can also help close the global heat budget. Additionally, because the ITCZ position also in turn largely affects the Hadley circulation (Held and Hou, 1980), it is hard to determine the causality between them. Chiang and Bitz (2005) further argued that the anomalous cross-equatorial SST gradient and the ITCZ shift combined to maintain their states by the water vapor, which is a greenhouse gas and thus keeps the relatively cooler hemisphere cool by transporting moisture to the relatively warmer hemisphere to reduce humidity in the relatively cooler hemisphere. This anomalous moisture transport results from the anomalous cross-equatorial pressure gradient associated with the anomalous cross-equatorial SST gradient. This suggests that SST does directly affect ITCZ shift. Therefore, the importance of the SST to the ITCZ shift needs to be reexamined, which is the focus of the second part of this thesis research.

For this purpose, we perform three additional AGCM-SOM hosing simulations (each is paired with a control simulation) that are similar to previous hosing simulation where the oceanic dynamics is turned off, and same Northern high-latitude

6

forcing (here the Northern high-latitude ocean surface cooling is seen as the forcing) but different ocean mixed layer depth is used. The change in the ocean mixed layer depth in these experiments is aimed to examine the sensitivity of SST response to changes in mixed layer depth. The results show that the high-to-low latitude surface cooling propagation is slower and the ITCZ southward shift is weaker when the mixed layer is deeper. This suggests that SST change is necessary for teleconnecting the ITCZ response to the high-latitude forcing. Now does the local SST change directly determine the ITCZ shift through affecting local pressure gradient, or does the large-scale SST pattern change indirectly affect ITCZ through affecting large-scale circulation? To answer these questions, we perform additional simulations using Lindzen and Nigam's (1987) simple model to examine the SST's direct effect. This model is simple but is able to capture SST's direct effect on the lower-tropospheric convergence, which characterizes the ITCZ, without indirect effect through large-scale circulation. The results show that the SST's direct effect is consistent with the ITCZ shift.

2. MODELING A YD-LIKE ABRUPT CLIMATE CHANGE USING AN COUPLED AOGCM

2.1 The community climate system model version 3

The Community Climate System Model Version 3 (CCSM3) (Collins et al., 2006) is a coupled AOGCM along with a land model and a sea ice model. Four component models are coupled and communicate among each other through a coupler. The four component models are: an atmosphere model - the Community Atmosphere Model Version 3 (CAM3) (Kiehl et al., 1996), an ocean model - the Parallel Ocean Program (POP) (Smith and Gent, 2002), a sea ice model - the Community Sea Ice Model Version 5 (Briegleb et al., 2004), and a land model - the Community Land Model Version 3 (CLM3) (Oleson et al., 2004). The coupled system is designed to conserve energy, mass, and water (not precisely, but outstanding among present AOGCMs). The CCSM3 can simulate both the atmospheric and oceanic circulations in realistic settings.

2.2 Modeling strategy and configurations

Although direct evidence of a sudden freshwater flux into the North Atlantic is absent, its effect can be simulated using fully coupled AOGCMs. In this section we will introduce the simulations carried out by Wan et al. (2011) using CCSM3. Their simulations include a 400-year climatological simulation and an ensemble of five 60-year freshwater hosing simulations. In the hosing simulations a virtual freshwater flux of 0.6 Sv (surface *salt* flux, instead of real freshwater flux, that is equivalent to the mentioned amount of freshwater flux) was uniformly applied to the subpolar North Atlantic Ocean over a latitude band between 50°N-70°N (shown in Fig. 2.1) to broadly simulate a freshwater influx from the ice sheet melt. The relation between

8

the surface salt flux and the virtual freshwater flux is given by the following equation:

$$F_{salt} = - \times F_{fw} S_{ref} / \rho_w \qquad (2.1)$$

where F_{salt} denotes the surface salt flux with unit msu·cm/s, F_{fw} the freshwater flux with unit $kg/m^2/s$, S_{ref} the reference ocean salinity, which is 34.7psu in CCSM3, and ρ_w the water density, which is $1g/cm^3$. "msu" denotes the model salinity unit, and "psu" the practical salinity unit, with a relation msu=psu/1000 (Smith and Gent, 2002). All fluxes are upward for positive values. This experiment setup follows the common design of coordinated experiments (so-called water hosing) under the WCRP Paleo-Modeling Intercomparison Project (PMIP) (Stouffer et al., 2006). The experiments were conducted under the current climate conditions with 1995 CO_2 value, solar constant and distribution of land cover types. The initial condition for each ensemble member was taken from a 400-year climatological simulation. A more detailed description of these hosing runs can be found in Wan et al. (2011). In this study we use the monthly mean output of the 400-year climatological simulation (CCSM3-CLIM) and the ensemble of five 60-year hosing runs (CCSM3-HOSE). To eliminate effect due to different initial conditions, we selected an ensemble of five 60-year segments from the 400-year climatological run (denoted as CCSM3-CTRL). The beginning of each segment corresponds to the initial condition used for each of the hosing simulations, so that the five segments can be paired with corresponding hosing runs by matching initial conditions. The resolution of the Atmospheric model is T42, which is approximately 2.8°latitude ×2.8°longitude, and the ocean model is set at around 1°latitude ×1°longitude. A summary of the simulation setups is given in Table 2.1.

Table 2.1: List of the CCSM3 simulations by Wan et al. (2011)

Simulation	Model used	Freshwater hosing	# ensemble	running time (years)
CCSM3-CLIM	CCSM3	NO	1	400
CCSM3-CTRL (segments from CCSM3-CLIM)	CCSM3	NO	5	60
CCSM3-HOSE	CCSM3	YES, 0.6 Sv uniformly in 50°N-70°N Atlantic	5	60
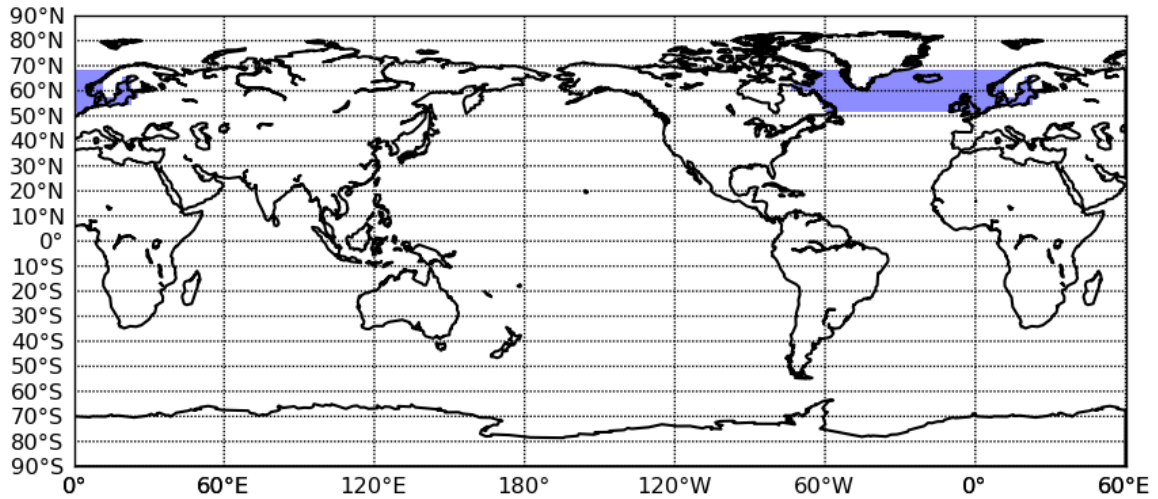
Figure 2.1: The geometry of the area (blue) where artificial anomalous freshwater input is applied.

2.3   Model results

As introduced in the previous section, Wan et al. (2011) simulated the climate responses to a freshwater hosing to the subpolar North Atlantic. The simulated climate responses present features that are broadly consistent with paleo-records during the

YD period. Fig. 2.2 shows the annual mean surface temperature and precipitation anomalies in the 6th decade after the freshwater onset. The anomalies are calculated using the hosing runs minus their corresponding segments from the climatological run (CCSM3-HOSE - CCSM3-CTRL), and hereafter all anomalies in this chapter are calculated this way. The ensemble average is taken over the 5 members to reduce sampling errors. The figure shows that after half century of hosing, the Northern Hemisphere broadly becomes cooler and the Southern Hemisphere warmer. The average cooling in the Northern Hemisphere and warming in the Southern Hemisphere are about 3K and 0.2K, respectively. The former is much stronger than the later, which is expected considering the fact that the freshwater forcing is added to the high-latitude North Atlantic. The cooling in the subpolar North Atlantic is particularly strong, which is over 8K. This is due to the increase in the upper ocean stratification in this region, which directly results from the freshwater forcing. The figure also shows that the precipitation decreases in the Northern Tropical Atlantic and increases in the Southern Tropical Atlantic, indicating a southward shift of the Atlantic ITCZ. These results are broadly consistent with the paleo-records (Council, 2002; Peterson et al., 2000). Additionally, the ITCZ in the Eastern Pacific and the Indian Ocean also shifts southward, while that in the Western Pacific weakens. Overall, the ITCZ shifts southward in a zonal mean view. These surface temperature and precipitation anomalies suggest that the Northern high-latitude freshwater forcing leads to a change in the interhemispheric contrast, of which the mechanism is under debate between the atmosphere-dominating (Chiang and Bitz, 2005; Kang et al., 2008) and the oceanic-dominating (Eisenman et al., 2009; Stouffer et al., 2006) hypotheses.

Note that a fully coupled CCSM3 simulation takes thousands of years to reach an equilibrium due to long adjustment time of deep ocean. Therefore, the results shown

in Fig. 2.2 are not equilibrium response. However, the patterns of climate responses do not change significantly after 20 years of integration, only the magnitudes may vary. Therefore, we may consider that the climate responses in equilibrium are quantitatively the same as those in the 6th decade. Fig. 2.3 is the same as Fig. 2.2, but shows the results in the 3rd decade. The two figures show that the anomalies in the 3rd decade have almost the identical patterns as in the 6th decade, except smaller magnitudes. Fig. 2.4 shows the ensemble averaged annual mean surface temperature anomaly and precipitation anomaly (CCSM3-HOSE minus CCSM3-CTRL) averaged over the Northern and Southern Hemispheres as functions of time. The magnitudes of the surface temperature anomalies in the Northern Hemisphere enlarge in around 1-25 years and hold hereafter. The magnitudes of the precipitation anomalies also enlarge in around 1-25 years but slightly enlarge continually hereafter. These results support the above statement that the 6th decade is not yet but near equilibrium. Hence we can view the 6th decade climate responses to gain an approximate picture of the equilibrium responses.
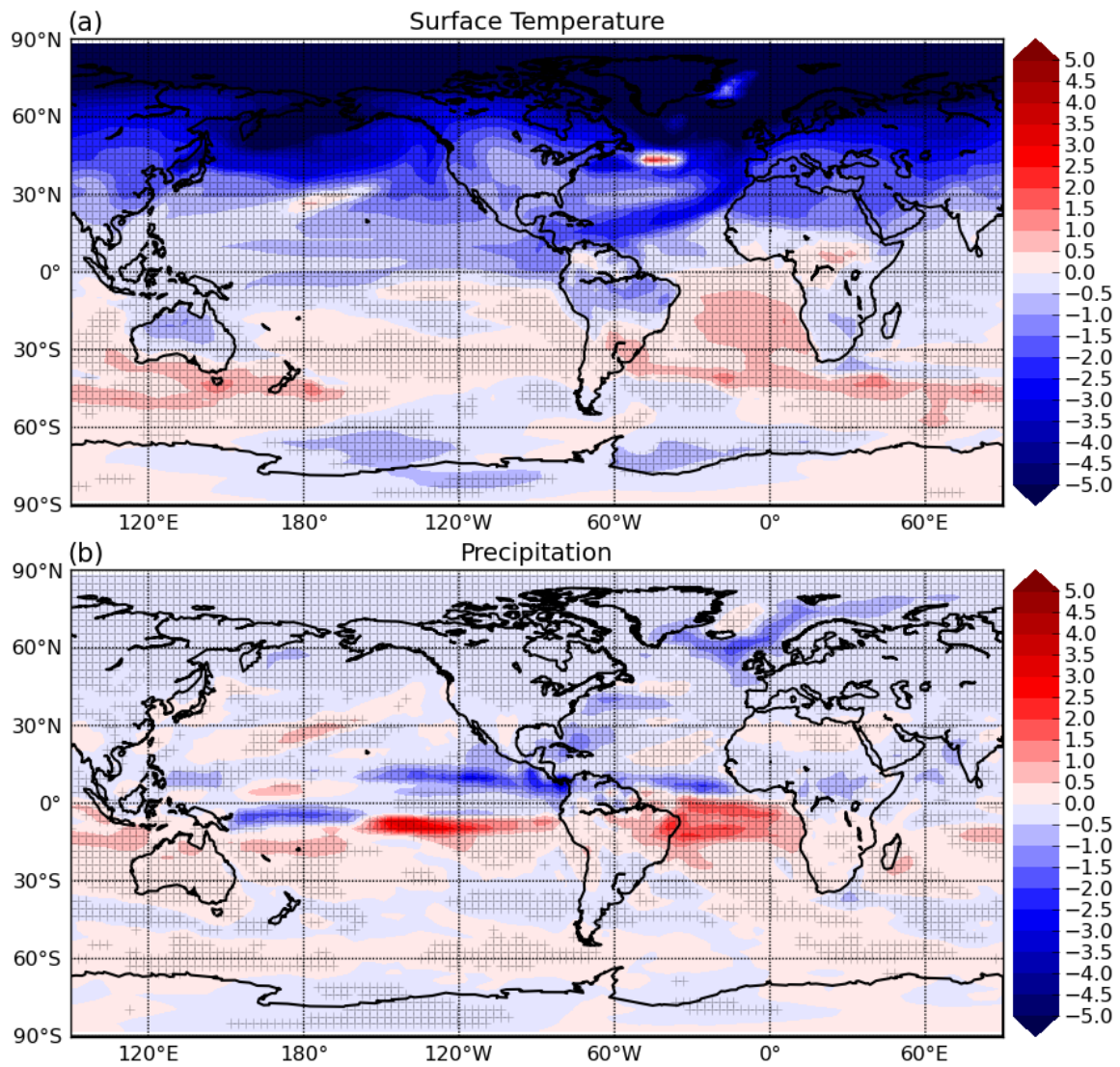
Figure 2.2: The (a) Surface Temperature and (b) Precipitation anomalies averaged over 51-60 years after the freshwater onset in the CCSM3 hosing simulation. Anomalies at spots with plus signs are nonzero with 95% confidence based on the student t-test. The units for surface temperature and precipitation are K and mm/day, respectively.
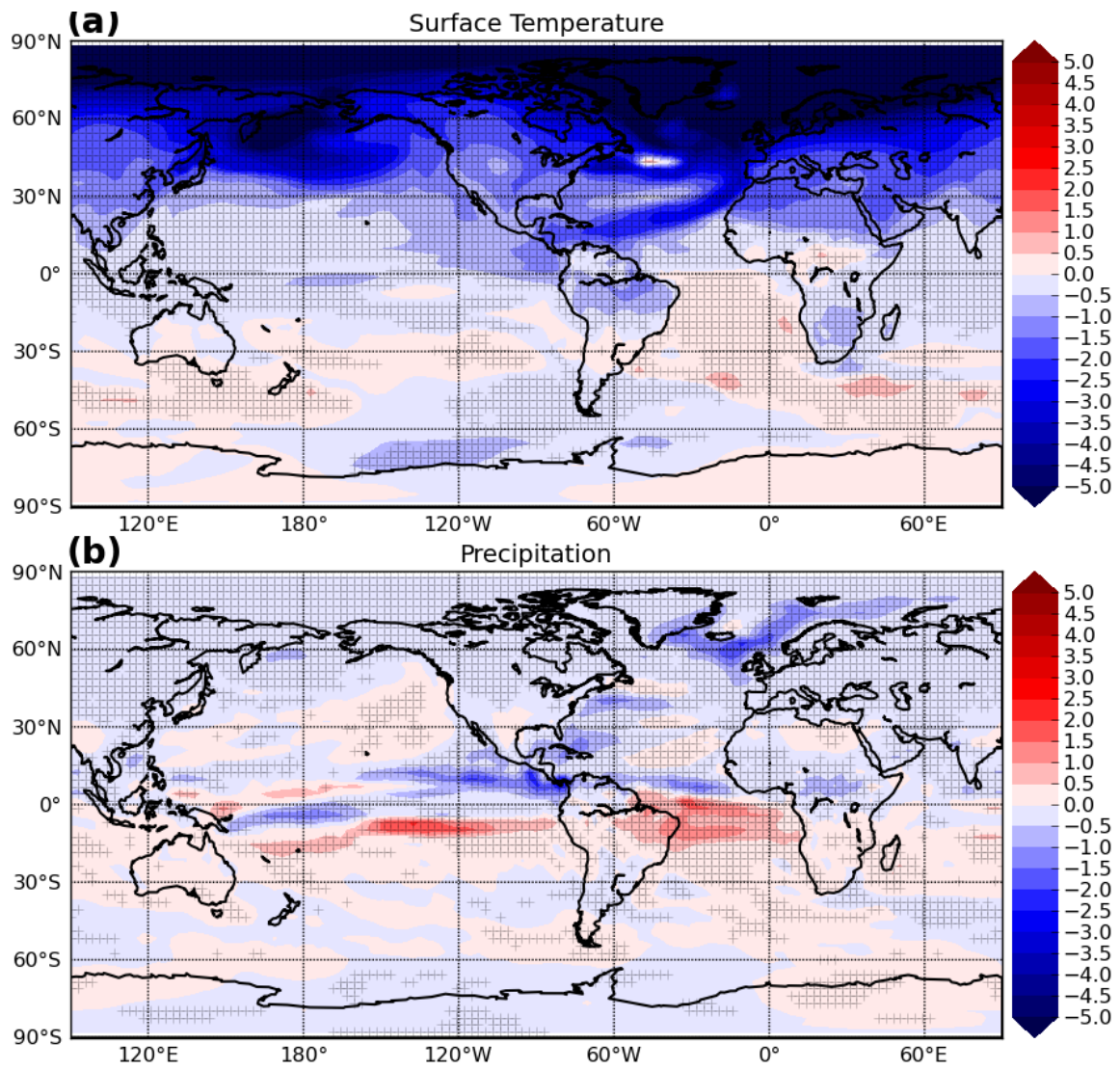
Figure 2.3: The same as Fig. 2.2 but showing 31-40 years after the freshwater onset.
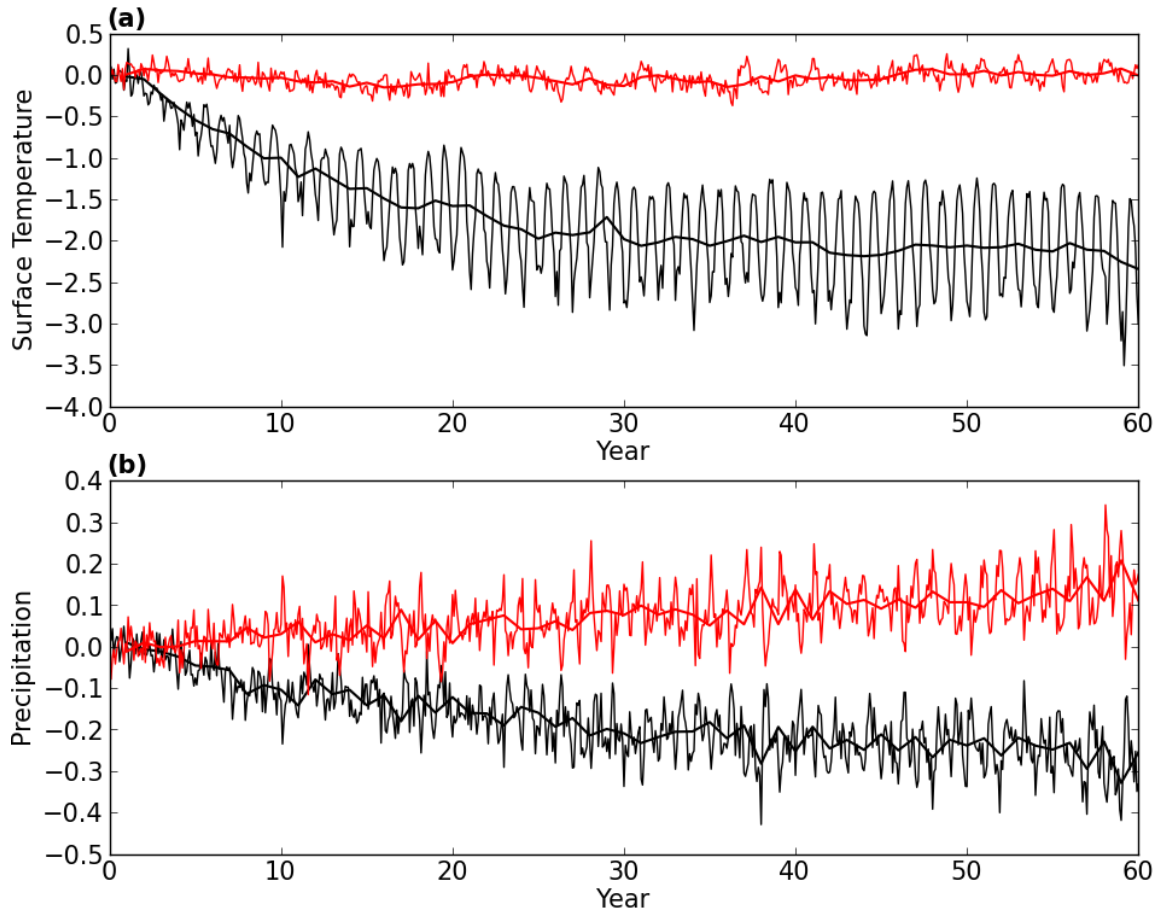
Figure 2.4: The ensemble averaged (a) Surface Temperature and (b) Precipitation anomalies averaged over the Northern Hemisphere (black lines) and the Southern Hemisphere (red lines). For each monthly mean plot (thinner lines) a corresponding annual mean is calculated (thicker lines).

The AMOC-associated explanation of the Northern Hemispheric cooling blames the northward cross-equatorial oceanic heat transport reduction resulting from the AMOC weakening. Fig. 2.5 shows the AMOC change overlaid on the AMOC climatology and the Global Northward Oceanic Heat Transport anomaly. The AMOC is characterized by the Atlantic Meridional Volume Stream Function, which is given by

the equation:

$$\overline{AMOC}(\theta, z) = 2\pi r cos(\theta) \int_{bottom}^{z} \left[\overline{V}(\theta, \lambda, z') H(\theta, \lambda) \right] dz' \qquad (2.2)$$

where

$$H(\theta, \lambda) = \begin{cases} 1, & \text{over Atlantic} \\ 0, & \text{elsewhere} \end{cases},$$

V denotes the meridional velocity, θ and λ the latitude and longitude. The overbar and the square bracket denote the temporal and the zonal averages, respectively. An AMOC weakening and an Atlantic northward oceanic heat transport reduction are evident. The AMOC is weakened by around 80% (the weakening is characterized by the fact that the highest value of the volume stream function of about 18Sv at 1000m depth and 40°N decreases by about 14Sv), and the associated Atlantic northward heat transport is reduced by the similar percentage over most latitudes. However, this heat transport anomaly peaks at around 20°N, suggesting that this anomaly cools the northern mid- and high- latitude Atlantic ocean and warms the Tropical Atlantic ocean. The global oceanic heat transport anomaly is similar to the Atlantic, which cools the Northern mid- and high- latitudes and warms the Tropics. This pattern contradicts the argument that the reduction of the northward oceanic heat transport simply cools the Northern Hemisphere and warms the Southern Hemisphere during a weakening of the AMOC (Eisenman et al., 2009; Stouffer et al., 2006). On the other hand, cooling over the Northern Hemisphere and warming in the Southern Hemisphere are observed (Fig. 2.2), suggesting that the AMOC-associated oceanic heat transport reduction alone cannot explain the high-to-low latitude teleconnection.

Thus, the atmospheric processes and other oceanic processes must be involved.

Kang et al. (2008) attributes the ITCZ southward shift to the increase in the cross-equatorial northward atmospheric heat transport as a compensation to the decrease in the cross-equatorial northward oceanic heat transport. Fig. 2.6 shows the northward atmospheric and oceanic heat transports of CCSM3-CTRL and CCSM3-HOSE in the 6th decade. The atmospheric heat transport is calculated by integrating the incoming vertical heat fluxes through the surface and the top of atmosphere from the South Pole:

$$\overline{AHT}(\theta) = 2\pi r^2 \int_{-\pi/2}^{\theta} \left(\overline{[F_{surf}]}(\theta') - \overline{[F_{TOA}]}(\theta') \right) cos(\theta')d\theta' \qquad (2.3)$$

where θ denotes the latitude, ranging from $-\pi/2$ (South Pole) to $\pi/2$ (North Pole). F_{surf} and F_{TOA} denote the net upward heat fluxes at the surface and the top of atmosphere (positive for upward). AHT represents the atmospheric northward heat transports. The overbar and the square bracket denote the temporal and zonal averages. A globally uniform adjustment is applied to $F_{surf} - F_{TOA}$ in order to conserve energy in the atmosphere. The northward oceanic heat transport (OHT) is directly from model output. There is a compensation between the AHT anomaly and the OHT anomaly over all latitudes between 60°S-60°N: the ocean transports less heat while the atmosphere transports more heat northward. However, we cannot simply conclude that the OHT anomaly causes the AHT anomaly, and vise versa. On the one hand, Stouffer et al. (2006) and Eisenman et al. (2009) argued that the freshwater forcing leads to AMOC slowdown, resulting in a decrease in OHT. On the other hand, Chiang and Bitz (2005) argued that the high-latitude cooling can result in increase in AHT when oceanic dynamics is absent. These previous studies suggest that both AHT and OHT can respond to the high-latitude freshwater forcing, but

neither of them necessarily results from the other. Additionally, these changes are coupled, meaning that any change in either of them can result in change in the other. For example, OHT change can lead to SST change (Chang et al., 2008; Wan et al., 2011; Wen, 2009), resulting in surface wind change, which can in turn change OHT through changes in wind driven circulation. Therefore, the compensation between the OHT decrease and the AHT increase cannot infer any causality between them. Nevertheless, the increase in cross-equatorial AHT is consistent with the southward shift of the ITCZ, which is consistent with Kang et al.'s (2008) results. However, this doesn't infer a causality between them because AHT and ITCZ are coupled. On one hand, a northward cross-equatorial AHT anomaly, implying a southward shift of Hadley circulation center (Kang et al., 2008), can result in a southward moisture transport anomaly, feeding precipitation in the Southern Tropics and reducing it in the Northern Tropics, which means a southward shift of ITCZ. On the other hand, a southward shift of ITCZ can in turn increase the Hadley circulation strength in the Northern Tropics and decrease it in the Southern Tropics (Held and Hou, 1980), resulting in a northward cross-equatorial AHT anomaly. Additionally, focusing on the role of large-scale circulation changes ignore the potential importance of SST's influence, which can affect local convergence through vertical mixing. Therefore, the mechanism of the ITCZ southward shift in response to the high-latitude freshwater forcing need to be further studied, which is the focus of Chapter 4.

These CCSM3 hosing simulation results infer that both the atmosphere and ocean may be important in linking the global climate response to the subpolar freshwater forcing. However, because both the atmosphere and the ocean are coupled, it is difficult to determine cause and effect from an AOGCM simulation. Therefore, a goal of this research is to find a way to distinguish their contributions to the teleconnection, which will be discussed in the next chapter.
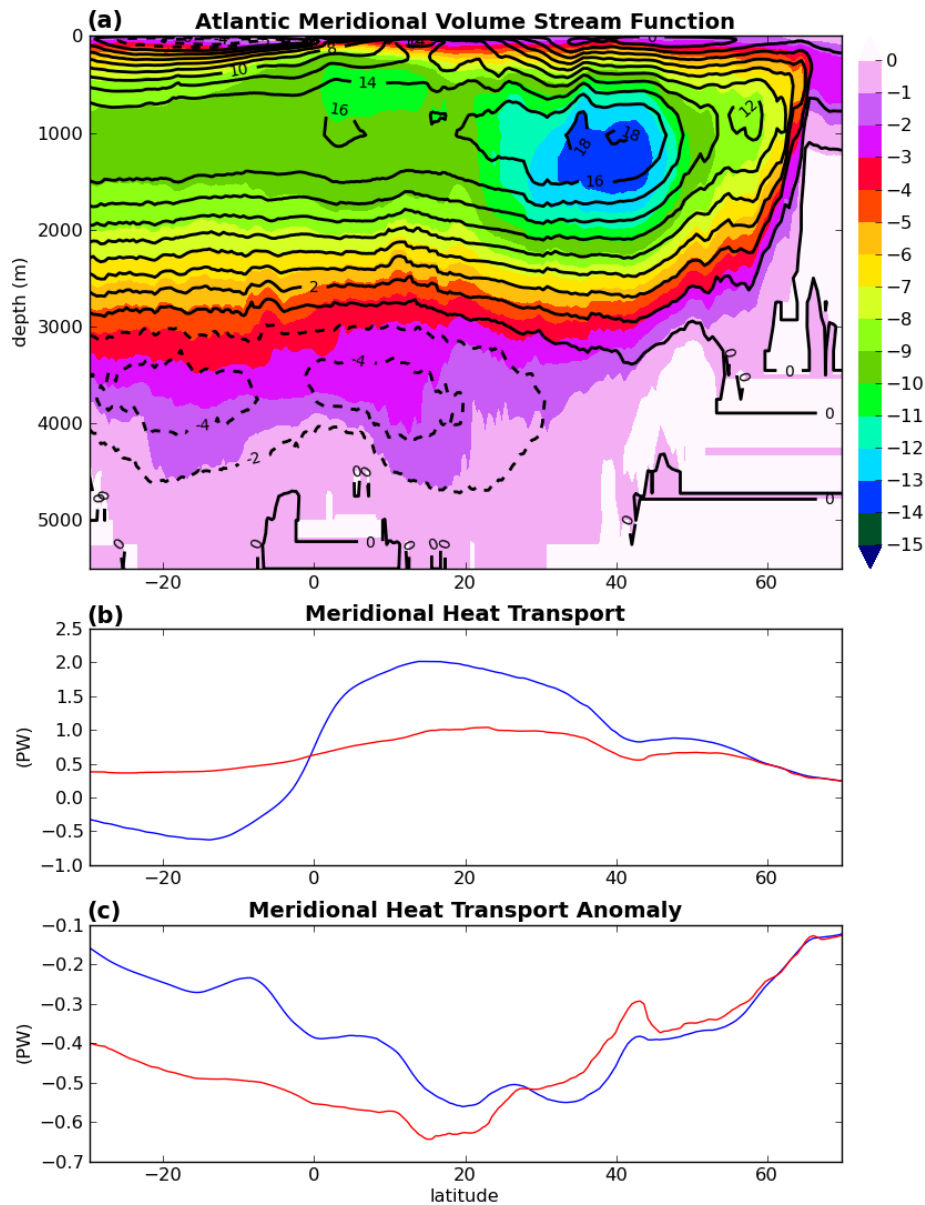
Figure 2.5: (a) The time-mean AMOC stream function (contour, with an interval of 2 Sv) in CCSM3-CTRL and its change in CCSM3-HOSE (color); (b) the time-mean Atlantic (red) and Global (blue) Northward Oceanic Heat Transports in CCSM3-CTRL and (c) their changes in CCSM3-HOSE. The changes are taken in the 6th decade. The units are Sv and PW for the AMOC stream function and the heat transports, respectively.
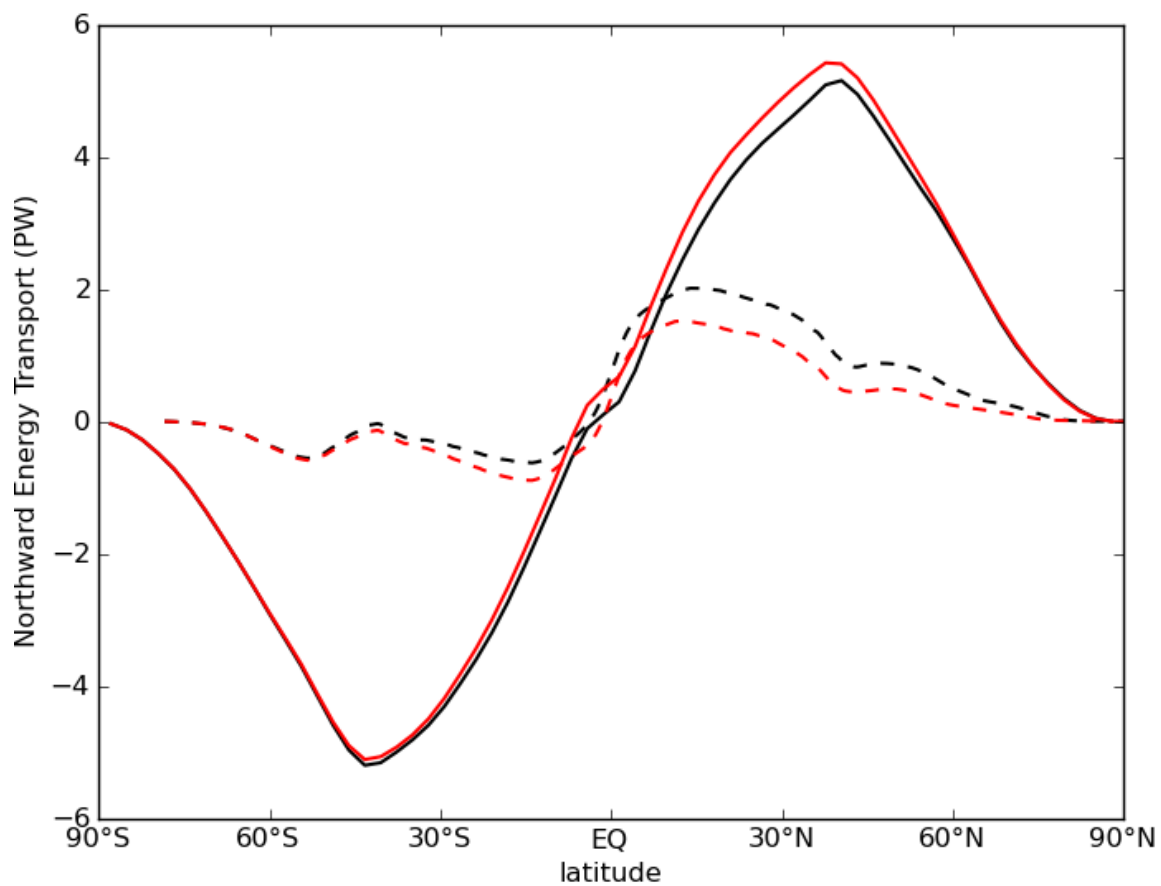
Figure 2.6: The annual mean atmospheric (solid) and oceanic (dashed) northward heat transports in the 6th decade of CCSM3-CTRL (black) and CCSM3-HOSE (red).

3. IDENTIFYING ATMOSPHERIC VERSUS OCEANIC CONTRIBUTIONS TO THE TELECONNECTION

3.1 Teleconnection in a fully coupled model

In last chapter we introduced a freshwater hosing experiment carried out by Wan et al. (2011) using CCSM3. In their hosing simulation a surface freshwater flux forcing is uniformly applied to the subpolar North Atlantic (50°N-70°N). The resultant global climate responses include a slowdown of the AMOC, a cooling over the Northern Hemisphere, a warming over the Southern Hemisphere, and a southward shift of the ITCZ. These responses are broadly consistent with paleo-records during the YD period. The responses develop rapidly, taking roughly 10-20 years to nearly reach a new equilibrium, which is also consistent with the abrupt climate change time scale at the beginning of YD (Alley et al., 1993). However, mechanisms teleconnecting these global climate responses to the regional freshwater forcing in the high-latitude North Atlantic are not yet clear. Previous studies suggest that both atmospheric and oceanic processes contribute to the teleconnection, but their relative importance has not been quantified. The goal of this chapter is to perform a series of model simulations to separate atmospheric contribution from oceanic contribution.

Because high-resolution paleo-records are not available, it is impossible to use them to separate atmospheric and oceanic contributions to the teleconnection during past abrupt climate changes. Fortunately, a fully coupled AOGCM can be used to simulate a YD-like abrupt climate change, providing a framework to address this issue. Wan et al. (2011) performed such simulations as we introduced in the previous chapter. These freshwater hosing simulations are used as a reference for other experiments.

However, because both the ocean and atmosphere are interactive in response to the high-latitude forcing, it can be a challenge to quantify their relative contributions to high-to-low latitude teleconnection in a fully coupled AOGCM hosing simulation. In the following we take SST as an example to explain the difficulty in using AOGCMs to distinguish the atmospheric and oceanic contributions. The sea surface, as the interface between the atmosphere and ocean, its temperature, SST, is a critical physical variable through which the ocean and atmosphere are communicated. SST not only affects both oceanic and atmospheric circulations, but also is affected by these circulations through surface heat fluxes and other dynamic processes. The governing equation for SST is given by ocean surface mixed layer heat budget:

$$\rho_w c_{pw} h_m \frac{\partial T}{\partial t} = -Q(T, \ldots) - F(T, \ldots) \tag{3.1}$$

where T, Q, F represents SST, divergence of oceanic heat flux integrated over the mixed layer depth, h_m (Q will be denoted as oceanic heat flux in following contexts) and the air-sea surface heat flux (positive upward), respectively. ρ_w and c_{pw} are the water density and specific heat. Q and F are complex functions of T and other variables associated with atmospheric and oceanic surface boundary processes, such as surface winds, cloud coverage, air temperature, oceanic surface currents, etc.

The equation for SST anomalies is given by (neglecting temporal change in mixed layer depth):

$$\rho_w c_{pw} h_m \frac{\partial \delta T}{\partial t} = -\delta Q(T, \ldots) - \delta F(T, \ldots) \tag{3.2}$$

where the prefix δ denotes anomalies from the climatology. From Eq. 3.2, it is evident that both δQ and δF contributes to δT when we introduce a forcing to the climate system. Superficially, one maybe attempt to simply denote δQ as the oceanic

22

contribution and δF as the atmospheric contribution to δT. However, this assertion is only meaningful if δQ and δF are independent. In this case, δT can be divided into two parts, one associated with oceanic contribution and the other associated with atmospheric contribution. In general, this will not be the case, because δQ and δF are related through SST as well as other dynamical processes. As such, it is generally difficult to separate oceanic versus atmospheric contributions to δT in a fully coupled AOGCM simulation, because it is not easy to eliminate oceanic processes while computing SST changes only through atmospheric surface heat fluxes, i.e.,

$$\rho_w c_{pw} h_m \frac{\partial \delta T}{\partial t} = -\delta F(T, \ldots) \tag{3.3}$$

Even if we succeed in eliminating oceanic processes in a fully coupled AOGCM simulation, δT and δF in Eq. 3.3 will be likely different from those in Eq. 3.2, because removing δQ in a fully coupled system can result in changes in both δT and δF. We can identify the δT in Eq. 3.3 as the atmospheric contribution and the δT in Eq. 3.2 as the total atmospheric and oceanic contribution as long as the same forcing is introduced to the two systems. The difference between the two can give an estimate of the oceanic contribution, assuming that linearity applies to the oceanic and atmospheric contributions to total SST changes. For this assumption to be valid, anomalies should be sufficiently small, so that the relationship among δT, δQ and δF are nearly linear. Although we are unable to fully validate this linearity assumption, we apply this assumption on the basis that SST anomalies in response to freshwater hosing, particularly in the tropics, are generally small compared to the seasonal SST variation. In the next section, we introduce the basic CAM3-SOM experimental scheme to separate out the atmospheric and oceanic contributions to the high-to-low latitude teleconnection.

3.2 CAM3-SOM and experimental scheme to separate atmospheric and oceanic contributions

Now we face the technical question of how to separate atmospheric and oceanic contributions. We illustrate below how this can be achieved using an AGCM-SOM modeling approach. In an SOM, the Q is prescribed and thus not interactive with other variables. Thus we can control the Q in AGCM-SOM simulations so that δQ is either present or eliminated. This allows us to separate out the atmospheric and oceanic contributions as follows: First, we reproduce an AOGCM hosing simulation using an AGCM-SOM by supplying a "correct" δQ to the model (details of computing δQ will be provided in the subsequent section). We then make another AGCM-SOM hosing simulation where δQ is removed outside of the freshwater hosing region, so that oceanic processes can be eliminated from the hosing simulation, giving us an estimate of the atmospheric contribution to the teleconnection. Finally, we take a difference between the above two experiments to obtain an estimate of the oceanic contribution. The validity of this approach requires that the AGCM-SOM "hosing" simulation can accurately reproduce climate responses in the AOGCM hosing simulation. We will demonstrate in the section 3.5 that this is indeed possible. In next section the technique of computing Q in CCSM3 experiments are described.

3.3 Computation of Q-fluxes using SST-restoring technique

In CAM3-SOM the ocean consists of merely an ocean mixed layer that is vertically uniform (supposing infinite vertical mixing within the mixed layer) and non-moving (Hansen et al., 1984; Kiehl et al., 1996). It exchanges energy, water and momentum with the overlying atmosphere (water and momentum changes in ocean mixed layer are excluded). The heat flux divergence due to the missing oceanic dynamics (Q in Eq. 3.1) is prescribed and referred to as Q-flux. Thus, the governing equation for

SST in CAM3-SOM is:

$$\rho_w c_{pw} h_m \frac{\partial T}{\partial t} = -Q - F(T, \ldots) \tag{3.4}$$

where Q is the Q-flux. Comparing Eq. 3.1 to Eq. 3.4 shows that Q is prescribed in CAM3-SOM while interactive in CCSM3. Therefore, to reproduce CCSM3 simulations using CAM3-SOM, we need to compute the Q-flux.

A possibly straightforward way to compute the Q-flux is to directly solve Eq. 3.1 about Q, because both T and F are known in the reference CCSM3 simulations. However, such an approach is problematic at coastal grid cells, where F is the average over the entire grid, contaminated by land surface heat fluxes. Therefore, we take a different approach to compute the Q-flux. In this study an *SST-restoring* technique is used to reproduce the CCSM3 climatological and hosing simulations. The technique follows that used by Knutson (2009) to reconstruct observed SST climatology using a Flexible Modeling System coupled to a slab ocean model. The approach to compute the Q-fluxes using this SST-restoring technique are described below.

A Newtonian damping term is added to the right hand side of Eq. 3.4 in CAM3-SOM, so that the governing equation for the SOM becomes:

$$\rho_w c_{pw} h_m \frac{\partial T}{\partial t} = -Q - F(T, \ldots) - \rho_w c_{pw} h_m \sigma (T - T_c) \tag{3.5}$$

where σ is a constant representing the reciprocal of the damping time scale, and T_c is a prescribed target SST. h_m is computed from the 400-year average mixed layer depth in CCSM-CLIM and thus varies only in space. This modified CAM3-SOM will be referred to as CAM3-RESTORE in this study.

Eq. 3.5 shows that T will be very close to T_c if σ is sufficiently large. We choose

it to be around 1/(2 hours), which will restrict $|T - T_c|$ to be less than around 0.03K in the simulation.

To compute the Q-flux climatology, we first run a CAM3-RESTORE simulation with T_c being the SST climatology in CCSM3-CLIM. Because Q in Eq. 3.5 is unknown, it is assigned zero everywhere in the first year of simulation. Then we recursively save and assign the value of $Q + \rho_w c_{pw} h_m \sigma (T - T_c)$ in preceding years to Q in following years. By doing so, Q converges to its final value as the value of the damping term gets smaller and smaller. The integration process lasts for 50 years before we calculate a 12-month annual cycle of Q using the last 49 years and denote it as the climatological Q-flux (CLIM-Q-flux).

Then we run another CAM3-RESTORE simulation to compute the hosing Q-flux. Here T_c is assigned the ensemble averaged transient SST of CCSM3-HOSE, and Q is assigned the CLIM-Q-flux. The simulation lasts for 20 years before the $Q + \rho_w c_{pw} h_m \sigma (T - T_c)$ term is saved as the hosing Q-flux (HOSE-Q-flux). The simulation includes an ensemble of runs with different initial conditions in order to reduce sampling errors. Because we focus on understanding the transition, Q-flux of only the first 20 years is computed.

The control Q-flux (CTRL-Q-flux) is computed following the same procedure as the hosing Q-flux, except that the T_c is assigned the ensemble averaged transient SST of CCSM3-CTRL. All the restoring simulations used to compute the Q-fluxes are listed in Table 3.1.

In the next section the experimental design using CAM3-SOM and the Q-fluxes computed above in order to separate the atmospheric and oceanic contributions to the teleconnection is described.

Table 3.1: The simulations' settings and procedure for computing the Q-fluxes.

Q-flux to compute	CLIM-Q-flux	CTRL-Q-flux	HOSE-Q-flux
Model used	CAM3-RESTORE	CAM3-RESTORE	CAM3-RESTORE
Initial condition	Random	Chosen from CLIM run above	Same as CTRL
# ensemble member	1	10	10
Running time (year)	50	20	20
Targeted SST (T_c)	Annual cycle of SST in CCSM3-CLIM	20-year SST in CCSM3-CTRL	20-year SST in CCSM3-HOSE
Q	Zero in 1st year. Thereafter $Q + \rho_w c_{pw} h_m \sigma(T - T_c)$ in each preceding year.	CLIM-Q-flux	CLIM-Q-flux
How Q-flux is computed	Annual cycle of Q in last 49 years	CLIM-Q-flux plus ensemble average of 20-year $\rho_w c_{pw} h_m \sigma(T - T_c)$	CLIM-Q-flux plus ensemble average of 20-year $\rho_w c_{pw} h_m \sigma(T - T_c)$

3.4 CAM3-SOM experimental design to separate atmospheric and oceanic contributions

Using the Q-fluxes derived from the above-mentioned SST-restoring technique, we conducted four sets of CAM3-SOM simulations, including: 1) a climatological experiment (CAM3-CLIM) using CLIM-Q-flux to reproduce the CCSM3 climatology;

27

2) an ensemble of five control experiments (CAM3-CTRL) using CTRL-Q-flux to reproduce ensemble-averaged CCSM3-CRTL; 3) an ensemble of five hosing experiments (CAM3-HOSE) using HOSE-Q-flux to reproduce ensemble-averaged CCSM3-HOSE; and finally 4) an ensemble of five CAM3-SOM hosing simulations where the HOSE-Q-flux is replaced by the CTRL-Q-flux outside of the hosing region between 50°N-70°N over the North Atlantic. We refer to this ensemble of runs as the CAM3-SOM hosing experiments with atmosphere-only processes (CAM3-HOSE-ATMO).

CAM3-CLIM is integrated for 100 years and the result will be compared to CCSM3-CLIM to give a basic sense of how well CAM3-SOM with the CLIM-Q-flux can reproduce the mean climate in CCSM3-CLIM. Each of CAM3-CTRL, CAM3-HOSE and CAM3-HOSE-ATMO ensemble is integrated for 20 years and is intended to gain understanding of the transient climate response to freshwater hosing. In particular, a comparison between CAM3-CTRL and CAM3-HOSE can tell us how well CAM3-SOM can capture atmospheric and oceanic processes' contribution to the high-to-low latitude teleconnection simulated by CCSM3. CAM3-HOSE-ATMO, where the Q-flux anomaly is suppressed except in high-latitude North Atlantic, can reveal the atmospheric contribution to the teleconnection. The five initial conditions for each of the ensemble members are taken from CAM3-CLIM and remain the same for all three ensembles. The external parameters, such as CO2, solar constant, orography and the distribution of land cover types are the same as the reference CCSM3 runs.

The basic settings of these experiments are listed in Table 3.2.

Table 3.2: The settings of CAM3-SOM simulations.

Experiment	Q-flux	# ensemble	Running time (year)
CAM3-CLIM	CLIM-Q-flux	1	100
CAM3-CTRL	CTRL-Q-flux	5	20
CAM3-HOSE	HOSE-Q-flux	5	20
CAM3-HOSE-ATMO	HOSE-Q-flux (50°N-70°N Atlantic) and CTRL-Q-flux (elsewhere)	5	20

3.5   Comparison between CCSM3 and CAM3-SOM simulations

In the following two subsections, CAM3-SOM simulations are compared to the CCSM3 simulations to examine the extent to which both the climatological and hosing CCSM3 simulations can be reproduced by the CAM3-SOM approach.

3.5.1   Comparison between CCSM3 and CAM3-SOM Climatological Simulations

In this subsection we will show how well the CAM3-SOM can reproduce CCSM3 climatology using CLIM-Q-flux.

As shown in Fig. 3.1, the resultant annual mean surface temperature of CAM3-CLIM resembles that of CCSM3-CLIM very well, with difference between the two less than 0.2K over ice-free ocean. Over land and ice-covered ocean the difference is also quite small, less than 1K and 4K, respectively. Totally the global root mean square (RMS) of the surface temperature difference between the two simulations is about 0.4K, which is less than 10% of the global mean standard deviation of either

simulation (around 4K).
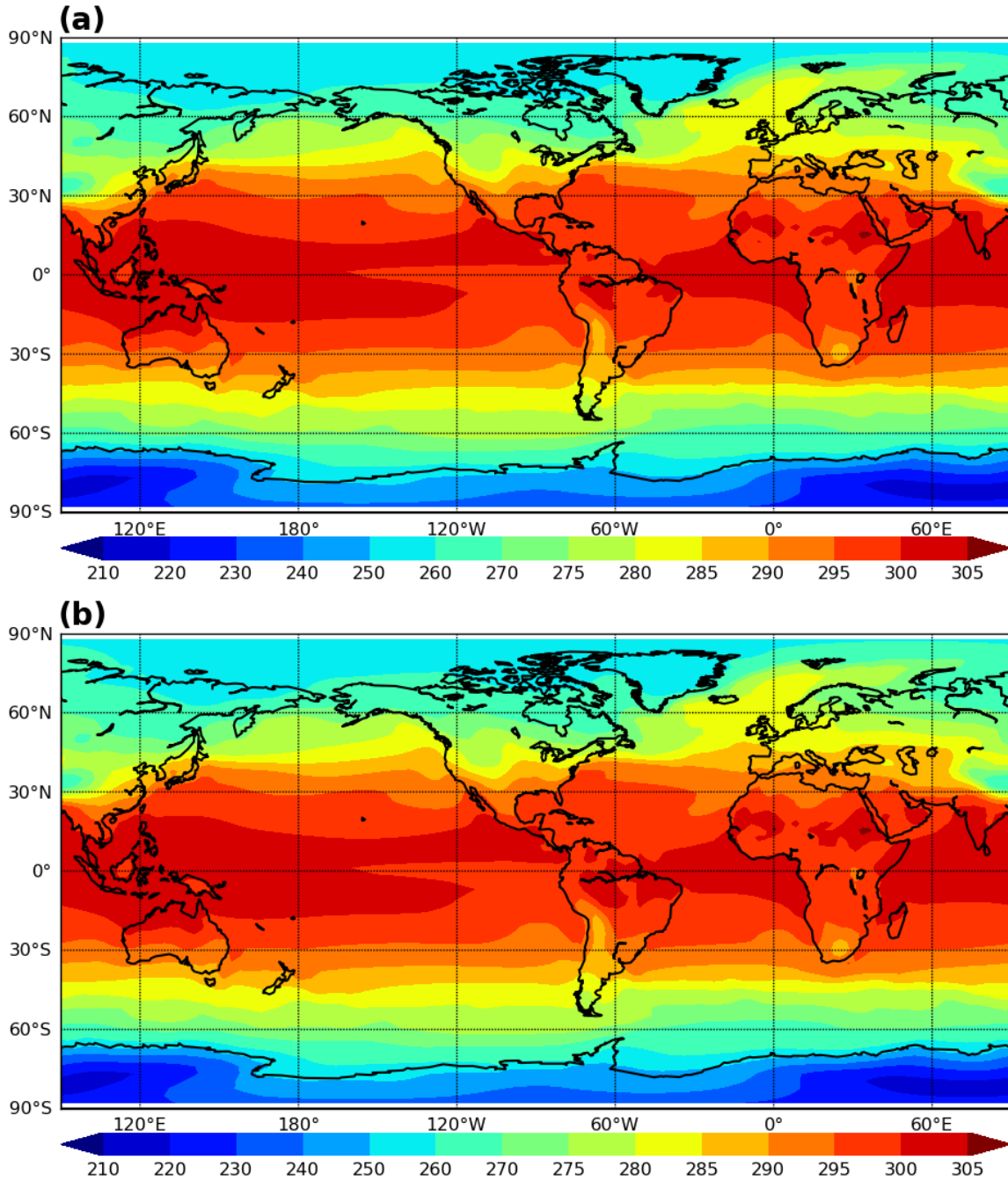
Figure 3.1: The annual average surface temperature in (a) CAM3-CLIM and (b) CCSM3-CLIM. The unit is K.

Reproducibility of the surface temperature seasonal variation in CCSM3-CLIM by CAM3-CLIM is shown in Fig. 3.2 as a Hovmoller diagram of zonally averaged surface temperature with annual mean removed. Similarity between CCSM3 and CAM3-SOM is evident. Further analysis indicates that the global RMS of the difference between the two surface temperature seasonal variations is less than 20% of the simulated surface temperature seasonal cycle amplitude, indicating that CAM3-SOM well reproduces the seasonal surface temperature variation in CCSM3. Basic features such as warming in summer and cooling in winter in each hemisphere are captured by both model simulations.
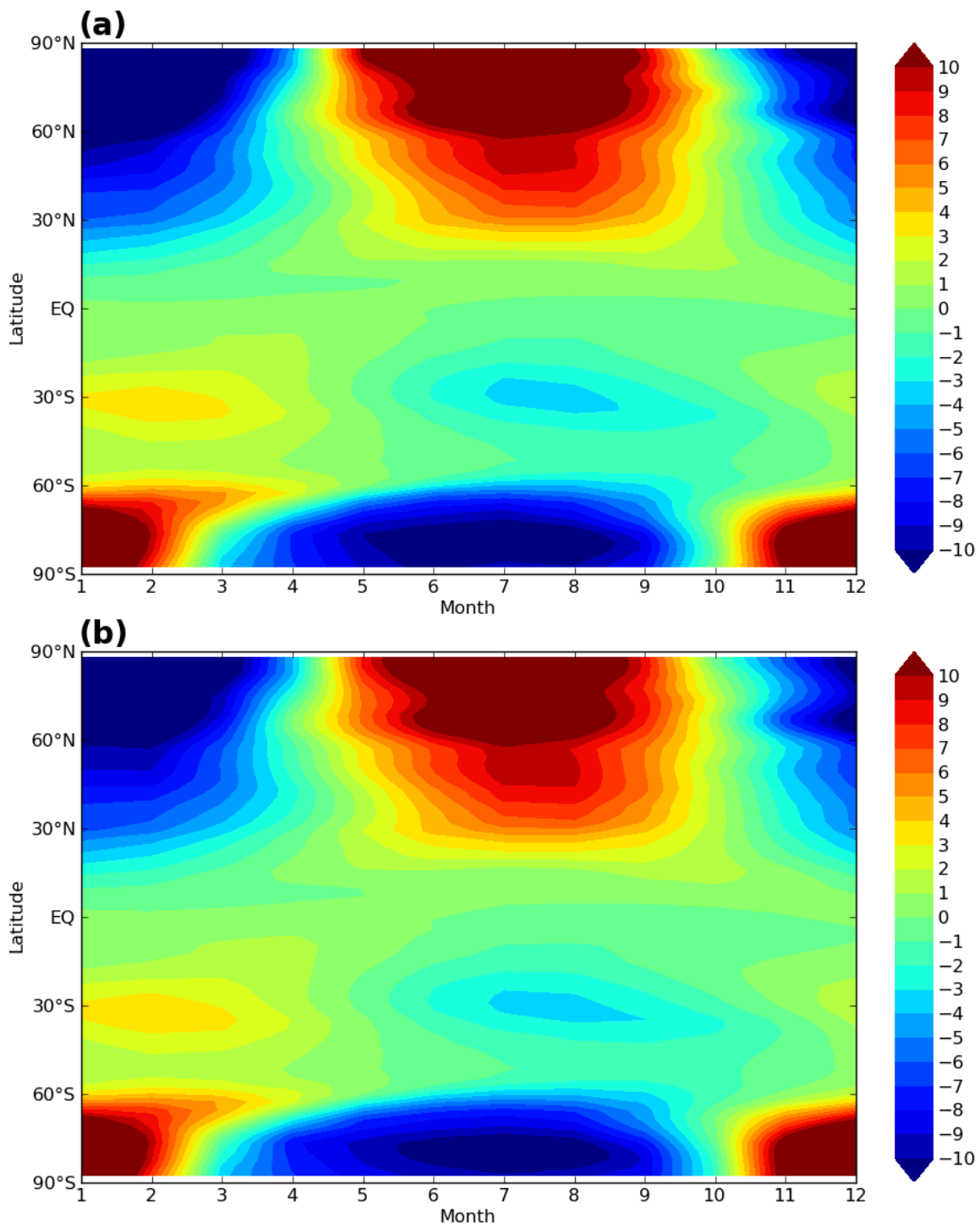
Figure 3.2: The seasonal variation of the zonally averaged surface temperature for (a) CAM3-CLIM, (b) CCSM3-CLIM with annual means removed. The unit is K

Fig. 3.3 shows a comparison of the annual mean surface heat flux between the two model simulations. Again, CAM3-SOM reproduces the CCSM3 surface heat flux mean climatology with high fidelity. The global RMS of the difference between the two model annual mean surface heat fluxes is 4 W/m2, which is less than 10% of the global mean standard deviation of the simulated surface heat fluxes. Basic features such as strong ocean-to-atmosphere heat release over subpolar North Atlantic and western boundary currents including the Kuroshio current along western Pacific boundary, the Gulf Stream along western Atlantic boundary, the Agulhas along African coast, the Brazil Current along western south Atlantic boundary, and the East Australia Current and strong heat gain over Equatorial ocean are captured by both model simulations. Fig. 3.4 shows a similar Hovmoller diagram of zonally averaged annual cycle of the surface heat flux to the annual cycle of surface temperature shown in Fig. 3.2. Similar to the surface temperature, the global RMS of difference between the two surface heat flux seasonal variations is less than 20% of the simulated globally averaged seasonal cycle amplitude. Basic features such as winter heat release and summer heat gain in both hemispheres are well simulated in both simulations. Based on these results, we conclude that the CAM3-SOM approach successfully reproduces the surface temperature and surface heat flux climatology of CCSM3. We next examine the reproducibility of CAM3-SOM in other important climate variables.
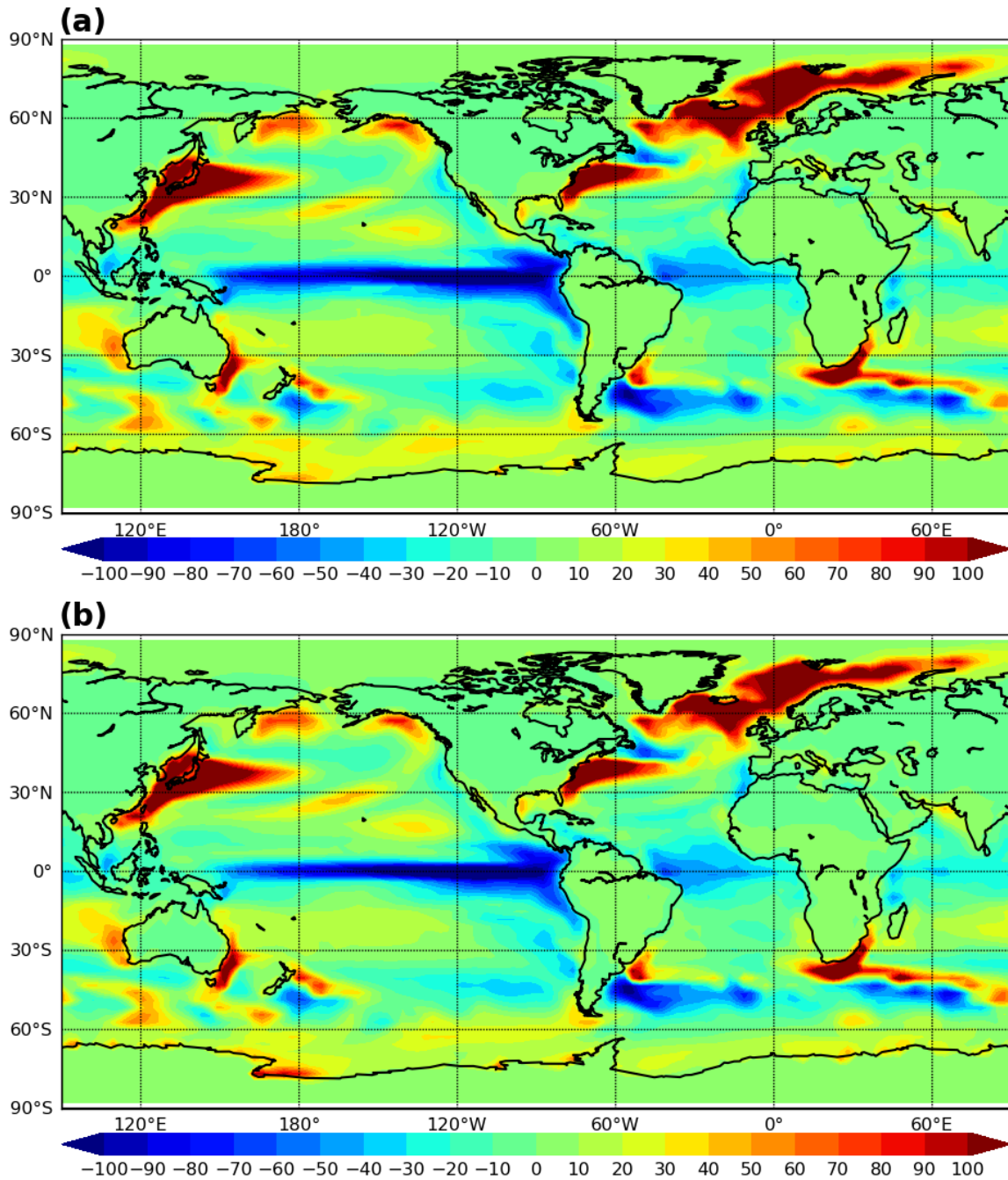
Figure 3.3: The same as Fig. 3.1 except showing the surface heat flux (positive upward). The unit is W/m2.
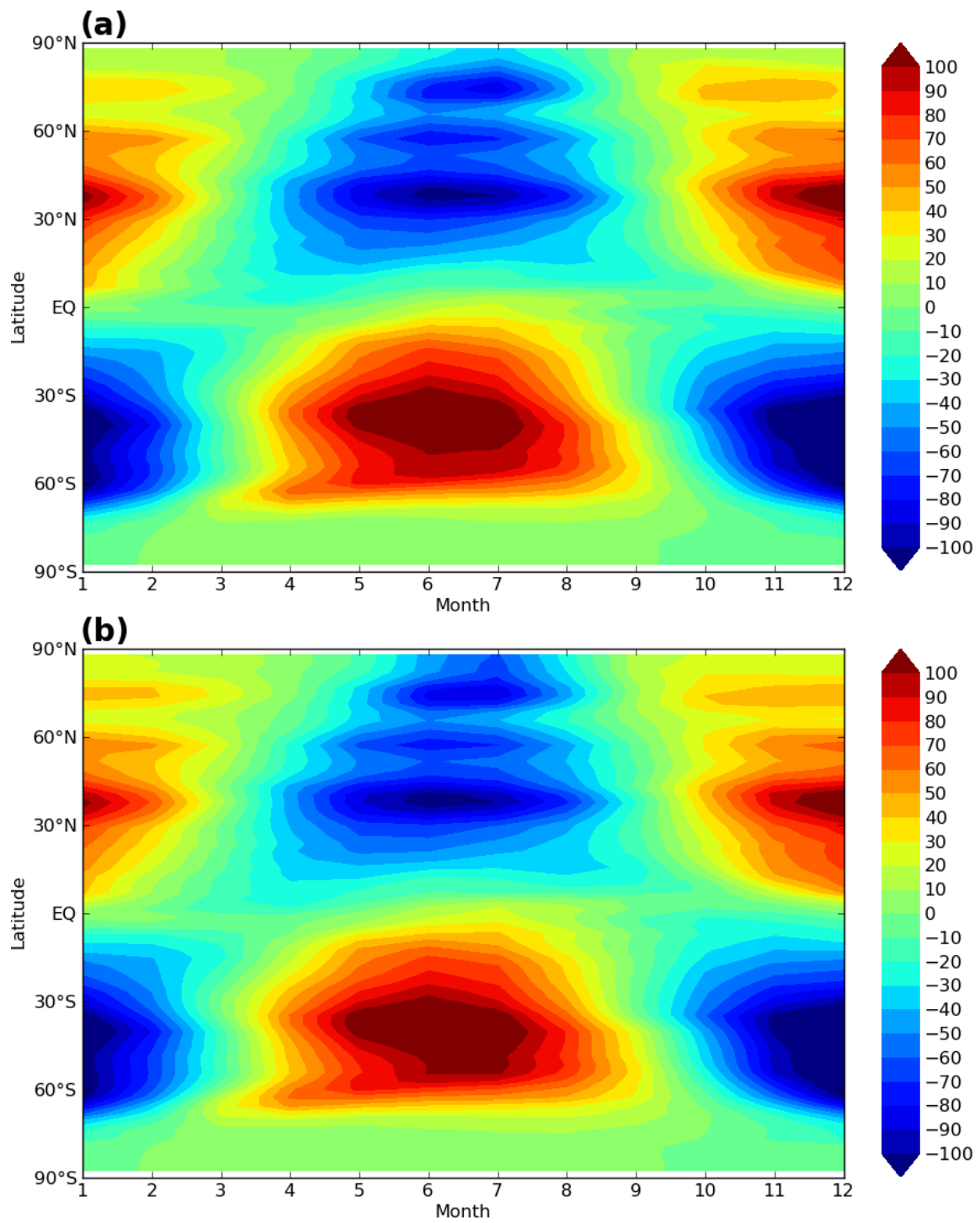
Figure 3.4: The same as Fig. 3.2 except showing the surface heat flux (positive upward). The unit is W/m2.

Fig. 3.5 shows a comparison of annual mean precipitation between CCSM3-CLIM and CAM3-CLIM. The global RMS of the difference is 4mm/day, which is about 10% of the global mean standard deviation of the simulated precipitation variability, indicating precipitation field is well reproduced. Both simulations present a double ITCZ in the tropical Pacific, which is a common issue of CCSM3 (Zhang and Wang, 2006). The precipitation associated with ITCZ and the Northern mid-latitude storm track are captured in both simulations. Further analysis shows that the annual cycle of the precipitation is also well reproduced (not shown).
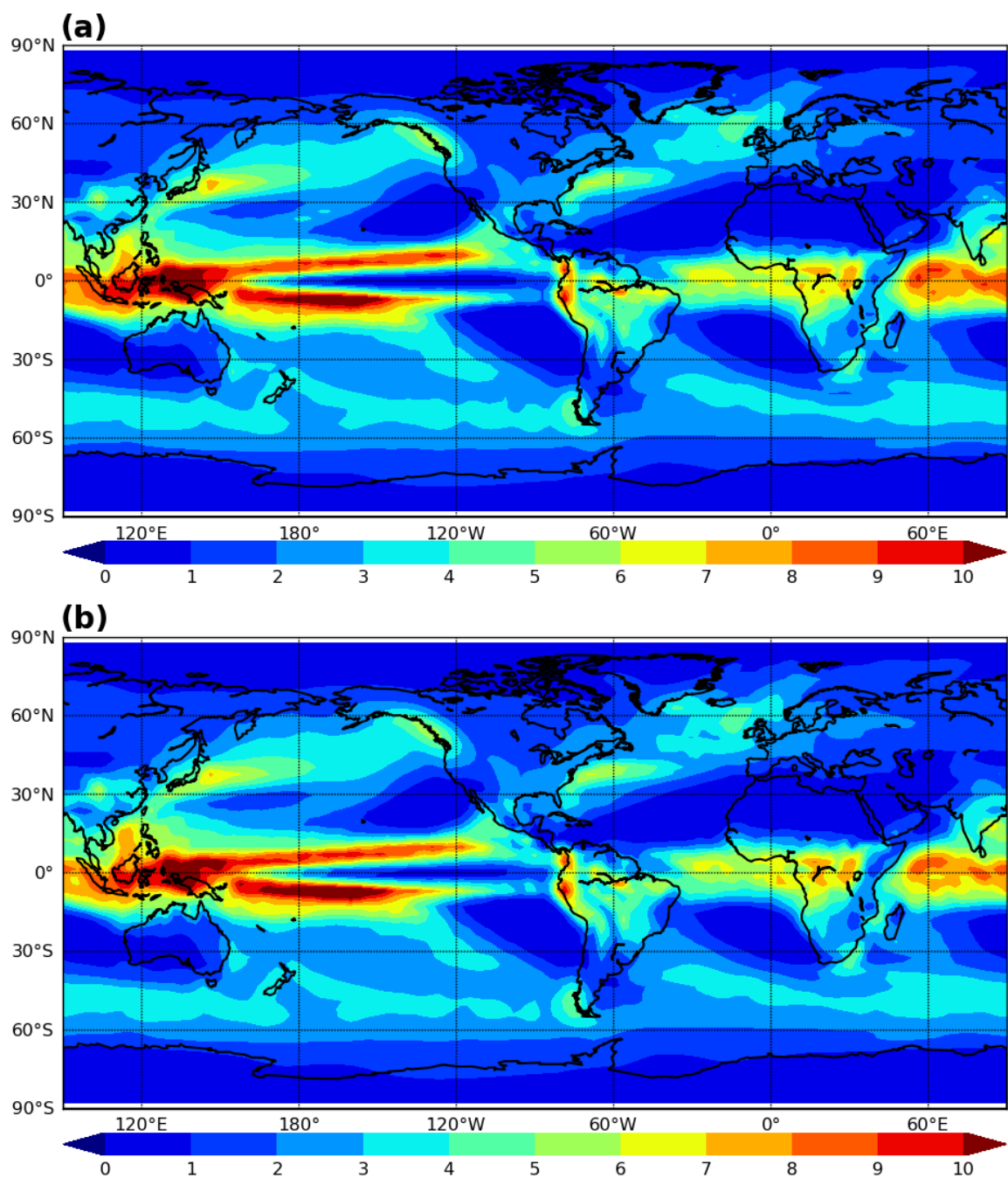
Figure 3.5: The same as Fig. 3.1 except showing the precipitation. The unit is mm/day

Fig. 3.6 shows a comparison of the zonally integrated heat fluxes at the surface

and at top of atmosphere (TOA) as functions of latitude between CAM3-CLIM and CCSM3-CLIM. The maximum difference between the two simulations occurs near 10°N and 10°S and 60°S, which is within 10% of the standard deviation of zonally integrated heat flux values at these latitudes. The TOA heat flux is downward (into the atmosphere) in tropics and upward (into outer space) in mid- and high- latitudes, indicating more incoming solar radiation than outgoing infrared radiation in tropics (35°S-35°N) and less in mid- and high- latitudes. The surface heat is particularly largely downward into the ocean over equatorial, indicating that the solar radiation the tropical ocean receives is more than the heat it releases. The difference between TOA and surface heat flux represents net heat flux into the atmosphere. This net heat flux into the atmosphere is positive in tropics and negative equatorward, which must be balanced by meridional atmospheric heat transport. Fig. 3.7 shows the implied northward oceanic and atmospheric heat transports in CCSM3-CLIM and CAM3-CLIM, which are computed by integrating the vertical heat fluxes into the ocean and atmosphere from the South Pole northward, respectively. The RMS differences between these two implied heat transports in the two models are again small compared to their respective standard deviation values at any given latitudes. The net heat flux into the tropical ocean and atmosphere (Fig 3.6 are transported to higher latitudes: both atmosphere and ocean transport the extra heat they receive in low-latitudes to high-latitudes where they release them. The atmospheric meridional heat transports can be carried by Hadley circulation in tropics, storm activities in mid-latitudes, etc, while the oceanic by AMOC and wind-driven circulation, etc. Changes in these physical processes can largely modify local climates. Therefore, investigation into these meridional heat transports can be very useful for understanding the high-to-low latitude teleconnection. These results further confirm that CAM3-SOM reproduces not only the mean climate state of CCSM3, but also

its mean energy transport.
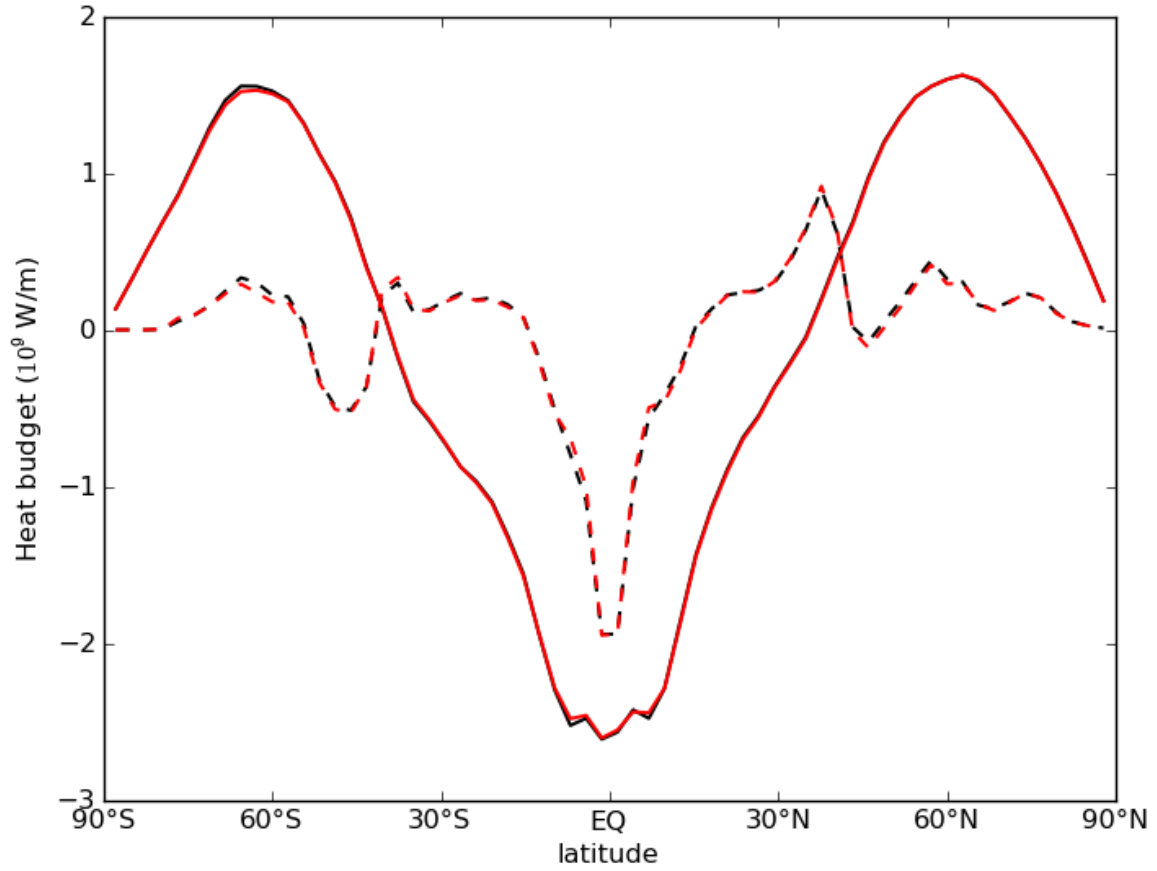
Figure 3.6: The annual mean zonally integrated heat fluxes at the TOA (solid lines) and the surface (dashed lines) of CAM3-CLIM (black lines) and CCSM3-CLIM (red lines). Positive values indicate upward fluxes. The unit is 10^9W/m.
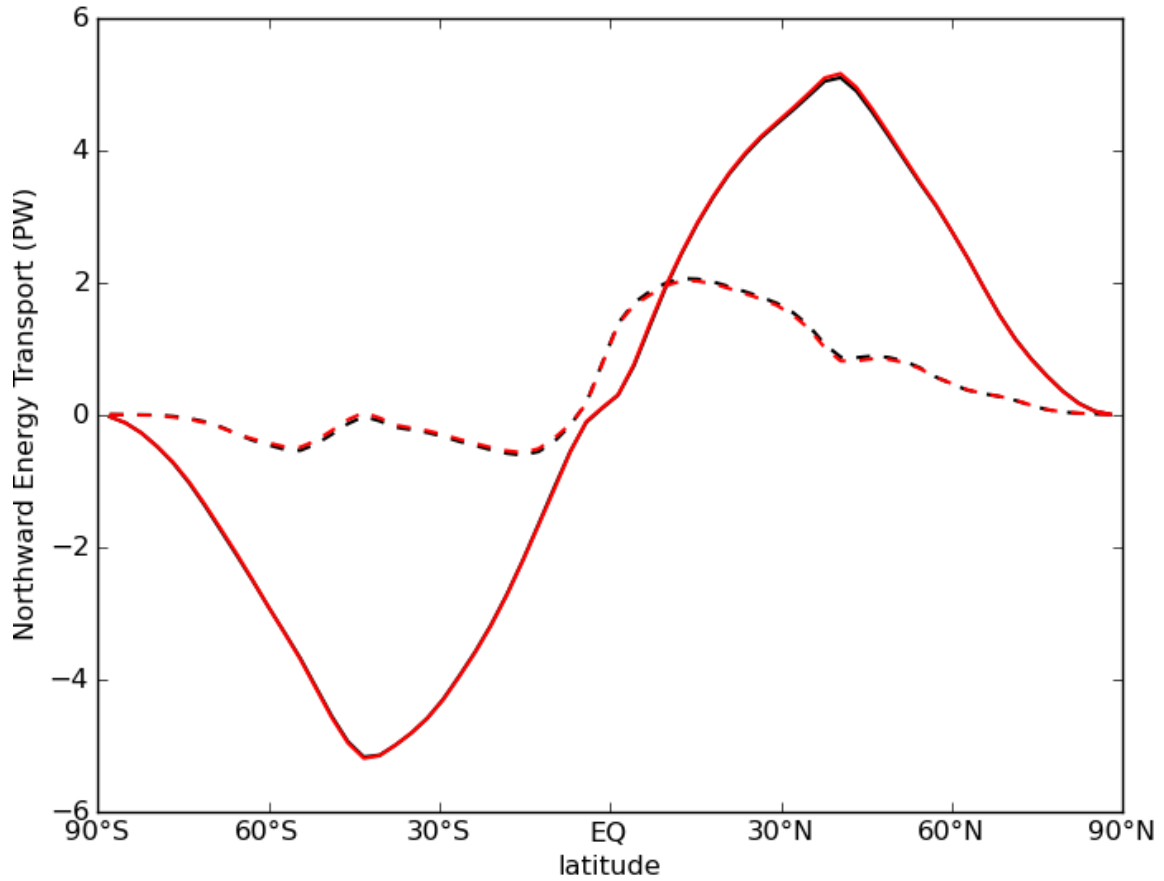
Figure 3.7: The annual mean Atmospheric (solid lines) and Oceanic (dashed lines) northward heat transports of CAM3-CLIM (red lines) and CCSM3-CLIM (black lines). The unit is 10^{15}W (PW)

In summary, we show in this section that the use of the climatological Q-flux computed using the SST-restoring technique in CAM3-SOM can effectively replicate the mean climate state and energy transport in CCSM3 simulation. In the following subsection, we will further demonstrate that the similar approach is also effective in reproducing CCSM3 hosing simulations.

3.5.2 Comparison between CCSM3 and CAM3-SOM Hosing Simulations

In this section we will compare CCSM3 and CAM3-SOM hosing simulations with a focus on the first 20 years of the simulations when high-to-low latitude teleconnection processes operate.

Fig. 3.8 shows anomalous surface temperatures in CAM3-SOM hosing simulation (CAM3-HOSE minus CAM3-CTRL) and in CCSM3 hosing simulation (CCAM3-HOSE minus CCSM3-CTRL). The anomalous surface temperatures averaged over the second decade of the simulations are shown in the left panel, while hovmoller diagrams of zonally averaged surface temperature anomalies over all the ocean points are shown in the right panel. Clearly, salient features of surface temperature anomalies in response to freshwater forcing in the subpolar North Atlantic in the CCSM3 hosing simulation are well reproduced by CAM3-SOM hosing simulation. These features include a propagation of surface cooling from the northern high-latitude equatorward, which takes around 10 years to reach the Equator, a broad cooling over the Northern Hemisphere, an extended cooling along North Atlantic subtropical gyre, and a warming over small areas of the Kuroshio and Gulf Stream extension regions. The global RMS of difference of the mean anomalous surface temperature between the two models (as shown in Fig. 3.8a, c) is about 0.2K, or 15% of the RMS of the anomalous surface temperature itself. The equatorward propagation speed of the surface temperature anomalies is also well reproduced by CAM3-SOM. In both model simulations, the surface cooling spreads at a rate of $7°$/year, reaching the equatorial zone after 8 years into the integration.

Fig. 3.9 shows zonally integrated anomalous heat fluxes averaged over the second decade at the surface and the TOA as functions of latitude. The global RMS differences of the TOA and surface anomalous heat fluxes between the two models are

both 0.01×10^9W/m. The TOA heat flux anomaly is smaller compared to the surface anomaly in most latitudes except near Equator, which broadly meets the requirement of the Bjerknes compensation (Bjerknes, 1964). The Bjerknes compensation states that changes in meridional atmospheric and oceanic heat transports should be equal and opposite if TOA surface heat flux does not change much. The surface heat flux anomaly is broadly downward in northern mid- and high- latitudes and upward in northern tropics, indicating a northward anomalous oceanic heat transport, which cools northern mid- and high- latitudes and warms the tropics. These can be more clearly seen in Fig. 3.10, which shows the anomalous implied northward oceanic and atmospheric heat transports averaged over the second decade in CCSM3 and CAM3-SOM hosing simulations. The global RMS differences of the heat transports between the two models are about 0.01 and 0.01 PW, or 15% and 6% of the respective RMS of the anomalies themselves. The compensation between the anomalous atmospheric and oceanic heat transports in CCSM3 hosing simulation is well reproduced by CAM3-SOM hosing simulation: the ocean transports less heat northward while the atmosphere transports comparable more heat northward in most latitudes. The anomalous oceanic heat transport peaks at around 30°N, with a maximum value of about 0.3 PW, indicating the oceanic processes cools northern mid- and high- latitudes and warms of tropics and the Southern Hemisphere, which is consistent with Fig. 3.9.
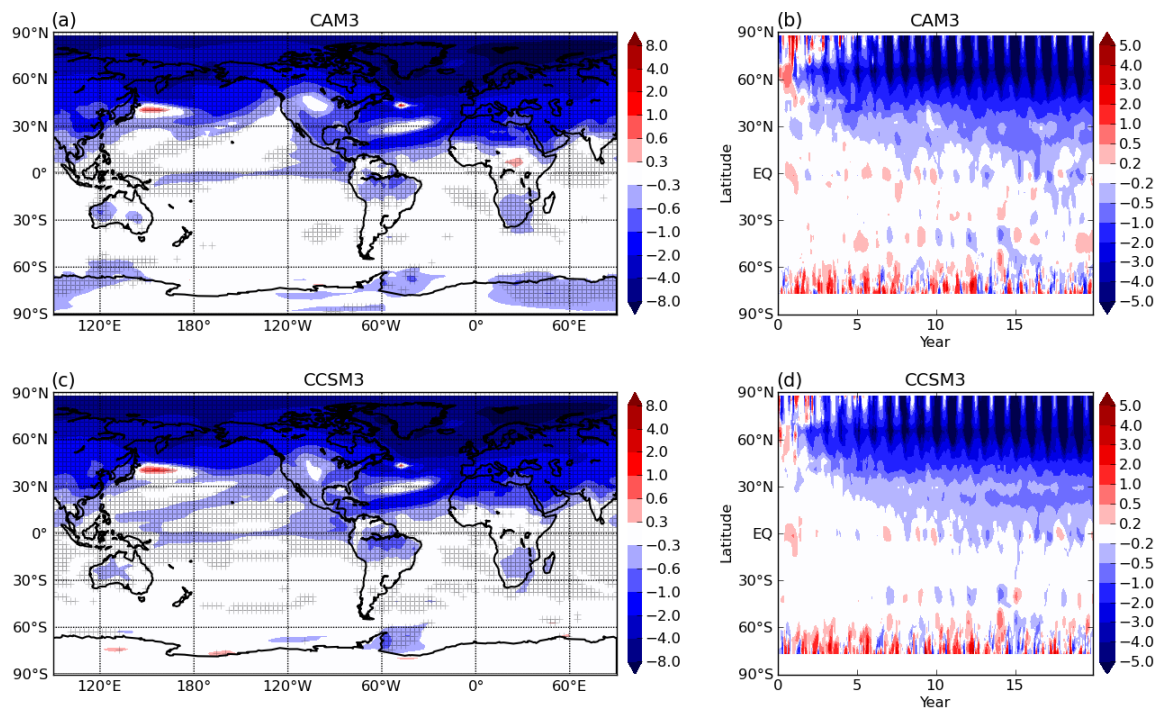
Figure 3.8: Left panel: the surface temperature anomaly averaged over 11-20 years after freshwater forcing onset. Right panel: he hovmoller diagrams of zonal average surface temperature anomaly over ocean points. (a) and (b) are from the CAM3-SOM hosing simulation (CAM3-HOSE minus CAM3-CTRL), and (c) and (d) are from the CCSM3 hosing simulation (CCSM3-HOSE minus CCSM3-CTRL).
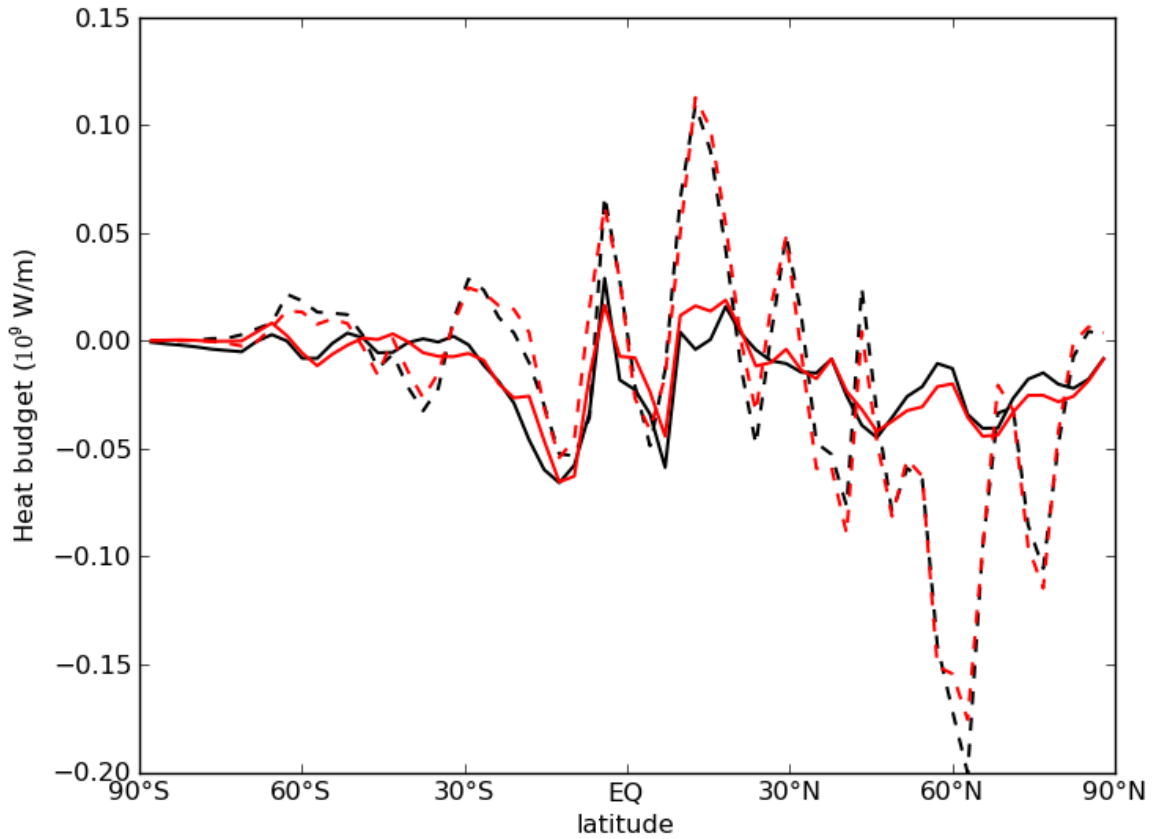
Figure 3.9: The zonally integrated anomalous heat fluxes at the TOA (solid lines) and the surface (dotted lines) of CAM3-SOM hosing simulation (CAM3-HOSE minus CAM3-CTRL, black lines) and CCSM3 hosing simulation (CCSM3-HOSE minus CCSM3-CTRL, red lines) averaged over the second decade of simulations. Positive values indicate upward fluxes. The unit is 10^9W/m.
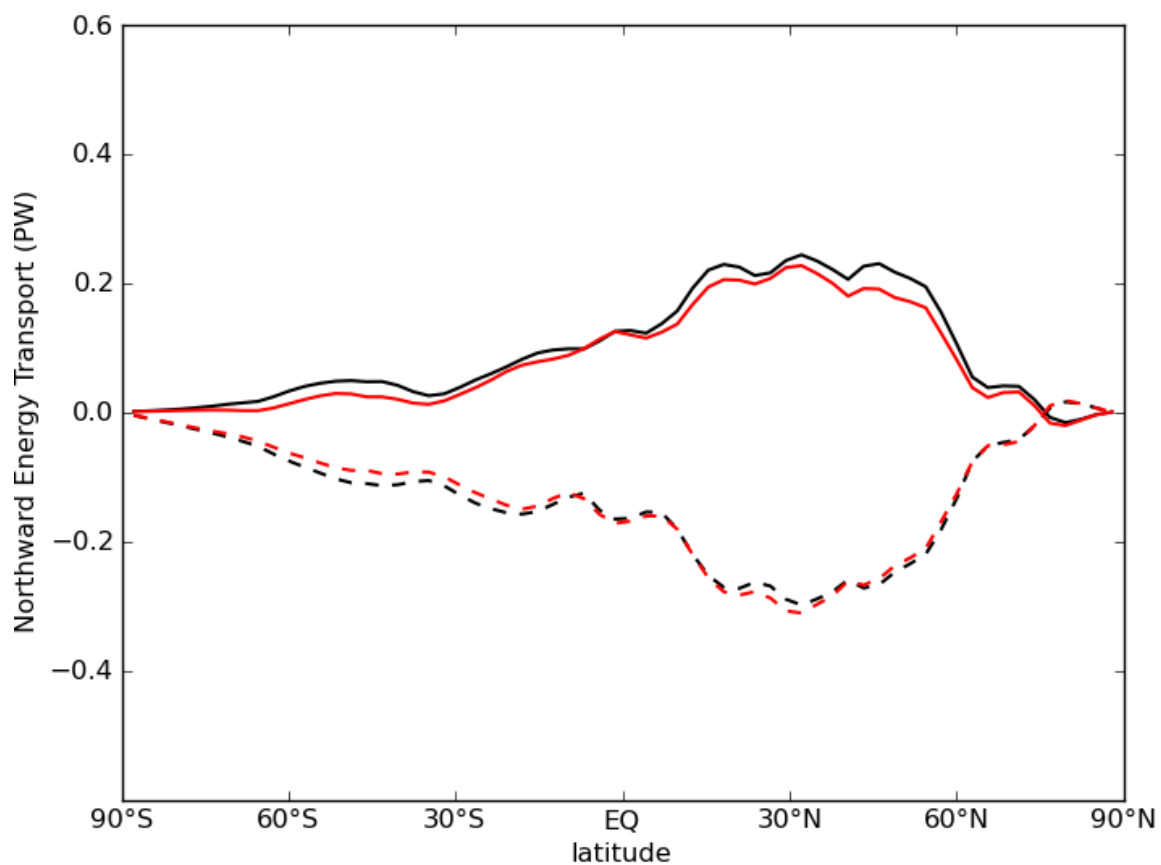
Figure 3.10: The anomalous Atmospheric (solid lines) and Oceanic (dashed lines) northward heat transports of CAM3-SOM hosing simulation (CAM3-HOSE minus CAM3-CTRL, red lines) and CCSM3 hosing simulation (CCSM3-HOSE minus CCSM3-CTRL, black lines) averaged over the second decade of simulations. The unit is 10^{15}W (PW)

In both CAM3-SOM and CCSM3 hosing simulations, we see a high-to-low latitude propagation of the surface cooling (Fig 3.8) and a southward shift of the Atlantic and Indian ITCZ (Fig. 3.11 a, b). This is the high-to-low latitude teleconnection in global climate response to the freshwater forcing in the high-latitude North Atlantic that we intend to focus in this investigation. Therefore, it is important that the modeling tools we used can simulate this feature well. In the following section, we will use CAM3-HOSE as a reference to separate out the atmospheric contribution to the teleconnection from the oceanic contribution.
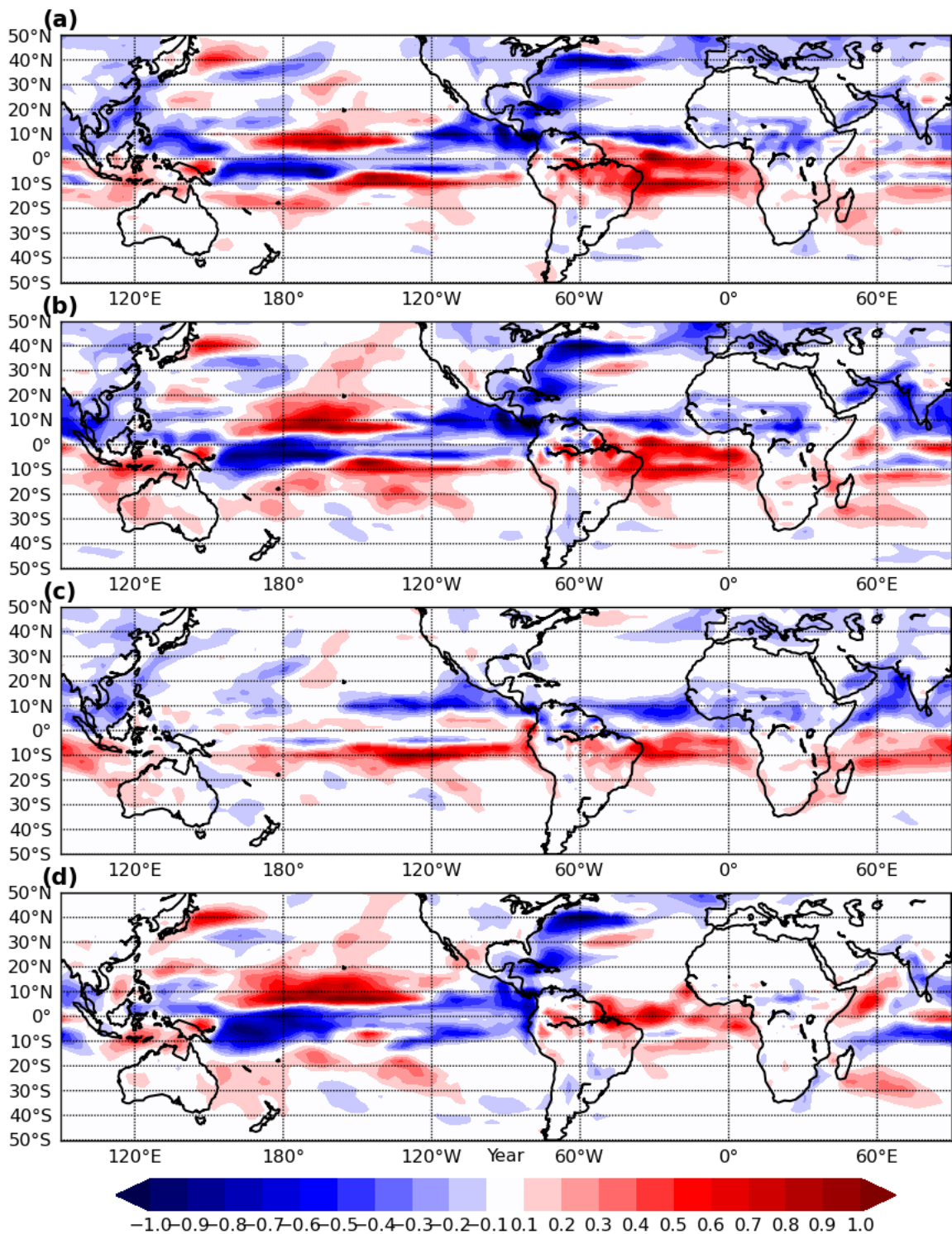
Figure 3.11: The precipitation anomaly in (a) CCSM3-HOSE (minus CCSM3-CTRL), (b) CAM3-HOSE (minus CAM3-CTRL), (c) CAM3-HOSE-ATMO (minus CAM3-CTRL), and the difference between CAM3-HOSE and CAM3-HOSE-ATMO (d) averaged over the 2nd decade. The unit is mm/day.

47

3.6 Assessment of atmospheric and oceanic contributions

As explained in the previous section, to eliminate the oceanic contribution in CAM3-SOM hosing simulation, we retained the hosing Q-flux only in the freshwater forcing region in the subpolar North Atlantic (50°N-70°N) and set its value to the control Q-flux outside this region. By doing so, the anomalous oceanic heat flux, which represents deep convection driven ocean circulation changes in the subpolar gyre of the North Atlantic, is only kept in the high-latitude North Atlantic, so that the SST change in the forcing region can be retained. Fig. 3.12 shows the anomalous Q-fluxes applied to CAM3-HOSE and CAM3-HOSE-ATMO, respectively. Evidently, only the anomalous Q-flux in the hosing region remains in the CAM3-HOSE-ATMO. Fig. 3.12c shows the annual mean anomalous Q-flux averaged over the forcing area. Clearly, the adjustment time of the oceanic heat flux is about 10 years, which is consistent with the adjustment time of global climate in CCSM3 hosing simulations.
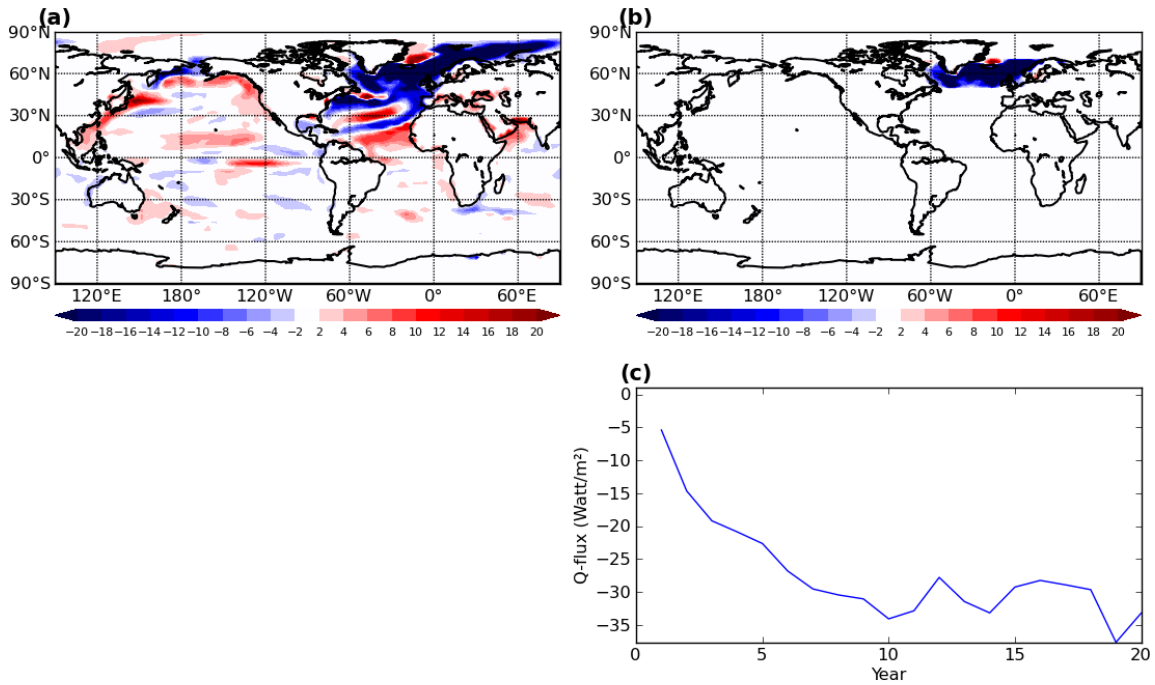
Figure 3.12: The anomalous Q-flux (Q-flux minus CTRL-Q-flux) applied to (a) the CAM3-HOSE and to (b) the CAM3-HOSE-ATMO averaged over 20 years of simulations. (c) is the inter-annual variation of the anomalous Q-flux averaged over the freshwater forcing region (50°N-70°N Atlantic). These Q-fluxes are in opposite sign to original, representing oceanic heat flux convergence.

Fig. 3.13 shows the anomalous surface temperature in CCSM3-HOSE (a, e), CAM3-HOSE (b, f) and CAM3-HOSE-ATMO (c, g), and the difference between the later two (CAM3-HOSE minus CAM3-HOSE-ATMO) (d, h), which represents the oceanic contribution to the teleconnection. A visual inspection indicates that the magnitudes of anomalous surface temperatures shown in Fig. 3.13c and d are comparable, suggesting that the atmospheric and oceanic contributions to the teleconnection are equally important. In fact, over the tropics between 30°S and 30°N the area-averaged surface temperature amplitudes shown in the two figures are nearly equal. However, the spatial distributions of the atmospheric and oceanic controlled

surface temperature anomalies are quite different. In CAM3-HOSE-ATMO, surface cooling occurs nearly over the entire Northern Hemisphere with moderate warming over the southeast tropical Pacific and Atlantic. Overall, the anomalous surface temperature in this case has a more or less zonally symmetric appeal. This is consistent with our understanding of the atmospheric controlled teleconnection, as shown by Chiang and Bitz (2005) and Kang et al. (2008). The mechanism of such atmospheric controlled teleconnection will be further discussed in subsection 3.6.1.

In contrast, the oceanic controlled teleconnection, obtained by subtracting CAM3-HOSE-ATMO from CAM3-HOSE, shows a more complex surface temperature anomaly pattern. Distinctive surface temperature anomalies are observed along some major ocean circulation system. For example, cold SST anomalies form along the North Atlantic subtropical gyre and a strong positive SST anomaly appears along the Kuroshio extension region. There is also a surface warming emanating from the northeastern Pacific towards the central equatorial Pacific. In the tropics, a broad cooling is observed in the eastern tropical Pacific, while a warming pattern occurs in the Arabian basin of the northern Indian Ocean. In the Southern Ocean, broad warming patterns appear throughout nearly all longitudes polewards of 40°S. Some of these SST anomalies are of opposite sign to those associated with the atmospheric controlled teleconnection, and thus tend to cancel out their influence, whereas others are of the same sign and tend to reinforce the anomalies induced by atmospheric processes. The complex spatial pattern of these oceanic process induced SST anomalies adds considerable zonal asymmetry to the surface temperature response to the freshwater forcing, which in turn can produce significant regional climate change patterns.

The mechanism governing this oceanic controlled teleconnection is more complex than its atmospheric counterpart. Because oceanic dynamics is not present in CAM3-HOSE-ATMO, all SST anomalies associated with oceanic dynamics are

included in the oceanic controlled teleconnection. These include the SST change produced by the AMOC weakening in response to the North Atlantic freshwater forcing. Also included are oceanic processes that are affected by the atmosphere, such as a change in local wind stresses, which can produce an ocean circulation change, resulting in SST anomalies that in turn can affect wind stresses. Additionally, a local oceanic controlled SST anomaly can affect SSTs in remote regions through atmospheric controlled teleconnection. Such response is also included in our defined oceanic controlled teleconnection.
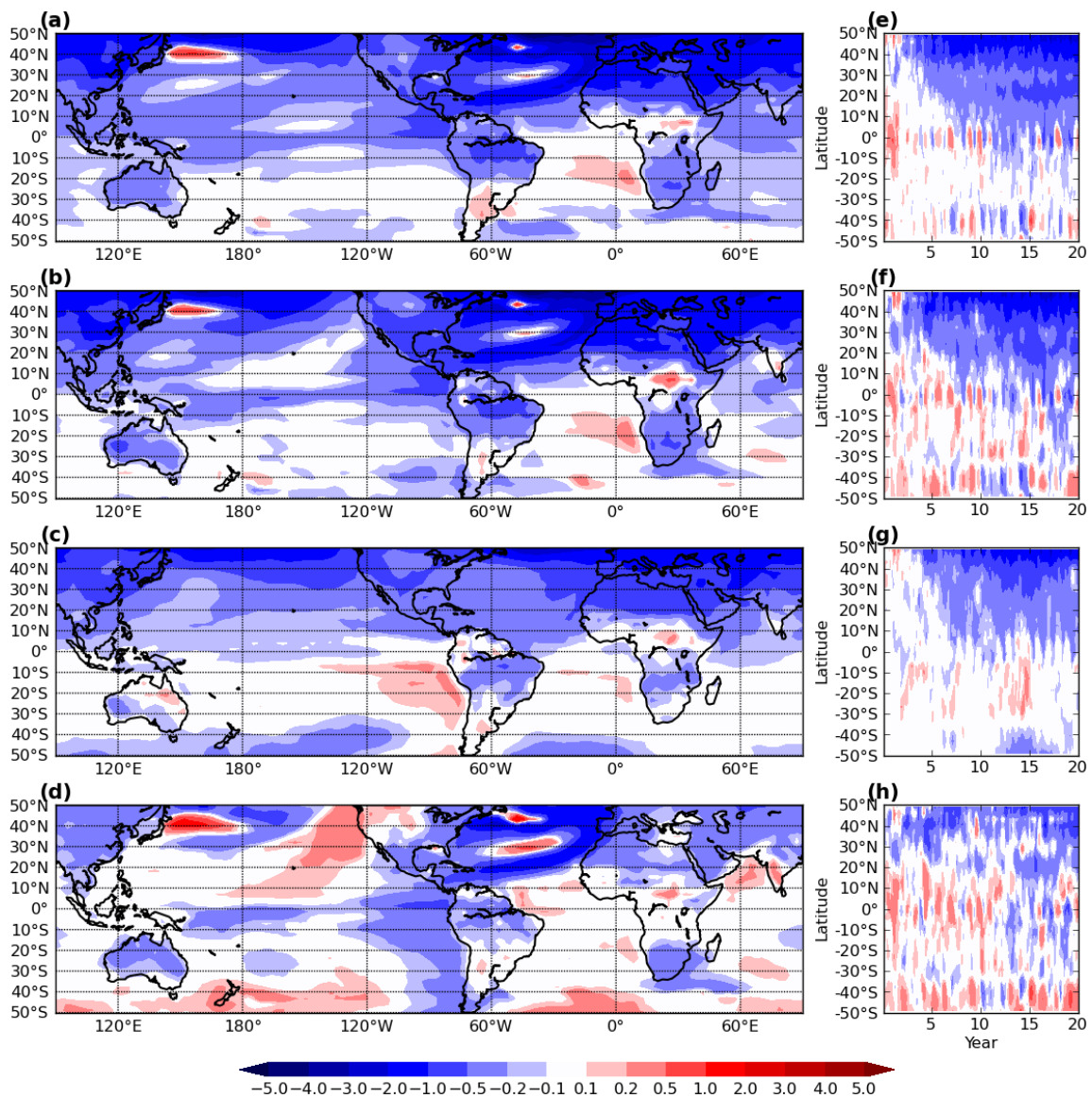
Figure 3.13: (he 11-20 year averaged surface temperature anomaly in (a) CCSM3-HOSE, (b) CAM3-HOSE, (c) CAM3-HOSE-ATMO, and the difference between CAM3-HOSE and CAM3-HOSE-ATMO (d). (e, f, g, h) are hovmoller diagrams of zonal average surface temperature anomalies over ocean points. The unit is K.

Insight into atmospheric versus oceanic contributions to the teleconnection can be gained by performing an energetic analysis on CAM3-HOSE and CAM3-HOSE-ATMO. Fig. 3.14 shows heat balances in different latitude bands based on 11-20 year

averages of CCSM3 and CAM3-SOM simulations. Five latitudinal bands are shown, including 1) the hosing region (50°N -70°N), 2) the Arctic region (70°N-90°N), 3) the northern hemisphere mid-latitude region (30°N-50°N), 4) the northern tropical region (Eq-30°N) and 5) finally the southern tropical region (30°S-Eq). The vectors represent the cumulative heat transport anomalies from hosing onsets, averaged over 11-20 years. In the hosing region, there is an increase in oceanic heat flux divergence, giving rise to a positive Q-flux, which cools the ocean and in turn causes a reduction of surface heat fluxes into the atmosphere. To compensate for this less heat input from the ocean, there is a considerable increase of atmospheric heat transport from the mid-latitude to the hosing region and a smaller increase of downward heat flux at TOA. Therefore, in response to the surface cooling in the hosing region the atmosphere draws heat primarily from the adjacent mid-latitude to compensate for the reduced heat input from the ocean. This is shown clearly in both CAM3-HOSE and CAM3-HOSE-ATMO. Physically, it implies that there is an increase in poleward atmospheric heat transport from the mid-latitudes, suggesting an enhanced eddy heat transport. Outside the hosing region, the heat balance in the CAM3-HOSE and CAM3-HOSE-ATMO displays some major differences. In CAM3-HOSE-ATMO (Fig. 3.14c), to compensate for the extra atmosphere heat transport from the mid-latitude to the hosing region, there is a considerable increase of atmospheric heat transport from the tropics to the mid-latitude and smaller increases of downward heat flux at TOA and upward heat flux at surface, which works to cool the mid-latitude ocean. However, in CAM3-HOSE (Fig. 3.14b), because there is an increase in oceanic heat flux divergence in northern mid-latitudes, giving rise to a positive Q-flux, the ocean draws heat from the atmosphere. Therefore, to compensate for this heat loss into the ocean, there is significantly more atmospheric heat transport from the tropics to the mid-latitude in CAM3-HOSE than in CAM3-HOSE-ATMO. This

53

increased atmospheric heat transport from the tropics to the mid-latitudes implies a stronger trade wind, which can enhance the Hadley circulation and can result from the increase in north-south SST gradient.

Moreover, in CAM3-HOSE-ATMO (Fig. 3.14c), to compensate for the extra atmospheric heat transport from the tropics to the mid-latitude, there is again a considerable increase of atmospheric heat transport northward across Equator and small increases of downward heat flux at TOA and upward heat flux at surface, which cools the northern tropical ocean. However, in CAM3-HOSE (Fig. 3.14b), because there is an decrease in oceanic heat flux divergence, giving rise to a negative Q-flux, the ocean releases more heat to the atmosphere to compensate for the significantly more atmospheric heat transport from the tropics to the mid-latitude, which allows a small increase of upward heat flux at TOA. Therefore, the increase of atmospheric heat transport from the southern tropics to the northern tropics is comparable between CAM3-HOSE and CAM3-HOSE-ATMO, which implies a southward shift of the Hadley circulation center, suggesting a southward shift of ITCZ in both simulations. Finally, in both simulations, there are considerable increase of downward heat flux at TOA in southern tropics to compensate for the extra atmospheric heat transport from the southern tropics to the northern tropics. This may be caused by a southward shift of the ITCZ, which blocks the upward infrared radiation in southern tropics. Although Chiang and Bitz (2005) argued that this increased downward TOA heat flux results from increase in water vapor through its greenhouse effect, our analysis does not show such increase in water vapor.

From these analysis we can conclude that the oceanic contribution primarily affects the northern tropics and mid-latitude. The effect of the Q-flux anomalies is basically to cool the mid-latitude and warm the northern tropics, which is broadly consistent with the anomalous oceanic heat transport shown in Fig. 3.10 and the SST responses in different simulations shown in Fig. 3.13d. However, as discussed previously, we cannot distinguish the sources of these Q-flux anomalies. They can be caused by either AMOC change in response to the high-latitude freshwater forcing or change in air-sea interaction.
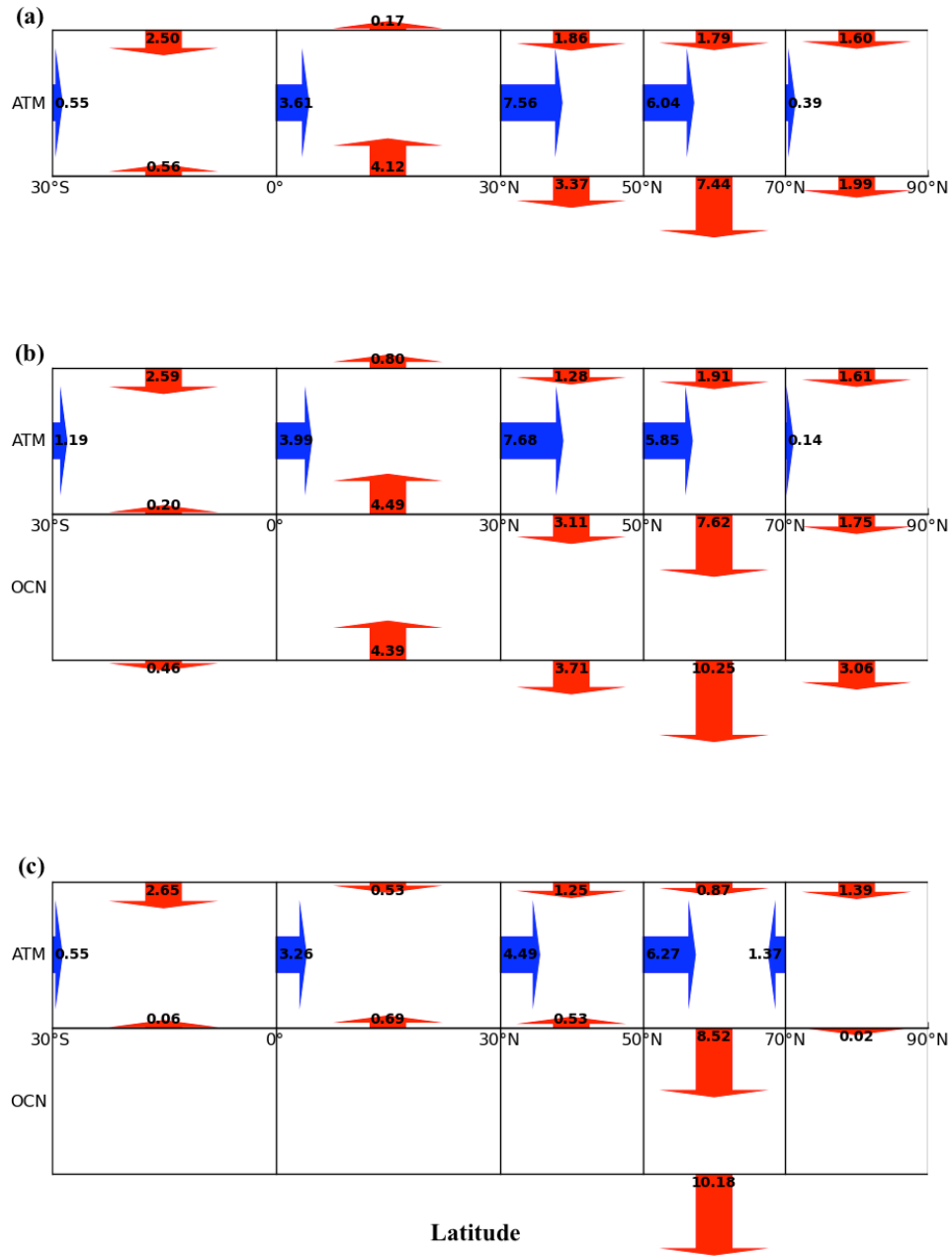
Figure 3.14: The cumulative heat transport anomalies from hosing onset, averaged over 11-20 years of (a) CCSM3-HOSE, (b) CAM3-HOSE and (c) CAM3-HOSE-ATMO. ATM and OCN represent the atmosphere and ocean mixed layer, respectively. Red (blue) arrows denote vertical (horizontal) heat transport anomalies across each box interface except the vertical arrows at the OCN bottom, which represent oceanic heat flux divergence anomaly, in other words the Q-flux (positive downward). The value of each arrow is placed around it, with a unit 10^{22}J.

The simulated precipitation response to freshwater forcing is shown in Fig. 3.11. Similar to the surface temperature, the atmospheric controlled teleconnection generates a dipole-like precipitation anomaly in all three tropical oceans, reconfirming the nearly zonally symmetric response. Kang et al. (2008) suggested a close correlation between the mean ITCZ position and the northward cross-equatorial heat flux: the more the northward cross-equatorial heat flux, the more southward the ITCZ shifts. Our results is consistent with their hypothesis (Fig. 3.14, Fig. 3.11). The extra northward cross-equatorial heat flux also implies a southward shift of the Haley circulation center (not shown). However, the cause-effect relationship between the Hadley circulation, the cross-equatorial heat flux and the ITCZ shift is not clear, because change in any of them can lead to change of the other two. In Chapter 4, we will analyze the mechanism of ITCZ shift, which shows that the tropical SST anomaly is primarily responsible for the ITCZ shift through affecting local pressure gradient. In contrast, the oceanic controlled precipitation responses are more complex, displaying considerable zonal asymmetries. In the eastern tropical Pacific, a precipitation deficit is observed along with a precipitation increase over much of the equatorial Atlantic. This pattern of precipitation change is consistent with a regional Walker circulation change over the eastern tropical Pacific and tropical Atlantic. Over the mid-latitudes, particularly along the Gulf Stream and Kuroshio extensions, the precipitation changes are almost entirely attributable to the oceanic controlled teleconnection. These mid-latitude precipitation anomalies are consistent with local SST anomalies.

Focusing on the Atlantic basin, the atmospheric controlled cooling signal propagates equatorward and reaches Equator in around 7-8 years, while the oceanic controlled propagation takes around 5 years to reach around 17°N without further propagation. One most distinctive SST difference between the atmospheric and

oceanic controlled climate response is the strong SST anomaly around the north Atlantic subtropical gyre that forms through oceanic controlled teleconnection, but absent in the atmospheric controlled climate response. These SST differences include a cold tongue in the northern subtropical and tropical Atlantic and a cold anomaly along the Gulf Stream, as well as weak warm anomalies in the center of the gyre and to the north of the Gulf Stream. These SST differences are likely attributed to the land surface temperature differences over the eastern US and northern Africa, and the precipitation difference over the Caribbean and along the Gulf Stream extension (Fig. 3.11). They also likely contribute to the difference in heat balance over the mid-latitude and tropics shown in Fig. 3.14. We further investigate these SST features in the subsequent section.

3.6.1 Atmospheric controlled teleconnection

As discussed above, neither the atmospheric nor the oceanic contribution to the high-to-low latitude teleconnection during a simulated YD-like abrupt climate change is negligible. However, the atmosphere spreads the surface cooling signal equatorward originating in high-latitude North Atlantic in a more zonally symmetric manner than the ocean does. This is understandable considering the fast atmospheric wave adjustment and that the atmosphere has no zonal bound. The mechanism of transient processes of the atmospheric controlled teleconnection proposed by Chiang and Bitz (2005) is demonstrated below: 1) the cooling originating in high-latitude North Atlantic Ocean surface leads to the cooling of the overlying atmosphere; 2) such a cooling then spreads meridionally rapidly into the mid-latitude atmosphere, as well as zonally into the high-latitude atmosphere, leading to cooling in the mid- and high-latitude ocean; 3) the increase in the north-south SST gradient leads to stronger trade wind, which subsequently cools the northern tropical ocean; 4) and finally, due to the

wind-evaporation-SST (WES) feedback (Xie, 1999), the anomalous cross-equatorial SST gradient is intensified, leading to a southward displacement of the ITCZ. The heat balance analysis (Fig. 3.14c) appears to be consistent with this hypothesis.

Below, this hypothesis is tested using the CAM3-SOM simulations. Fig. 3.15 shows the zonally averaged surface heat flux anomalies cumulated since freshwater forcing onset in CAM3-HOSE-ATMO (CAM3-HOSE-ATMO minus CAM3-CTRL), which reflects atmospheric controlled surface heat flux change. The figure clearly shows that the sensible heat flux anomaly (Fig. 3.15b) dominates the surface cooling in the northern mid-latitudes and subtropics, and the latent heat flux anomaly dominates the cooling in the deep northern tropics (0-10°N). The clear sky radiative flux anomaly (Fig. 3.15c) plays a secondary role in the northern hemispheric cooling between 0-45°N. The upward clear sky radiative flux anomaly (primarily longwave radiative heat flux anomaly) observed in northern tropics and mid-latitudes indicates that the cooling of lower-troposphere leads the cooling of ocean surface, suggesting that the mid-latitude lower-troposphere cools the ocean (primarily by sensible heat flux and secondarily by radiation) after feeling the cooling signal from higher latitudes. Further analysis shows that the northern mid-latitude upward surface sensible heat flux anomaly primarily results from local cooling of surface air rather than surface wind speed change. Such surface air cooling results from the strengthened mid-latitude eddy activity. In contrast, the northern equatorial upward surface latent heat flux anomaly primarily results from trade wind strengthening as a result of increase in the north-south surface temperature gradient.
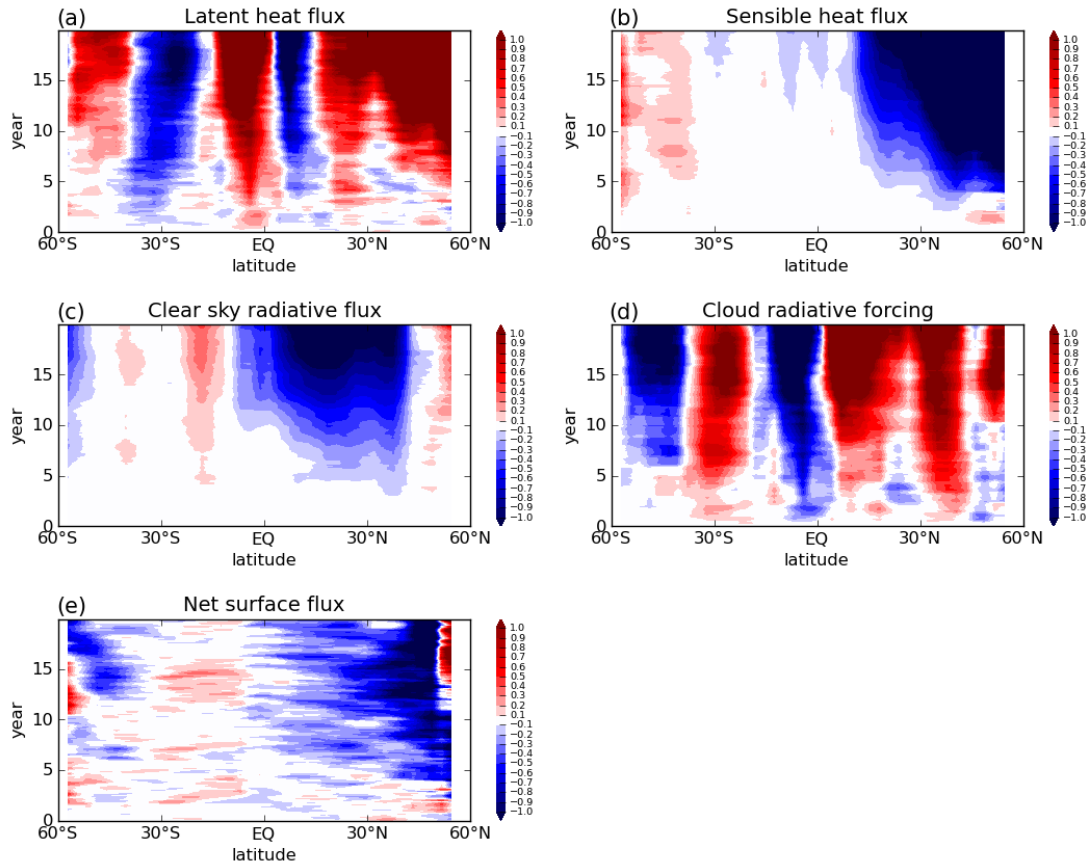
Figure 3.15: The zonal averaged (e) surface heat flux anomaly and its four terms, (a) latent heat flux anomaly, (b) sensible heat flux anomaly, (c) surface net radiative flux anomaly, and (d) radiative cloud forcing anomaly cumulated since freshwater forcing onset as functions of latitude and time in CAM3-HOSE-ATMO (Positive for downward). These heat flux anomaly cumulations are divided by the water heat capacity, $4.2{\times}10^3$J/kg/K, the water density, $1.0{\times}10^3$kg/m3 and a depth of 50m of water. Thus the unit is K.

3.6.2   Oceanic controlled teleconnection

Fig. 3.13 and Fig. 3.11 show that the oceanic contribution to the high-to-low latitude teleconnection during a YD-like abrupt climate change is as important as the atmospheric contribution but results in distinctive climate responses. The oceanic contribution dominates cooling around the North Atlantic subtropical gyre and over

60

the eastern tropical Pacific, as well as warming along the Kuroshio and Gulf Stream extension regions. In this sub-section the mechanism of such oceanic controlled teleconnection is analyzed.

In a fully dynamical ocean, oceanic temperature of surface layer (annual average mixed layer) is governed by the following equation:

$$\frac{\partial \overline{T}}{\partial t} = -\overline{\nabla \cdot \left(\vec{V} T\right)} + \overline{A_H \nabla_H^2 T} + \kappa \frac{\partial T}{\partial z}\bigg|_{z=-h_m} - \frac{1}{\rho_w c_{pw} h_m} Q_{ice} - \frac{1}{\rho_w c_{pw} h_m} F \quad (3.6)$$

where T is sea surface temperature, V velocity, F net surface heat flux (positive for upward), A_H the horizontal diffusion coefficient, κ the vertical diffusion coefficient, h_m the annual average mixed layer depth, Q_{ice} the heat fluxes due to ice formation. Overbar means vertical average over the mixed layer (surface to h_m deep). ρ_w is the water density, taken as a constant, 1000kg/m3 in this study. This equation shows that sea surface temperature is affected by surface heat flux, heat advection, diffusion and mixing, heat flux due to ice melting and formation.

Taking Eq. 3.6 for both CCSM3-HOSE and CCSM3-CTRL, making a subtraction between the two, and then integrating from the freshwater forcing onset yields (assuming that incompressibility of water holds):

$$\{\overline{T}\}_a (t) = -\int_0^t \overline{\left\{\vec{V} \cdot \nabla T\right\}}_a dt' - \frac{1}{\rho_w c_{pw} h_m} \int_0^t \{F\}_a dt' + R \quad (3.7)$$

where $\{\}_a$ denotes the anomaly (CCSM3-HOSE minus CCSM3-CTRL) of the enclosed term, and the integral denotes integration from freshwater forcing onset ($t = 0$) till the desired time t. R is the residual of the former three terms, representing the heat exchange with deep ocean and mixing processes. In Eq. 3.7 the four terms represent the mixed-layer-average temperature anomaly, the cumulated mixed-layer-

average oceanic heat advection anomaly, the cumulated upward net sufrace heat flux anomaly, and the residual, respectively, counted left to right.

Fig. 3.16a, b, c, d shows the 4 terms in Eq. 3.7 averaged over 11-20 years after freshwater forcing onset focusing on the North Atlantic basin. From Fig. 3.16a we can observe an anomalous SST pattern that is identical to Fig. 3.13a in the same region, including cooling along the North Atlantic subtropical gyre, warming at around 30°N in Central Atlantic and along the Gulf Stream extansion region. This SST anomaly is attributed to the combination of the three different terms: the surface heat flux, oceanic heat advection and the residual (shown in Fig. 3.16b, c, d, respectively). Cooling in vast high- and mid- latitude ocean north of 40°N is largely driven by the residual term. Such cooling is presumably dominated by strenthening of winter stratification (Fig. 3.16d) due to freshwater forcing. The cooling along the North Atlantic subtropical gyre and warming at around 30°N are donimated by the oceanic heat advection (Fig. 3.16c). The cooling south to this gyre is dominated by the surface heat flux (Fig. 3.16b). The warming along the Gulf Stream extension region is dominated by both the oceanic heat advection and the residual term (Fig.. 3.16c,d). These results are consistent with the oceanic contribution separated from the CAM3-SOM simulations. Fig. 3.16e, f show a further decomposition of the oceanic heat advection into vertical advection and horizontal advection, respectively, which indicate that the horizontal advection is primarily responsible for the cooing along the subtropical gyre and warming at around 30°N.
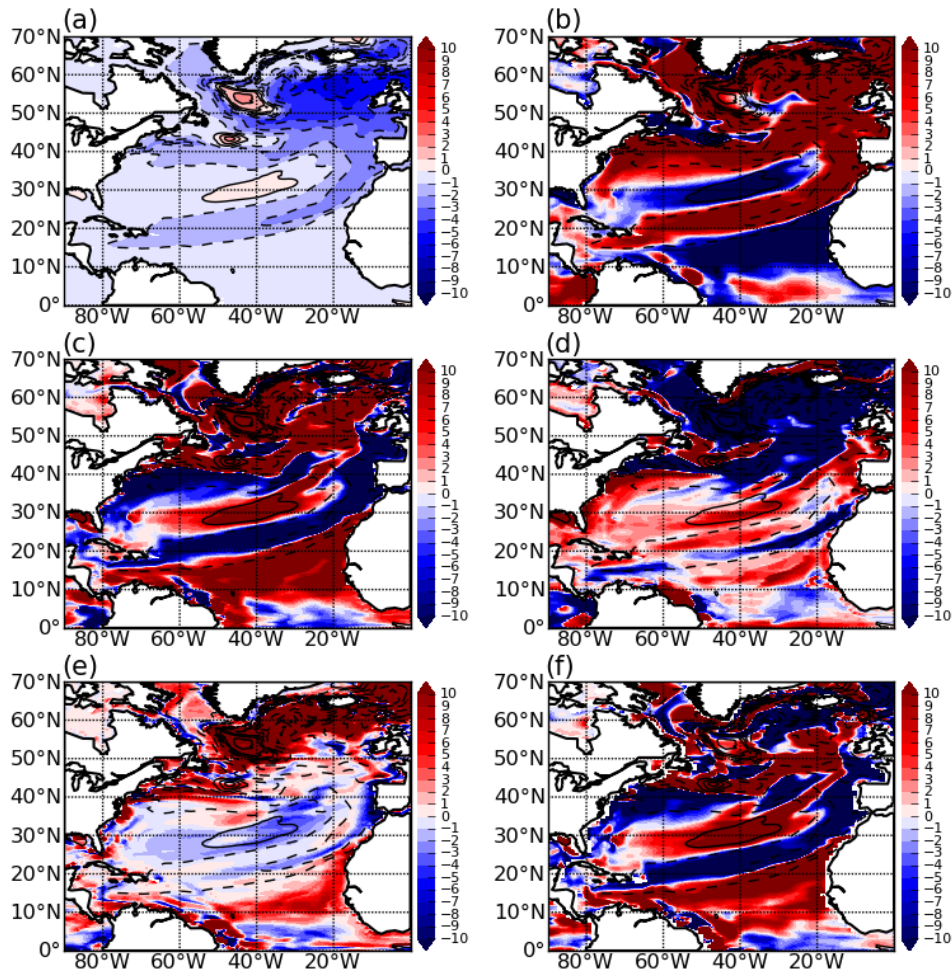
Figure 3.16: The anomalous (CCSM3-HOSE minus CCSM3-CTRL) (a) surface temperature, (b) cumulated surface heat flux, (c) cumulated oceanic heat advection, (d) the residual of the former 3 terms, (e) cumulated vertical oceanic heat advection, and (f) cumulated horizontal oceanic heat advection averaged over 11-20 years after freshwater forcing onset. All fluxes in (b, c, d, e, f) are divided by the mean CCSM3-CTRL mixed layer depth, water heat capacity, and water density so that their dimensions are the same as temperature as in (a). A contour of anomalous surface temperature is added to every panel to assist comparison, where real (dash) lines indicate positive (negative) values. The units are K for all panels.

Because the horizontal heat advection (Fig. 3.16f) is responsible for the strong SST anomaly pattern over the North Atlantic subtropics, understanding it is important for understanding the oceanic controlled teleconnection in this region. Is it primarily due to horizontal velocity anomaly, or SST gradient anomaly? To answer this question, we further decompose the anomalous horizontal heat advection term shown in Fig. 3.16f into 3 terms:

$$ -\int_0^t \overline{\left\{\overrightarrow{V}\cdot\nabla_h T\right\}}_a dt' = -\int_0^t \overline{\left\{\overrightarrow{V}\right\}}_a \cdot \nabla_h \left\{T\right\}_c dt' - \int_0^t \overline{\left\{\overrightarrow{V}\right\}}_c \cdot \nabla_h \left\{T\right\}_a dt' + R \quad (3.8) $$

where $\{\}_c$ denotes the value in CCSM3-CTRL of the enclosed term, and ∇_h the horizontal gradient operator. The horizontal heat advection anomaly on the left hand side of Eq. 3.8 can be affected by both horizontal velocity anomaly and SST anomaly, which are represented separately on the right hand side. The last term is the residual, which represents nonlinear advective effect and is assumed to be small.

Fig. 3.17 shows the decomposition of the cumulated horizontal heat advection anomaly into 3 terms shown on the right hand side of Eq. 3.8 averaged over 11-20 years after freshwater forcing onset. Clearly both the SST anomaly and horizontal velocity anomaly contribute to the anomalous horizontal advection (b, c), though the former plays a primary role while the latter a secondary role. The residual term (d) is small compared to the other two terms, which supports the linearity assumption.
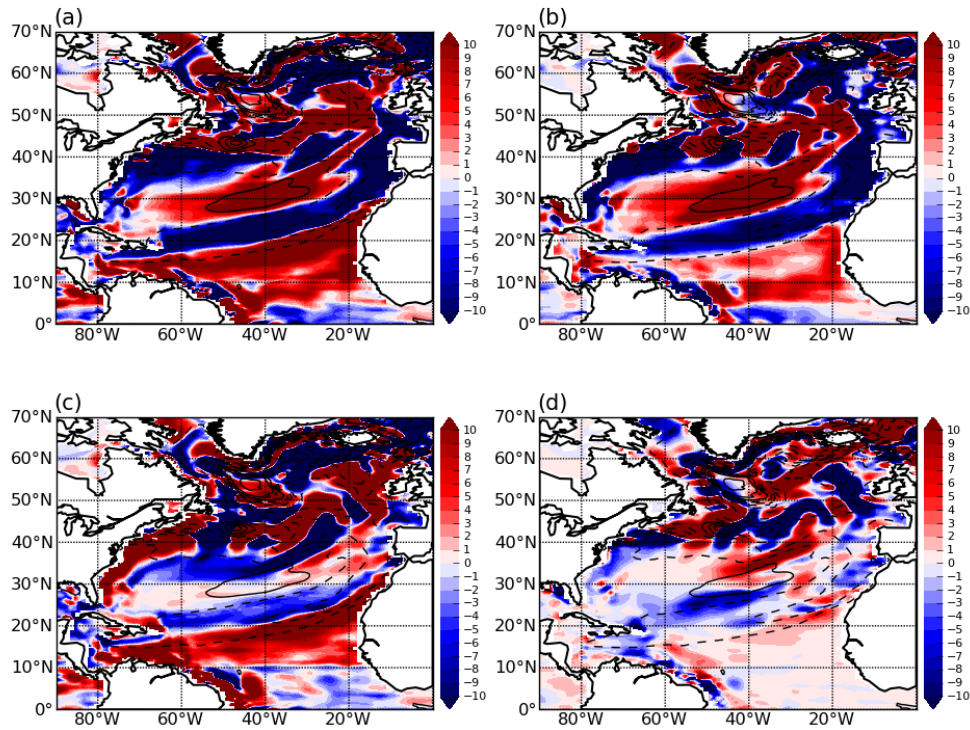
Figure 3.17: The decomposition of temporal accumulation of anomalous oceanic heat flux regard to horizontal advection shown in Fig. 3.16f into 3 terms shown on the right hand side of Eq. 3.8, with the four terms representing the effect of (a) both anomalous horizontal velocity and anomalous SST, (b) the anomalous SST, and (c) the anomalous horizontal velocity, and (d) the residual. The unit and the contours are the same as in Fig. 3.16.

From the above analysis we can conclude that the anomalous SST pattern formed between 20°N and 40°N in Atlantic predominantly results from change in ocean surface current. South to the cold tongue, around 10°N-20°N, the warming predominantly results from the change in SST gradient. Note that oceanic surface currents in this region are nearly in geostrophic balance, which allows us to understand the change in oceanic current by analyzing sea surface height (SSH) anomalies.

Fig. 3.18a shows the anomalous SSH averaged over 11-20 years after freshwater forcing onset. Due to rotation of the Earth, geostrophic current is along SSH contours and toward the left of the SSH gradient in the Northern Hemisphere. According to this relationship, the anomalous geostrophic current over the cold tongue region is southwestward, which results in a cold advection anomaly. Over the area to the north of the cold tongue region where the ocean experiences warmer anomaly, the anomalous geostrophic current is northeastward, which results in a warm anomalous advection. As the above analysis of SSH anomaly confirms that the cold tongue is mainly due to change in ocean surface current, which is reflected from the anomalous SSH, we further show that such anomalous SSH results from the freshening of ocean surface, but not from wind-driven circulation changes. This freshening is speculated to result from the freshwater originating in high-latitude North Atlantic and flowing along the North Atlantic subpolar and subtropical gyres. For this purpose we decompose anomalous SSH into 3 terms along with a residual according to conservation of mass (Steele and Ermold, 2007):

$$
\begin{aligned}
\{\eta\}_a = & \left(\{\eta\}_a + \int_{bottom}^{0m} \frac{\{\rho\}_a}{\rho_0} \right) - \int_{bottom}^{0m} \frac{\{T\}_a}{\rho_0} \left(\frac{\partial \rho}{\partial T} \right)_{\{T\}_c, \{S\}_c} dz \\
& - \int_{bottom}^{0m} \frac{\{S\}_a}{\rho_0} \left(\frac{\partial \rho}{\partial S} \right)_{\{T\}_c, \{S\}_c} dz + R
\end{aligned}
\tag{3.9}
$$

where η is the SSH, ρ_0 is the reference water density, which is 1000kg/m3, S is the salinity of the sea water, $\left(\frac{\partial \rho}{\partial S} \right)_{\{T\}_c, \{S\}_c}$ and $\left(\frac{\partial \rho}{\partial T} \right)_{\{T\}_c, \{S\}_c}$ are partial derivatives from the state equation for sea water. The anomalous SSH on the left hand side of the equation is thus divided linearly into changes due to anomalous mass per water column, ocean temperature, and salinity on the right hand, which are shown in Fig. 3.18(b, c, d). The higher SSH observed in Fig. 3.18a in the subtropical

Atlantic cold tongue area mainly results from change in salinity, while change in ocean temperature plays an opposite role, and change in mass per water column is small. The residual (Fig 14e) is small enough to prove the validity of the linear division employed in Eq. 3.9.
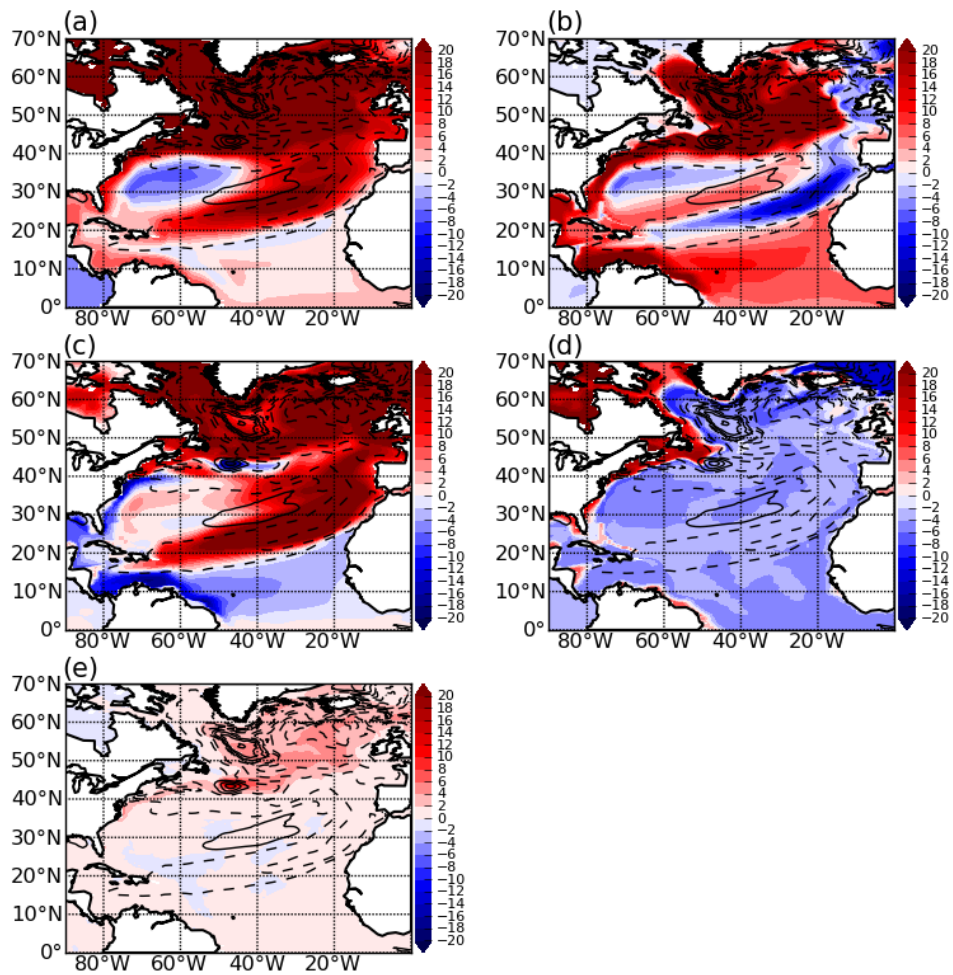
Figure 3.18: (a) The anomalous SSH in the CCSM3 hosing experiment (CCSM3-hose minus CCSM3-cntl in 11-20 years), which is divided linearly following Eq. 3.9 into changes due to anomalous (b) ocean temperature, (c) ocean salinity, and (d) mass per water column, with (e) a residual. The unit is cm. The contours are the same as in Fig. 3.16.

3.7 Summary

In this chapter, we used the CAM3-SOM to separate the atmospheric and oceanic contributions to the high-to-low latitude teleconnection during the YD-like abrupt climate change simulated using CCSM3 introduced in last chapter. The results show that the atmospheric contribution is comparable to the oceanic contribution: the magnitudes of atmospheric controlled and oceanic controlled surface temperature responses averaged over tropics are comparable. However, their controlled teleconnection are very different. The atmospheric controlled teleconnection expands the surface cooling originating from the subpolar North Atlantic equatorward in a zonally symmetric manner. The cooling reaches the Equator in about 10 years. The ITCZ shifts southward in all three oceanic basins. In contrast, the oceanic controlled teleconnection forms a complex SST anomaly pattern, including cooling around the North Atlantic subtropical gyre and eastern equatorial Pacific and warming at the center of North Atlantic subtropical gyre and along Kuroshio and Gulf Stream extension regions.

Subsequently, mechanisms of the atmospheric and oceanic controlled teleconnection are analyzed respectively. The atmospheric controlled teleconnection is found to be consistent with the hypothesis proposed by Chiang and Bitz (2005). Based on energetics analysis, the atmospheric teleconnection consists of:

- The freshwater input in subpolar North Atlantic results in strengthening of upper ocean stratification, which results in downward heat flux anomaly from the mixed layer to deep ocean as a result of reduced oceanic deep convection, cooling the high-latitude surface ocean (Fig. 3.14c).

- The lower troposphere in the northern mid-latitudes is cooled due to strengthening in storm activity, which extracts more sensible heat northward from the

69

mid-latitude to high-latitude (Fig. 3.14c).

- The cooler lower troposphere in the northern mid-latitudes leads to cooling of the the ocean primarily by surface sensible heat flux (Fig. 3.15b) and secondarily by infrared radiation (Fig. 3.15c).

- Lower SST in northern subtropics leads to increase in north-south SST gradient, which results in a stronger trade wind. This stronger trade wind results in evaporation increase in the Northern tropics, leading to a cooling in the Northern tropical region (Fig. 3.15a).

The mechanism of the oceanic controlled teleconnectin in the North Atlantic is also analyzed. The freshwater flowing from the subpolar North Atlantic along the subpolar and subtropical gyres is primarily responseible for the cooling along the North Atlantic subtropical gyre. The freshwater that reaches the North Atlantic subtropics forms a surface height anomaly pattern through halosteric effect, resulting in surface geostrophic current anomaly, which leads to SST anomaly through anomalous horizontal heat advection.

The SST anomaly in the tropical Pacific indicates a perminant La Niña condition, which, however, is not consistent with oceanic heat flux divergence (Q-flux).

4. THE ROLES OF SST IN THE HIGH-TO-LOW LATITUDE TELECONNECTION AND THE ITCZ SHIFT DURING YD-LIKE ABRUPT CLIMATE CHANGES

4.1 Introduction

The tropical precipitation is mostly related to deep convection; therefore its distribution is largely determined by the distribution of convection. Lindzen and Nigam (1987), based on simplified momentum equations, show that the convection, which is closely associated with near surface convergence, is determined by the lower-tropospheric horizontal pressure gradient. According to their analysis, a low- (high-) pressure center in the planetary boundary layer (PBL) along with surface drag, can lead to convergence (divergence) of lower-tropospheric airflow. Additionally, according to the hydrostatic equation, the pressure field at a given height is determined by the mass of the air column above it, and thus by the air density distribution. Furthermore, according to the equation of state for air, the air density at certain pressure level depends on its temperature. Together, these result in a simple relation between the pressure gradient and air temperature distribution. On one hand, the lower-tropospheric air temperature in the boundary layer and up to as high as 3000m is closely related to the surface temperature due to strong Planetary Boundary Layer (PBL) mixing. On the other hand, the air temperature is largely affected by advection associated with horizontal and vertical motions and latent heat release in cumulus clouds. Therefore, the surface temperature distribution, the large-scale circulations such as Hadley and Walker Circulations, and the latent heat release in upper troposphere, etc., are all factors that affect the precipitation distribution in Tropics. Additionally, these factors also interact with each other (Held and Hou,

1980), which may make it difficult to understand the causality. Although the upper-tropospheric latent heat release associated with deep convection is often considered as the primary source of the lower-tropospheric convergence, studies have shown that this latent heat release contributes little to the convergence (Schneider, 1977; Schneider and Lindzen, 1977; Stevens and Lindzen, 1978; Stevens et al., 1977). Currently, the relative importance of the direct contribution of SST via vertical mixing and the contribution of large-scale circulations to the tropical precipitation is still not well understood.

The ITCZ southward displacement during Younger Dryas (Alley, 2000) -like abrupt climate changes has been observed in sediment record (Stouffer et al., 2006) and simulated using general circulation models (Chang et al. 2008; Cheng et al. 2007; Chiang et al. 2005; Stouffer R.J. 2006). While most of these studies explain the ITCZ shift as a result of decrease in south-to-north interhemispheric surface temperature gradient, they did not offer a clear physical explanation of the underlying dynamics. Recently, Kang and Held (2012) argue that the large-scale circulation (i.e., the Hadley Circulation) plays a more important role in the ITCZ shift than the SST-associated lower-tropospheric pressure gradient. They conducted a suite of experiments with an aqua-planet AGCM coupled to an SOM using artificial cooling in Northern extratropical oceans and warming in Southern extratropical oceans. In one experiment the surface evaporation is prescribed (so as to eliminate the wind-evaporation-SST (WES) feedback (Xie, 1999)) and in the other it is not. The two simulations result in different SST anomaly but similar ITCZ shift. They thus argue that the surface temperature is not important to the ITCZ shift. They further conducted simulations with prescribed surface temperature and found that the cross-equatorial atmospheric meridional heat transport, which reflects the position of the Hadley circulation center (Kang et al., 2008), is in a good statistical linear relation-

ship with the ITCZ shift. They argue accordingly that the large-scale circulation is responsible for the ITCZ shift. However, the difference of SST anomalies in their two AGCM-SOM simulations is relatively small compared with the surface temperature anomalies themselves. Therefore, if we consider the anomalies as the first order changes and the differences of anomalies between the two simulations as the second order changes, the first order ITCZ shift may still largely depend on the surface temperature anomaly, while the second order effect becomes subtle. Additionally, the construction and strength of the Hadley Circulation is largely dependent on the location of heating center in the troposphere (such as upper-tropospheric latent release heating in tropical deep clouds) and the tropical surface temperature distribution (Held and Hou, 1980), which means that the ITCZ shift may lead to change in the Hadley circulation. Therefore, the linear relationship between the Hadley circulation and ITCZ shift may not necessarily indicate a causality, but the former may be only a reflection of the later. The causality deserves a further look.

Therefore, in the second part of this dissertation we will focus on understanding the importance of SST in ITCZ shift as well as the high-to-low latitude teleconnection during Younger Dryas-like abrupt climate changes.

4.2   Experimental design

We use the NCAR Atmosphere Model version 3 (CAM3) (Kiehl et al. 1996) coupled to a thermodynamic slab ocean model (CAM3-SOM) to perform three sets of experiments, each containing a climatological simulation (C1, C0.1 and C10) and a perturbed simulation (P1, P0.1 and P10) with a sudden and continuing cooling in the high-latitude Northern Hemisphere, as listed in detail in Table 4.1. The slab ocean contains a motionless mixed layer that is vertically uniform (Hansen et al., 1984; Kiehl et al., 1996). As before, the high-latitude cooling is introduced by perturbing the

Q-flux (a prescribed term representing the vertical integration of heat flux divergence over the ocean mixed layer) (Hansen et al., 1984; Kiehl et al., 1996). The Q-fluxes are computed using the SST-restoring technique described in Chapter 3. Three 12-month climatological Q-fluxes, CLIM-Q-flux-1, CLIM-Q-flux-10, CLIM-Q-flux-1/10, and three 20-year hosing Q-fluxes, HOSE-Q-flux-1, HOSE-Q-flux-10, HOSE-Q-flux-1/10 are computed accordingly. The suffix numbers represent the ratio of the mixed layer depth in the CAM3-SOM-RESTORE simulations to a standard mixed layer depth that is obtain from CCSM3-CLIM by taking the 400-year time mean. In each CAM3-SOM-RESTORE simulation, to compute the climatological Q-fluxes, T_c is prescribed as the 12-month SST climatology in CCSM3-CLIM, and in each simulation computing the hosing Q-fluxes, T_c is prescribed as the first 20-year SST in CCSM3-HOSE. Note that CLIM-Q-flux-1 and HOSE-Q-flux-1 are the same as CLIM-Q-flux and HOSE-Q-flux described in Chapter 3. The mixed layer depths (constant in time) are different among the three sets of experiments. In one set (C1 and P1) it is the standard mixed layer depth. In the other two sets it is increased (C10 and P10) and decreased (C0.1 and P0.1) by a factor of 10 of the standard depth, respectively. In each climatological simulation, the corresponding climatological Q-flux is applied, while in each perturbed simulation, the corresponding hosing Q-flux is applied in 50°-70°N North Atlantic and 70°-90°N (blue area in Fig. 4.1), and the climatological Q-flux applied elsewhere. In such a way the Q-flux is only perturbed in high-latitude Northern Hemisphere in the perturbed simulations. Based on the procedure computing Q-fluxes, we are confident that the three climatological runs result in the same climate as CCSM3-CLIM, and the three perturbed runs result in the same cooling over the perturbed area as CCSM3-HOSE. Each climatological simulation lasts for 100 years and each perturbed simulation lasts for 20 years with five ensemble members. The model resolution is set as T42. The sea ice coverage in

each climatological simulation is prescribed as its climatology in CCSM3-CLIM, and in each perturbed simulation as in CCSM3-HOSE.

Table 4.1: The experimental setups.

Simulation	Ocean Mixed Layer Depth	Q-flux in 50° N-70° N Atlantic and 70° N-90° N	Q-flux elsewhere
C1	Standard × 1	CLIM-Q-flux-1	CLIM-Q-flux-1
P1		HOSE-Q-flux-1	
C10	Standard × 10	CLIM-Q-flux-10	CLIM-Q-flux-10
P10		HOSE-Q-flux-10	
C0.1	Standard × 1/10	CLIM-Q-flux-1/10	CLIM-Q-flux-1/10
P0.1		HOSE-Q-flux-1/10	
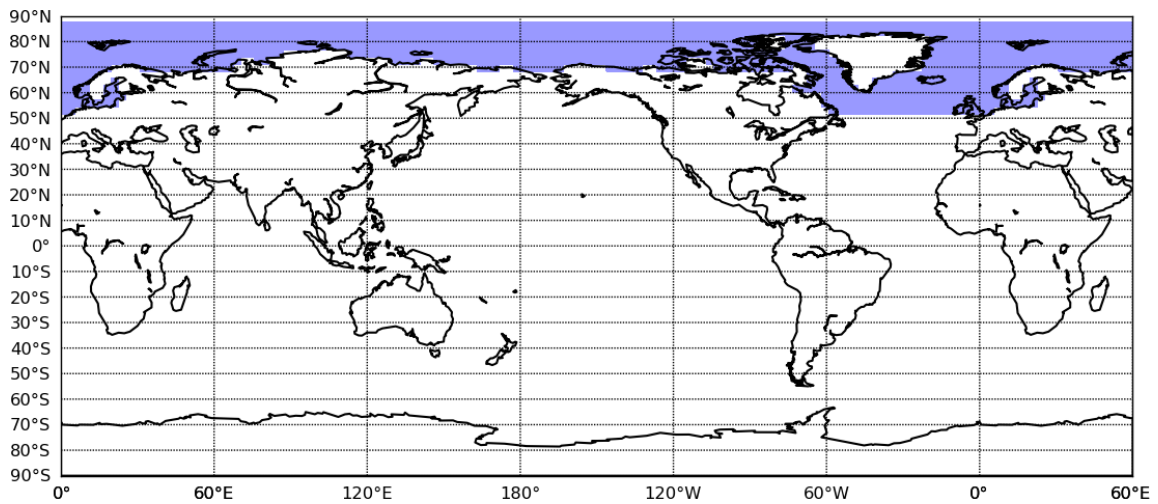
Figure 4.1: The geometry of the area (blue) where Q-flux perturbation is applied.

Fig. 4.2 shows the anomalous surface temperature as functions of time after Q-flux perturbation onset. The anomalous surface temperature is averaged over the forcing area as shown in Fig. 4.1 in blue color. The three lines represent the three sets of experiments. The cooling of surface temperature is partly due to the perturbed Q-flux and partly due to the increasing of sea ice in this area. From the figure we can see that the high-latitude Northern Hemispheric cooling remains approximately the same in the three perturbed runs. The differences among them are much smaller than the coolings themselves. We will denote such cooling as the high-latitude forcing in following analysis and assume that the three perturbed runs have the same high-latitude cooling forcing.
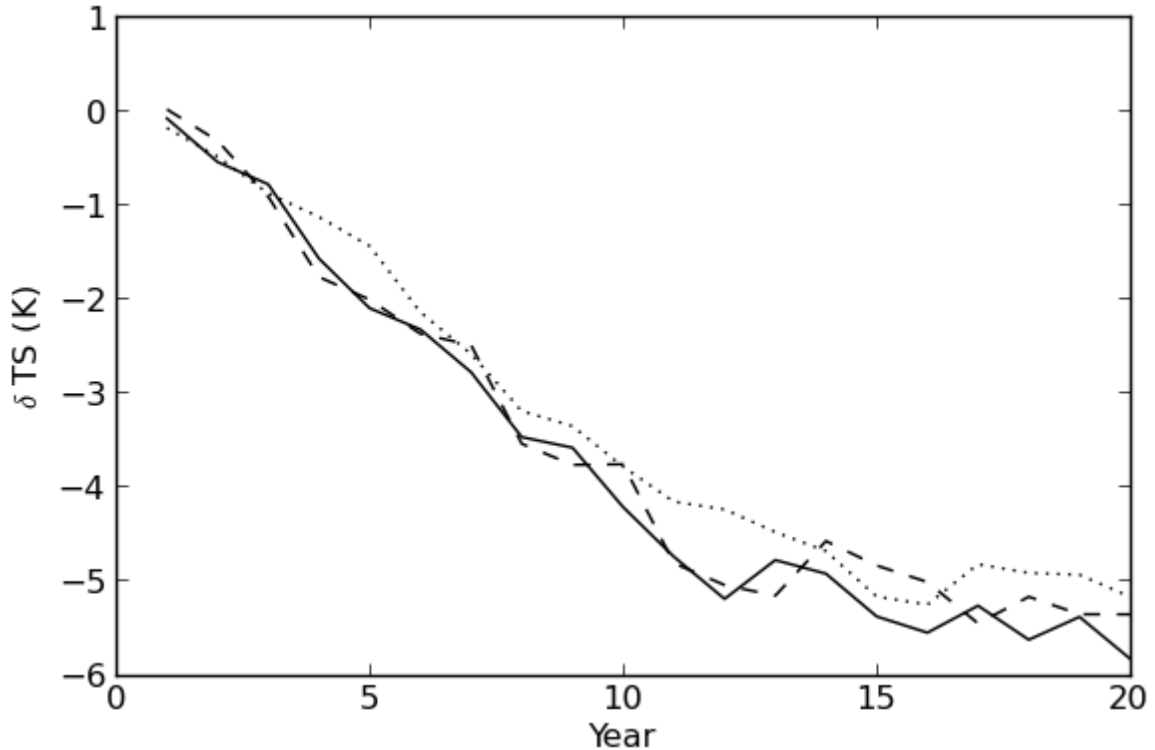
Figure 4.2: The annual average anomalous surface temperature in P1 (solid, P1-C1), P0.1 (dash, P0.1-C0.1), and P10 (dotted, P10-C10) as functions of time. An area average is taken over the blue area shown in Fig. 4.1.

4.3 Propagation of surface cooling and development of precipitation anomaly

4.3.1 SST

By introducing the same high-latitude Northern Hemispheric cooling forcing while varying mixed layer depth, different SST responses in lower latitudes are expected. This is because the slab ocean with different mixed layer depth has different heat capacity, which means that SST response in a deeper slab ocean is less sensitive to heat flux forcing than in a shallower slab ocean.

Though not shown here, by design the resultant surface temperature in the three climatological runs are the same. Surface temperature responses from the three perturbed runs, however, are quite different. Fig. 4.3 shows the surface temperature anomalies (perturbed runs minus corresponding climatological runs) from the three perturbed simulations. We see from Fig. 4.3a, b, c that in the 2nd decade the extent of the cooling in the Northern Hemisphere is different among the three perturbed runs. In P1 and P0.1 the cooling extends over the entire Northern Hemisphere with temperature anomalies ranging in 0K-8K, while in P10 the extent of the surface cooling is less broad. Especially over the northern tropical oceans the cold surface temperature anomaly in P10 is much weaker. As previously discussed, this is caused by the fact that the deeper mixed layer makes it more difficult to change its temperature. This result is seen more clearly in Fig. 4.3(d, e, f), which shows high-to-low latitude propagations of cooling surface temperature anomaly in a zonal mean viewpoint. In P1 it takes about 10 years for the surface cooling (estimated as 0.1K cooling contour line) to reach Equator. In P0.1 it takes much shorter time, only around 2-3 years, while in P10 longer than 20 years. At the 20th year, the cooling only reaches about 10°N in P10. The propagation speeds are about 7°/year, 23°/year and 2°/year for P1, P0.1 and P10, respectively, following a linear fit of the 0.1K contour of the

Hovemollar plots. From Fig. 4.3(g, h, i) we can see that in the second decade the cooling already reaches the Equator in P1 by cooling the equatorial region by about 0.2K. In comparison, the cooling extends across the Equator and reaches about 15°S in P0.1, and in P10 the extent of the cooling is confined to the north of the equator. At 30°N, the northern bound of the tropics, the cooling in the second decade is about 0.4K, 0.5K and 0.2K in P1, P0.1 and P10, respectively.
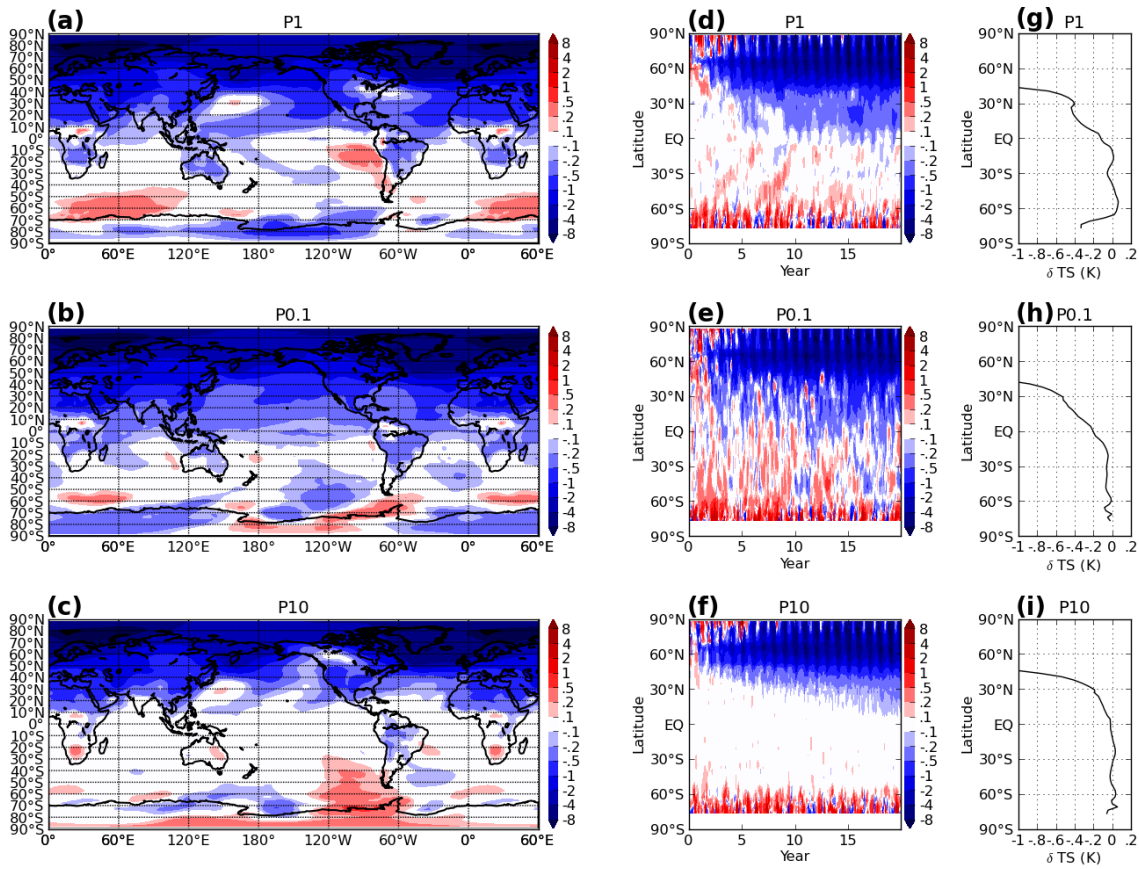
Figure 4.3: The surface temperature anomaly in 3 sets of experiments. (a, b, c) are the 11-20-year average surface temperature anomalies (here and later in this chapter, anomalies are calculated by hosing simulations minus their paired segments from the climatological simulations with the same initial conditions). (d, e, f) are the Hovemoller diagram of the zonal average surface temperature anomalies over ocean spots. (g, h, i) are the 11-20-year-zonal average surface temperature anomalies over ocean spots. The unit is K.

78

4.3.2 Heat budgets

As discussed in the previous chapter, investigation into meridional and vertical heat flux changes provides a good insight into the high-to-low latitude teleconnection. Fig. 4.4 shows the cumulative heat transport anomalies from hosing onset, averaged over 11-20 years, for P1, P0.1 and P10, respectively. In high-latitudes (50°N-90°N), all three experiments show large decreases in surface heat release, which is driven by the Q-flux forcings. Note that the Q-flux forcings are larger than the surface heat flux changes, indicating that the ocean is cooled. The difference between Q-flux forcing and surface heat flux change in P10 is particularly large, which is due to the large heat capacity in P10: it requires more heat release to cool an ocean mixed layer with larger heat capacity by the same degree. These surface heat flux changes are compensated primarily by extra meridional atmospheric heat transport from the mid-latitudes and secondary by increase of downward heat flux at TOA. In the mid-latitudes and tropics, these three experiments present significant different energetic responses. In P1 and P0.1 (Fig. 4.4a,b), the extra atmospheric heat transports from the mid-latitudes to the high-latitudes are primarily compensated by extra atmospheric heat transports from the tropics to the mid-latitudes and secondarily by increase of downward TOA radiation fluxes and upward surface heat fluxes. In P10 (Fig. 4.4c), however, the increase of upward surface heat flux is comparable with the extra heat transport from the tropics to the mid-latitudes. This is also due to the large heat capacity of the ocean mixed layer in P10, which can supply more heat to the atmosphere when being cooled. In the northern tropics there is a similar story. In P1 and P0.1, the extra atmospheric heat transports from the tropics to the mid-latitudes are compensated primarily by the extra atmospheric heat transports from the southern tropics to the northern tropics and secondarily by

the increase of downward TOA radiation fluxes and upward surface heat flux. In P10, however, the increase of surface heat flux is larger than the atmospheric from the southern tropics to the northern tropics. In all three experiments, there are significant increase in downward TOA radiation fluxes in the southern tropics, compensating the extra atmospheric heat transports from the southern tropics to the northern tropics, which is speculated to result from increase of cumulus clouds. However, the meridional atmospheric heat transports from the southern mid-latitudes to the tropics are quite different, especially in P10, where this heat transport change is opposite to those in the other two experiments. Overall, the smaller meridional atmospheric heat transport change in P1 (Fig. 4.4c) indicates a weaker high-to-low latitude teleconnection, which is consistent with the surface temperature anomalies (Fig. 4.3).
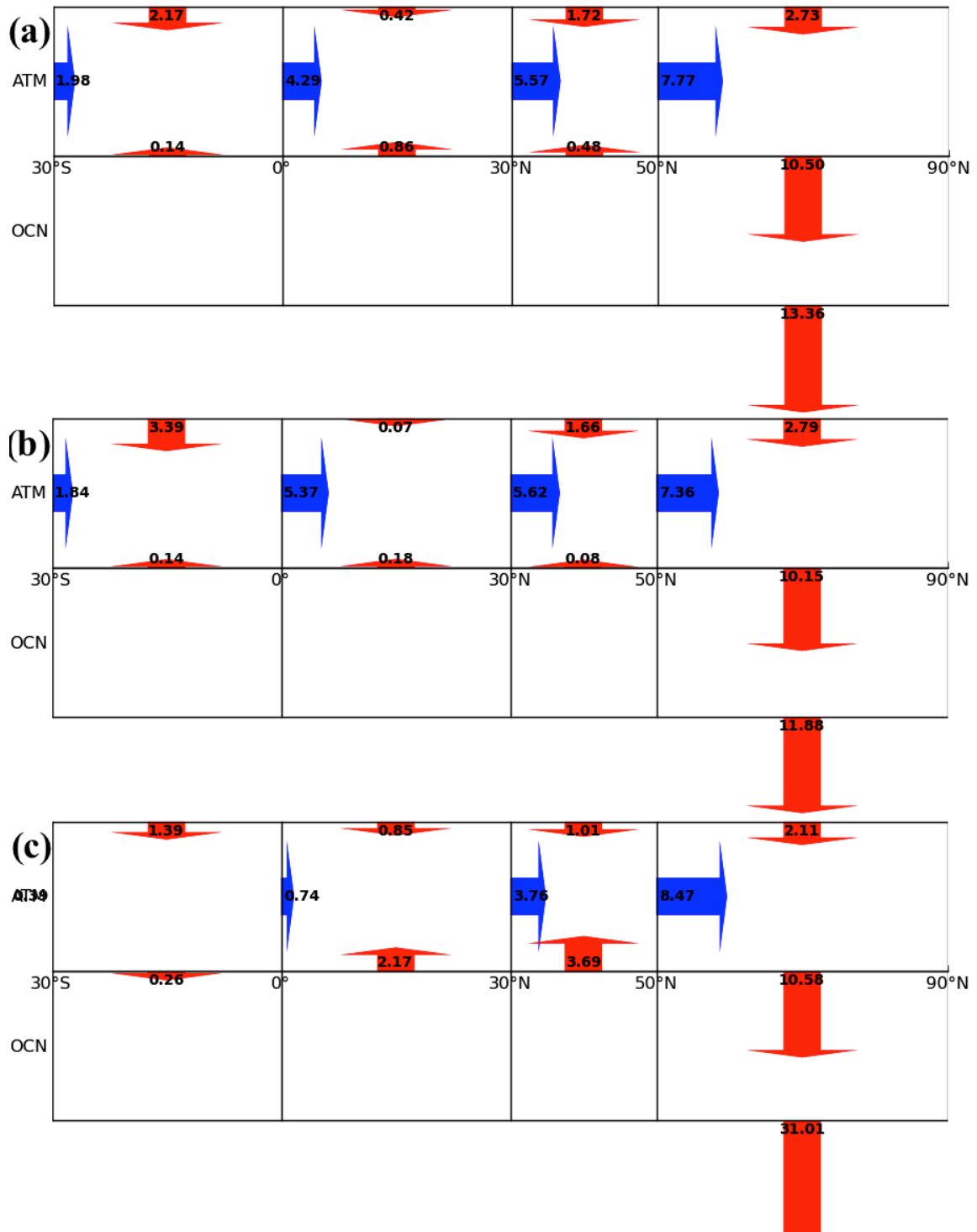
Figure 4.4: The same as Fig. 3.14 but showing anomalies in (a) P1, (b) P0.1 and (c) (P10)

4.3.3   Tropical climate response: precipitation

The main feature of the tropical climate response to the high-latitude cooling forcing is the southward shift of the ITCZ. Fig. 4.5 shows the 11-20-year average tropical precipitation anomalies in P1, P0.1 and P10, as well as the climatological precipitation in C1 (C0.1 and C10 are similar as they simulate the same mean climate and thus are not shown). The CAM3 shows a double ITCZ (Fig. 4.5a, e) in the tropics. Nevertheless, we see clearly a southward shift of ITCZ in P1 and P0.1,but not obviously in P10. The precipitation increases in Southern Tropics by about 0.2mm/day and decreases in Northern Tropics by about the same amount in P1 and P0.1 (Fig. 4.5e, f), while it only increases by less than 0.05mm/day in $10°$S-$0°$in P10 (Fig. 4g). Moreover, the ITCZ in P0.1 (Fig 4.5g) is shifted further southward than in P1 (Fig. 4.5f) by about $5°$, which is understandable considering that the surface cooling spreads further southward in P0.1 than P1. In detail, in P1 the Atlantic ITCZ shifts and strengthens, the northern branch of Pacific ITCZ shifts and the southern branch strengthens, and the Indian ITCZ shifts and strengthens; in P0.1 the Atlantic and Indian ITCZ undergoes the same as in P1, the northern branch of Pacific ITCZ weakens and the southern branch shifts; in P10 the Atlantic ITCZ shifts vaguely, both branches of the Pacific ITCZ strengthens, and the Indian ITCZ shifts.
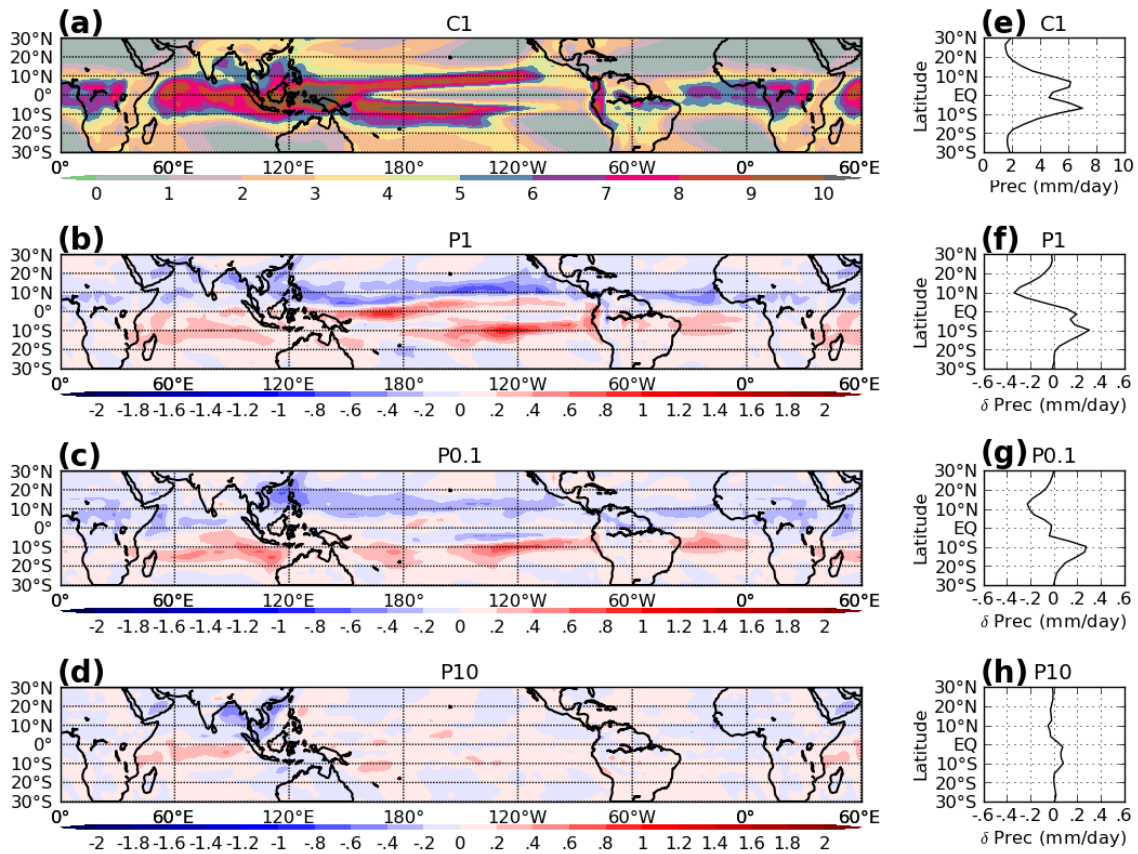
Figure 4.5: The tropical precipitation for (a) Climatology in C1, (b) Anomaly in P1 (P1-C1), (c) Anomaly in P0.1 (P0.1-C0.1), and (d) Anomaly in P10 (P10-C10), as well as their zonal average over oceanic spots in the right corresponding panels, (e, f, g, h). The anomalies are obtained from 11-20-year average. The unit is mm/day.

These results suggest that the SST change plays an important role in linking the low-latitude climate response to the high-latitude cooling forcing. Deeper mixed layer slows down the propagation through increasing the heat capacity of the ocean. When the SST is made difficult to change, the high-to-low latitude teleconnection becomes weak: tropical SST response (Fig. 4.3c,f,i), meridional atmospheric circulation response (Fig. 4.4c) and tropical precipitation response(Fig. 4.5d,h) all becomes weak. We can also speculate that there is no so-called "atmospheric bridge" connecting the

high-latitude and tropical climates through upper troposphere without SST changes. For example, the meridional atmospheric heat transport change is closely related to the SST change. In the mid- and high- latitudes, the meridional atmospheric heat transport is carried primarily by storm activities, which is strengthened when the meridional SST gradient is larger through strengthened baroclinic instability. In the tropics, it is carried primarily by the Hadley circulation, which is also strengthened when the meridional SST gradient is larger ((Held and Hou, 1980)).

4.4 Understanding ITCZ southward shift in response to high-latitude forcing

As we discussed in the previous section, surface temperature is crucial for the high-to-low latitude teleconnection. The fact that the ITCZ responds more strongly to the same high-latitude forcing in the experiments where mixed layer depth is shallow and SST anomalies are strong indicates that SST plays a critical role in affecting tropical convection. In this section, we take a further look at the underlying dynamics linking the high-latitude forcing to tropical precipitation response.

4.4.1 Tropical convection response

Observations show that tropical precipitation is mostly convective driven. Like in other AGCMs, CAM3 simulates tropical precipitation using a cumulus parameterization scheme (Kiehl et al., 1996). A cumulonimbus cloud in the tropics usually occupies altitudes from hundreds of meters up to thousands of meters and peaks at around 6000 meters. Within those clouds there is strong convection and heavy rain. The air flow, carrying rich water vapor, converges horizontally in the lower troposphere under cumulonimbus clouds; then it goes upward, releasing its water vapor to feed the heavy rain before it reaches the cloud top and diverges in the upper troposphere. Thus the tropical precipitation is tightly related to convective activity. The convective activity can be characterized by the upward flow at a certain height that

is typical for cumulonimbus clouds. We choose this height to be Z_T=3000m (around 700mb). This height is also about the base of the free atmosphere. According to the mass conservation equation, and neglecting the term of density change in Eulerian Coordinate, which is small compared with the other terms, we have the vertical velocity expressed by convergence in lower troposphere:

$$w_T = \frac{1}{\rho_T} \int_0^{Z_T} -\rho \nabla \cdot \overrightarrow{V} dz \tag{4.1}$$

where the subscripts T denote the 3000m height.

Fig. 4.6 is the same as Fig. 4.5 but showing the vertical average convergence under Z_T. We can see that the spatial pattern, not only the zonal average, agree very well with the precipitation patterns shown in Fig. 4.5. Therefore, it is reasonable to conclude that the tropical precipitation is very well characterized by the lower tropospheric convergence.
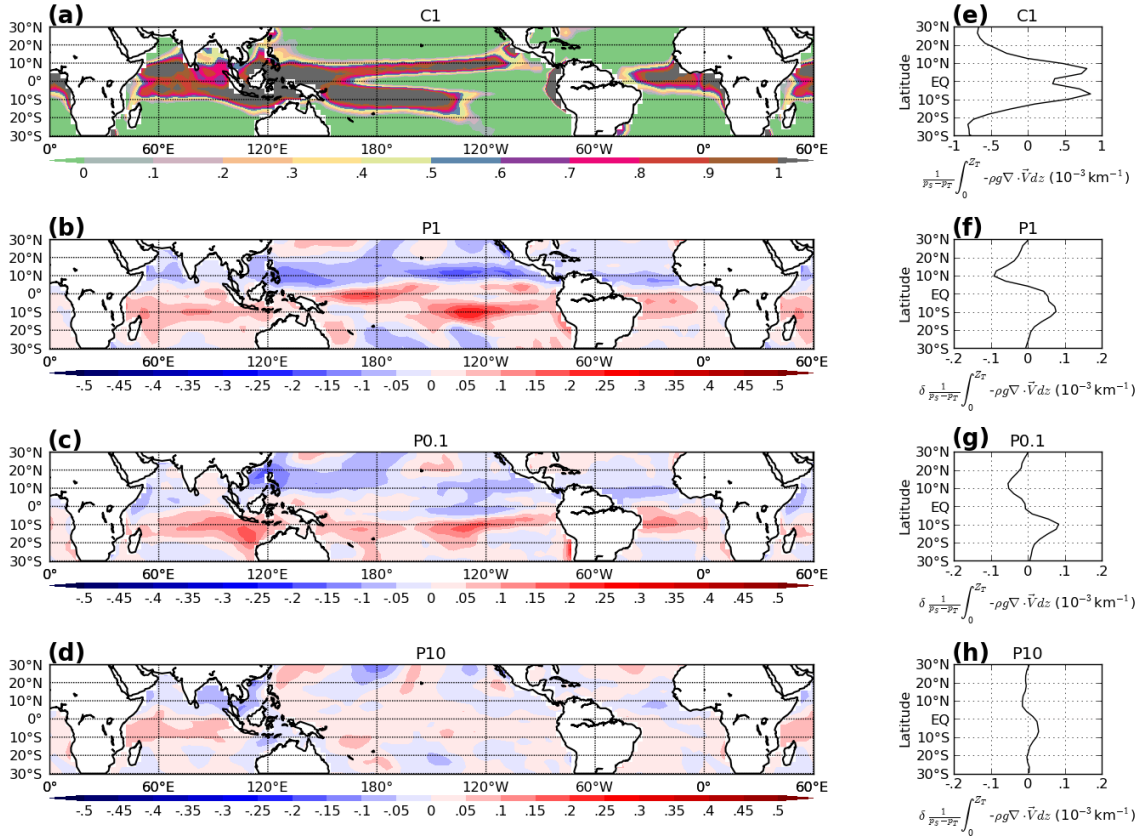
Figure 4.6: The same as Fig. 4.3 except showing the vertical average convection from surface to 3000m. The unit is (1000km)-1.

4.4.2 Lindzen and Nigam's simple model

In this subsection, we will show the SST's direct effect on ITCZ shift excluding the large-scale circulation's effect using Lindzen and Nigam's simple model. As we discussed in the Introduction, the lower tropospheric convergence/divergence is affected by many factors including near surface temperature, large-scale circulations, latent release heating, etc. In the following discussion the focus will be on the effect of near surface temperature. The lower tropospheric convergence/divergence can be understood in a simple model framework as a combined action of pressure gradient and the surface drag (Lindzen and Nigam, 1987). In the lower troposphere, because

of strong vertical mixing, the air temperature is very well related to the surface temperature. Fig. 4.7 and Fig. 4.8 show the air temperature anomalies at 850mb and 700mb, respectively. It is evident that their patterns bear strong resemblance to that of the surface temperature anomalies (Fig. 4.3) over ocean.
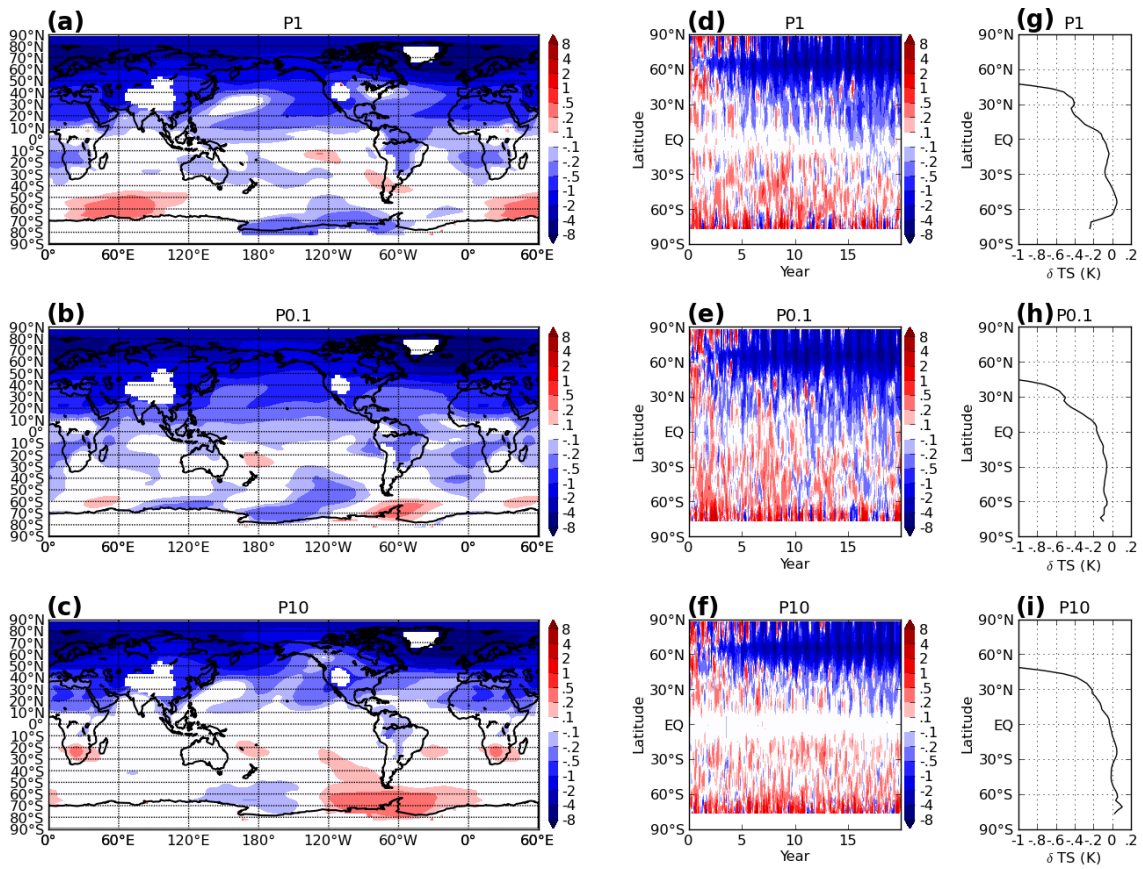
Figure 4.7: The same as Fig. 4.3 except showing the air temperature at 850mb.
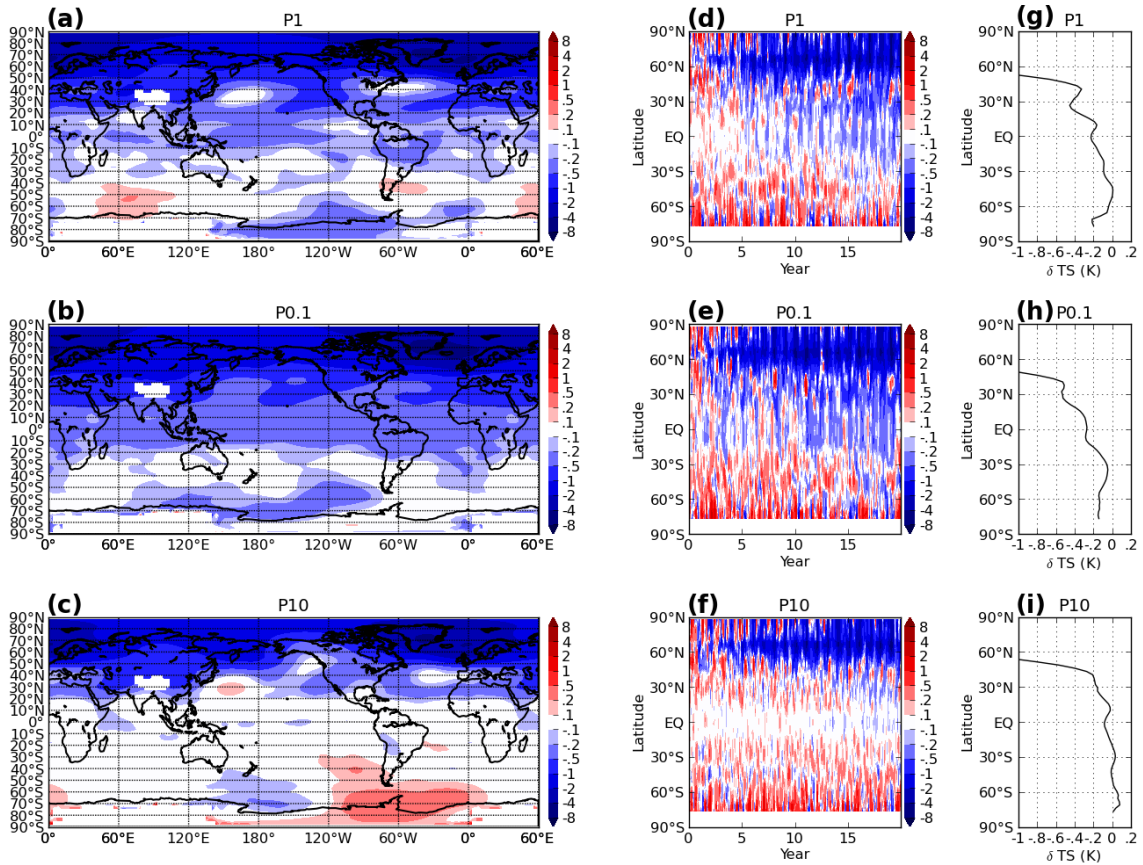
Figure 4.8: The same as Fig. 3 except showing the air temperature at 700mb.

To physically relate the lower-tropospheric convergence to the surface temperature, Lindzen and Nigam (1987) developed a simple model from momentum balance, which accounts for the direct contribution of the SST to the lower-tropospheric convergence. Contributions from large-scale circulations and mid- and upper- tropospheric latent release heating are assumed to be secondary, so is the feedback from the convergence to the SST. In this model the pressure gradient is only determined by the surface temperature, which determines the lower-tropospheric air temperature explicitly, and is affected by a so-called back pressure as a result of the lagged vertical flow response at Z_T (top of lower troposphere) to the conver-

88

gence. We force this simple model using surface temperatures from our simulations by solving the equation (10, 6c, 7c) combined with (12) in their paper to compute the lower tropospheric convergence, with back pressure coefficient τ being 3min and all other coefficients being the same. We employ a finite difference scheme to solve the equations. The result is given in Fig. 4.9. We will denote the vertical average lower-tropospheric convergence shown in Fig. 4.9 computed using Lindzen-Nigam's model as LN-convergence, and that computed using the results from our model experiments as CAM-convergence. In C1 LN-convergence captures the basic horizontal structure of the ITCZs in each ocean basin. For example, the double ITCZ in the tropical Pacific, the ITCZ over equatorial Atlantic and Indian basins. However, it overestimates the ITCZs by about 10-20% in Atlantic and Indian basins. In the middle of each ocean basin over subtropics, 20°-30°latitudes, LN-convergence shows a convergence zone that is absent in CAM3. These inconsistent convergences are likely to be balanced by the divergences driven by high-pressure associated with subsidence that is a part of the Hadley Circulation. Along the coast LN-convergence also shows disagreement with the CAM3-convergence, which is speculated to be because the land has too small heat capacity, thus its surface temperature feels too much feedback from the atmosphere, as well as of the complex topography. The basic structures of the anomalous CAM-convergences in P1, P0.1 and P10 are also captured to some extent: in P1 the shift and strengthening of Atlantic ITCZ, and the shift of northern branch of Pacific ITCZ and strengthening of southern branch are captured, while the shift of Indian ITCZ not so well; in P0.1, shift and strengthening of Atlantic ITCZ is captured, while the other basin not so well. However, the zonal average is captured well. Again, because of small oceanic heat capacity in P0.1, the ocean feels much more feedbacks from the atmosphere, which make noise to LN's SST-deterministic result. In P10 the Atlantic ITCZ shift and the strengthening of Pacific ITCZs are

captured, while the Indian ITCZ shift not. Again the zonal averages (Fig. 4.9e,f,g,h) are captured well.

The LN's model does not consider any feedback from the atmosphere, i.e. the cloud formed from convergence in turn change surface temperature by changing Cloud Radiative forcing. Additionally, change in latent heating due to change in precipitation also manipulates in turn the lower-tropospheric pressure field. All these feedbacks are not considered. Therefore, these model results only reflect the pure contribution from the SST and vertical mixing to the lower-tropospheric convergence. Fig. 4.10 shows that the magnitude of the LN-convergence anomalies in tropics are close to that of the CAM-convergence (there is a linear relation between the two convergences with 95% confidence). This suggests that the SST-vertical mixing-lower air temperature process does contribute a lot to the lower-tropospheric convergence anomalies during YD-like abrupt climate changes. SST is important and plays its role in the ITCZ shift through manipulating lower-tropospheric air temperature and thus the pressure gradient. The ITCZ shift in P1 and P0.1 is stronger than in P10 because the SST change is stronger. However, the shift in P0.1 is much weaker than in P1, while the surface temperature change is similar (Fig. 4.3g,h). This is because in P0.1 the oceanic heat capacity is too small and it feels much feedbacks from the atmosphere.
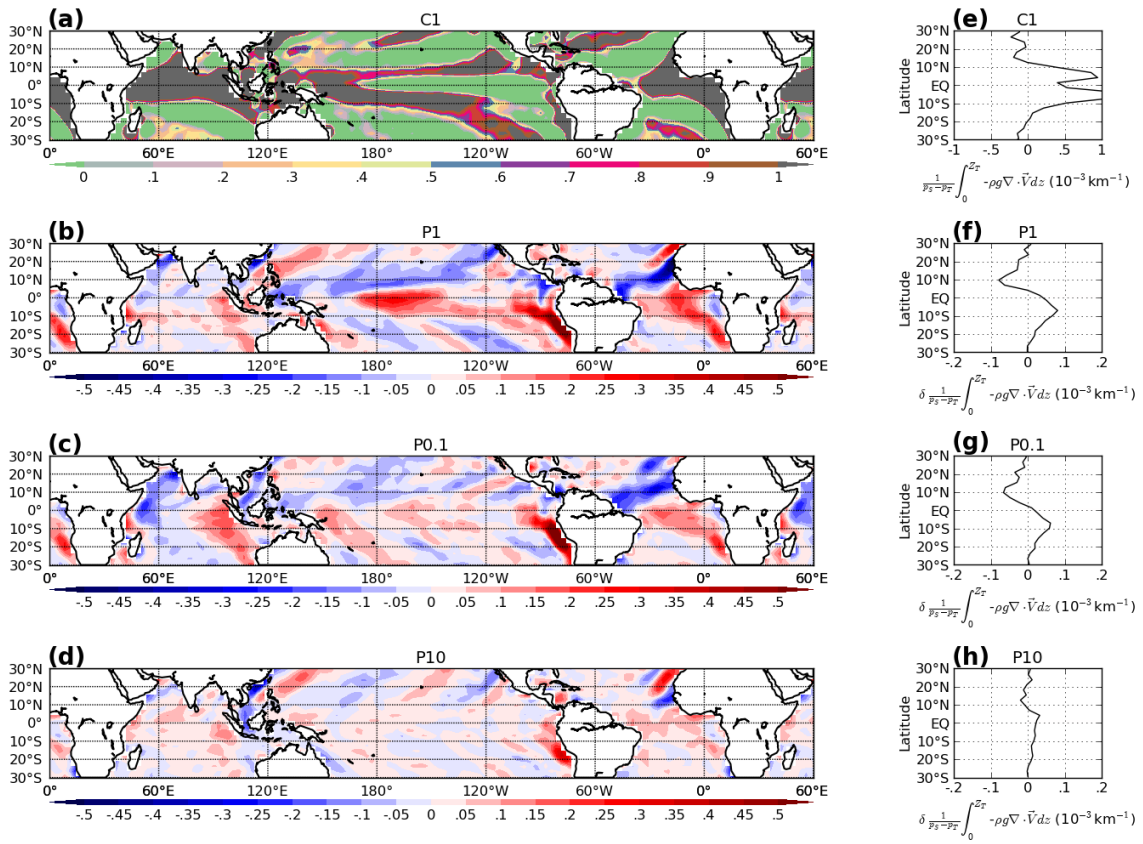
Figure 4.9: The same as Fig. 4.6 except that the convergence is calculated using Lindzen and Nigam's model.
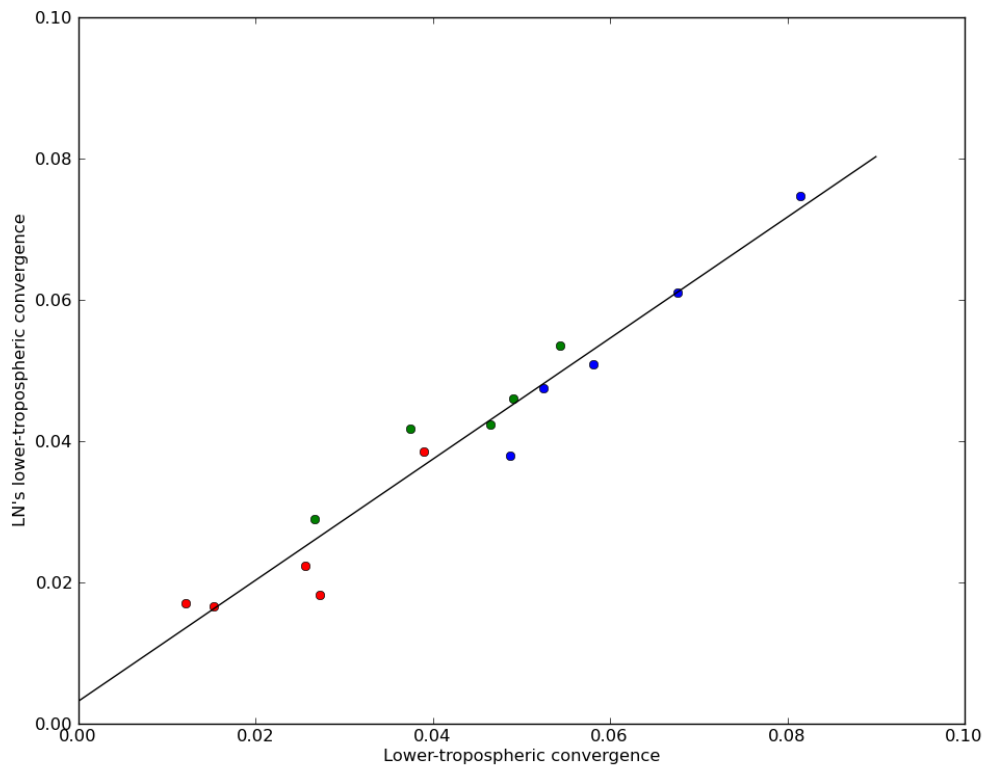
Figure 4.10: The 11-20-year and 20°S-20°N average of the magnitude of the zonal mean LN-convergence anomalies as a function of the CAM-convergence anomalies. Each circle represents an ensemble member of P1 (blue), P0.1 (green) and P10 (red). The least square fit is plotted in a solid line. The unit is $(1000\text{km})^{-1}$

4.5   Summary

Three sets of experiments were carried out using CAM3-SOM to understand the role of SST in linking high-latitude to tropical climate changes during a YD-like abrupt climate change event. Each set of experiments includes a climatological run and a perturbed run. In each perturbed run, the Northern Hemispheric high-latitude ocean is artificially cooled by introducing Q-flux perturbation (Q-flux is perturbed in 50-70N Atlantic and whole Arctic, blue area in Fig. 4.2). The ocean mixed layer

depths are various among the three sets of experiments (1x, 0.1x and 10x standard depth, respectively). The lower-latitude climate responses are different in the three perturbed runs due to the different ocean heat capacity. All perturbed runs exhibit surface cooling over Northern Hemisphere and a high-to-low latitude propagation of surface cooling, although extent of the cooling and the propagation rate differ considerably (Fig. 4.3). These differences are expected considering the fact that SST change is more difficult when the oceanic heat capacity is larger. An energetic analysis (Fig. 4.4) makes this clearer. The basic processes leading to SST changes for the three experiments from an energetic point of view are described as follows:

- High-latitude Q-flux forcing cools the ocean, reducing surface heat flux into the atmosphere, which is compensated by increase of downward TOA radiation and extra atmospheric heat transport from the mid-latitude. Such increase of meridional atmospheric heat transport is carried by strengthened storm activities, which results from stronger baroclinic instability due to stronger meridional SST gradient.

- The extra atmospheric heat transport from the mid-latitudes to the high-latitudes is compensated by the extra atmospheric heat transport from the tropics to the mid-latitudes and increased TOA and surface heat fluxes into the atmosphere. This increased upward surface heat flux cools the ocean. This extra heat transport from the tropics to the mid-latitudes is carried by strengthened Hadley circulation, which results from stronger meridional SST gradient (Held and Hou, 1980).

- The extra atmospheric heat transport from the tropics to the mid-latitudes is further compensated by the extra atmospheric heat transport from the southern tropics to the northern tropics and increased TOA and surface heat fluxes

93

into the atmosphere, which cools the ocean. This extra atmospheric heat transport from the southern tropics to the northern tropics can also be carried by strengthened Hadley circulation.

However, the teleconnections in the three experiments also exhibit significant differences. The most noticeable difference is that the surface heat flux change over the northern tropics and mid-latitudes in P10 (Fig. 4.4c) is significantly larger than in P1 and P0.1 (Fig. 4.4a,b), which is understandable considering the larger ocean heat capacity in P10. This larger surface heat flux change compensates considerably to the extra atmospheric heat transport to the higher latitudes, leading to less atmospheric heat transport change from the lower latitudes, which indicates a weaker high-to-low latitude teleconnection in P10. As discussed, the physical processes that carry the atmospheric heat transport is largely affected by the meridional SST gradient, indicating that SST plays an important role in the high-to-low latitude teleconnection.

We further investigate into the tropical climate response to the high-latitude forcing. The main feature of tropical climate response is the southward shift of ITCZ (Fig. 4.5). Briefly the ranking of the shifting magnitudes among the three perturbed runs is P1¿P0.1¿P10. Considering the convective nature of the tropical precipitation, and estimating the convection using the lower-tropospheric (3000m-surface) flow convergence, we see that the lower-tropospheric convergence is in very good agreement with the precipitation in both climatological runs and perturbed runs. From this we conclude that the ITCZ shift is associated with change in convective activity in CAM3 simulations.

Furthermore, we consider possible sources of change in convective activity. The lower-tropospheric convergence is driven by pressure gradient cooperating with surface drag according to the momentum equations (Lindzen and Nigam, 1987). There-

94

fore, what contribute to the lower-tropospheric pressure field are essential for the convective activity. These factors that contribute include the surface temperature, which largely affects the lower-tropospheric temperature (thus density) through vertical mixing, large-scale circulations, which manipulates air temperature through advection, and latent release heating in cumulus clouds, which changes upper-tropospheric air temperature, etc. We focus on the role of surface temperature. We apply the simple model developed by Lindzen and Nigam (1987) and force the model with surface temperature field from our model results. In the model the pressure field on the top of lower troposphere (3000m) is not affected by upper-troposphere and the lower-tropospheric temperature is only associated with the surface temperature, which means factors such as the large-scale circulation and the latent release heating, etc. are absent. We present the lower-tropospheric convergence again but from the simple model results (Fig. 4.9). The results show that the convergence due to SST-vertical mixing agrees very well with the convergence shown in our CAM3-SOM results (Fig. 4.6). A good linear relationship between the convergence anomalies and the SST's direct contribution is found (Fig. 4.10). Now we can try to understand why the ranking of ITCZ shift magnitudes is P1 >P0.1 >P10. The ITCZ shift in P1 and P0.1 is larger than in P10 because the surface temperature anomaly is larger. The ITCZ shift in P0.1 is smaller than in P1 possibly because of negative feedbacks from the atmosphere to SST: when warmer (cooler) surface temperature favors (harms) convection and precipitation, the formed cloud decreases (increases) solar radiation reaching surface, and the strengthened surface wind increases surface heat fluxes, which tends to in turn decrease SST; and because ocean contains less heat capacity in P0.1, it feels more negative feedback.

5. SUMMARY AND FUTURE WORK

This dissertation addresses three primary questions: 1) what is the relative contributions from the atmospheric and oceanic processes to the high-to-low latitude teleconnection during a YD-like abrupt climate change event; 2) what is the physical processes for the contributions from the tow components; and 3) how important is SST in the teleconnection.

The current understandings that lead to our questions are:

- A freshwater forcing over subpolar North Atlantic is widely believed to have triggered the YD event (Johnson and McClure, 1976).

- The high-to-low teleconnection are believed to be through weakening of AMOC, which is driven by the stronger stratification over the subpolar North Atlantic due to freshwater forcing (Carlson, 2010; Kang et al., 2008).

- Chiang and Bitz (2005) argued that atmospheric processes plays a role in linking high-latitude forcing to low-latitude climate responses, without oceanic process changes.

- Kang et al. (2008) and Kang and Held (2012) proposed that the ITCZ shift in response to high-latitude forcing is controlled by cross-equatorial atmospheric heat transport through affecting Hadley circulation. However, the direct effect from SST change has not yet been examined.

We address these questions in the framework of freshwater fluxes in subpolar North Atlantic triggering YD-like abrupt climate change events. A simulation of such a YD-like abrupt climate change event Wan et al. (2011) shows global climate

changes in response to a freshwater forcing in subpolar North Atlantic: a weaken of AMOC (Fig. 2.5), a cooling over most of the Northern Hemisphere and a southward shift of ITCZ (Fig. 2.2), with an adjustment time of about one or two decades (Fig. 2.4). These results are broadly consistent with paleo-records during YD event (Alley et al., 1993; Council, 2002; Peterson et al., 2000).

To separate the atmospheric contribution from the oceanic contribution to the high-to-low latitude teleconnection, we performed a series of experiments using CAM3-SOM. A control and a hosing simulations are performed to reproduce the reference CCSM3 control and hosing simulations, respectively. The comparison between them shows the total atmospheric and oceanic contribution. An additional perturbed hosing simulation is performed where only atmospheric process changes are present. The comparison between this simulation and the control simulation then shows the atmospheric only contribution. The comparison between the perturbed hosing simulation and the hosing simulation shows the oceanic only contribution, assuming a linear combination of the two contributions.

The results show that the atmospheric and oceanic controlled climate responses in the tropics have similar magnitudes (Fig. 3.13, Fig. 3.11), indicating that the two contributions to the high-to-low latitude teleconnection are comparable. However, the patterns of the atmospheric and oceanic controlled climate response are very different, indicating that both atmospheric and oceanic processes play distinctive roles in the high-to-low latitude teleconnection.

An energetic analysis of the two hosing simulations (Fig. 3.14b,c) gives more insight into the involved physical processes. For the atmospheric controlled teleconnection (Fig. 3.14c), the basic physical processes are as follows:

- The high-latitude freshwater forcing leads to cooling of ocean surface through

intensified upper-ocean stratification. This ocean surface cooling reduces heat release to the atmosphere, which is compensated primarily by extra atmospheric heat transport from the mid-latitudes to the high-latitudes and secondarily by increase of downward TOA radiation and extra atmospheric heat transport from the polar region. This extra atmospheric heat transport from the mid-latitudes to the high-latitudes is carried by strengthened storm activities, which results from stronger baroclinic instability due to stronger meridional SST gradient.

- The strengthened storm activities over the mid- and high- latitudes leads to cooler near surface air in the mid-latitudes, which further cools beneath ocean through increased surface sensible heat flux (Fig. 3.15b). The extra atmospheric heat transport from the mid-latitudes to the high-latitudes is also compensated primarily by the extra atmospheric heat transport from the tropics to the mid-latitudes and secondarily by the increased surface and TOA heat fluxes into the atmosphere. This extra atmospheric heat transport from the tropics to the mid-latitudes is speculated to be carried by stronger Hadley circulation, which results from the stronger meridional SST gradient (Held and Hou, 1980).

- The stronger Hadley circulation leads to stronger trade wind in the northern tropics, cooling the beneath ocean through increased surface latent heat flux (Fig. 3.15a). The heat budget undergoes the same story in the northern tropics as in the mid-latitudes. The extra atmospheric heat transport from the southern tropics to the northern tropics is also likely to be carried by the Hadley circulation change.

- The extra atmospheric heat transport from the southern tropics to the northern

tropics is primarily compensated by the increased downward TOA radiation in the southern tropics, which mainly results from the cloud forcing change (Fig. 3.15d) due to the southward shift of ITCZ (Fig. 3.11c).

This is broadly consistent with the results of Chiang and Bitz (2005). The oceanic processes cools the northern mid-latitudes and warms the northern tropics (comparing Fig. 3.15b and c): in the mid-latitudes, there is increased oceanic heat flux divergence, which cools the ocean, while in the northern tropics, there is decreased oceanic heat flux divergence, which warms the ocean. This is inconsistent with previous studies (Dong and Sutton, 2002) arguing that the AMOC reduction simply cools the Northern Hemisphere and warms the Southern Hemisphere. We speculate that this is because the wind-driven circulation also plays a role in this oceanic controlled high-to-low latitude teleconnection. The oceanic processes also adjusts the atmospheric circulation, increasing atmospheric heat transport from the northern tropics to the mid-latitudes, which is carried by even stronger Hadley circulation due to stronger meridional SST gradient.

The physical oceanic processes are also analyzed in order to understand the distinctive SST anomaly pattern (Fig. 3.16a) over North Atlantic. The physical processes are as follows:

- The freshwater input flows along the subpolar and then the subtropical North Atlantic gyre, freshening the subtropical gyre, and partly sinking into deeper ocean over the Caribbean sea.

- SSH over the subtropical gyre is increased through halosteric effect (Fig. 3.18), which induces change in surface geostrophic current.

- The surface geostrophic current change forms the pattern of cooling along the

99

subtropical North Atlantic gyre and warming in the middle mainly through horizontal heat advection change (Fig. 3.16c,f, Fig. 3.17)

We perform additional three sets of CAM3-SOM experiments to examine the SST's role in the high-to-low latitude teleconnection. The three sets of experiments have the same high-latitude cooling forcing but different ocean mixed layer depth (different oceanic heat capacity), and they simulate the atmospheric controlled high-to-low latitude teleconnection. The results show that the surface cooling propagation rate is smaller when the oceanic heat capacity is larger (Fig. 4.3). This is understood by performing an energetic analysis (Fig. 4.4). The physical processes in the three perturbed runs are the same as in the perturbed hosing simulation simulating the atmospheric controlled teleconnection (Fig. 3.14c). However, the main difference is of the strength of teleconnection. The thicker ocean mixed layer weakens the teleconnection(Fig. 4.4c), because the ocean can supply more heat to compensate for local heat flux changes, thus requires less atmospheric heat transport changes from adjacent latitudes.

We further examine the SST's direct effect on the ITCZ southward shift. The SST's direct effect excluding effects from large-scale circulations and latent release heating is obtained by forcing Lindzen and Nigam's (1987) simple model using CAM3's resultant SST response. Our results show that there is a very good linear relationship between the tropical precipitation response and the SST's direct contribution to it (Fig. 4.10), suggesting that the SST change does contribute a lot to the tropical precipitation change by manipulating local pressure pattern through vertical mixing. We speculate that the SST's direct effect contribute more than the large-scale circulation when the ocean heat capacity is larger, while less when the oceanic heat capacity is smaller, because smaller heat capacity increases negative

100

feedbacks from the precipitation to SST, reducing SST's direct effect. The experiments by Kang and Held (2012) corresponds to the smaller oceanic heat capacity case (they used a mixed layer depth of 2m, which is similar to that in our P0.1 simulation). But examining this speculation requires further investigation into the large circulation's effect on precipitation. The contribution from wind-driven circulation change to the high-to-low latitude teleconnection also needs to be analyzed. In the future we may separate the contributions from thermohaline circulation change and wind-driven circulation change to understand the oceanic processes (cooling the northern mid-latitudes and warming the northern tropics, Fig. 3.14b)

We did not analyze oceanic controlled SST responses over the tropical Pacific, which is very inconsistent with local Q-flux anomalies, leading to difficulty in understanding them. Constrained in the modeling world is another shortcoming of this research. For example, our conclusion that SST's direct effect contributes to the majority of ITCZ response may be only a consequence of the convective parameterization scheme of CAM3.

REFERENCES

Alley, R., Meese, D., Shuman, C., Gow, A., Taylor, K., Grootes, P., White, J., Ram, M., Waddington, E., Mayewski, P., et al. Abrupt increase in greenland snow accumulation at the end of the younger dryas event. *NATURE-LONDON-*, 362: 527–527, 1993.

Alley, R. B. The younger dryas cold interval as viewed from central greenland. *Quaternary Science Reviews*, 19(1):213–226, 2000.

Augustin, L., Barbante, C., Barnes, P. R., Barnola, J. M., Bigler, M., Castellano, E., Cattani, O., Chappellaz, J., Dahl-Jensen, D., Delmonte, B., et al. Eight glacial cycles from an antarctic ice core. *Nature*, 429(6992):623–628, 2004.

Bjerknes, J. Atlantic air-sea interaction. *Advances in geophysics*, 10(1):82, 1964.

Briegleb, B., Bitz, C., Hunke, E., Lipscomb, W., Holland, M., Schramm, J., Moritz, R., et al. Scientific description of the sea ice component in the community climate system model, version three. *Technical Note TN-463STR, NTIS# PB2004-106574, National Center for Atmospheric Research, Boulder, CO, 78 pp*, 2004.

Broecker, W. S. Was the younger dryas triggered by a flood? *Science*, 312(5777): 1146–1148, 2006.

Carlson, A. E. What caused the younger dryas cold event? *Geology*, 38(4):383–384, 2010.

Chang, P., Zhang, R., Hazeleger, W., Wen, C., Wan, X., Ji, L., Haarsma, R. J., Breugem, W.-P., and Seidel, H. Oceanic link between abrupt changes in the north atlantic ocean and the african monsoon. *Nature Geoscience*, 1(7):444–448, 2008.

Cheng, W., Bitz, C. M., and Chiang, J. C. Adjustment of the global climate to an abrupt slowdown of the atlantic meridional overturning circulation. *Ocean*

Circulation: Mechanisms and Impacts-Past and Future Changes of Meridional Overturning, pages 295–313, 2007.

Chiang, J. C. and Bitz, C. M. Influence of high latitude ice cover on the marine intertropical convergence zone. *Climate Dynamics*, 25(5):477–496, 2005.

Chiang, J. C. and Friedman, A. R. Extratropical cooling, interhemispheric thermal gradients, and tropical climate change. *Annual Review of Earth and Planetary Sciences*, 40(1):383, 2012.

Collins, W. D., Bitz, C. M., Blackmon, M. L., Bonan, G. B., Bretherton, C. S., Carton, J. A., Chang, P., Doney, S. C., Hack, J. J., Henderson, T. B., et al. The community climate system model version 3 (ccsm3). *Journal of Climate*, 19(11): 2122–2143, 2006.

Council, N. R. *Abrupt Climate Change: Inevitable Surprises.* The National Academies Press, Washington, DC, 2002. ISBN 978-0-309-07434-6. URL `http://www.nap.edu/catalog/10136/abrupt-climate-change-inevitable-surprises`.

Dong, B.-W. and Sutton, R. Adjustment of the coupled ocean–atmosphere system to a sudden change in the thermohaline circulation. *Geophysical Research Letters*, 29(15):18–1, 2002.

Eisenman, I., Bitz, C. M., and Tziperman, E. Rain driven by receding ice sheets as a cause of past climate change. *Paleoceanography*, 24(4), 2009.

Friele, P. A. and Clague, J. J. Younger dryas readvance in squamish river valley, southern coast mountains, british columbia. *Quaternary science reviews*, 21(18): 1925–1933, 2002.

Hansen, J., Lacis, A., Rind, D., Russell, G., Stone, P., Fung, I., Ruedy, R., and Lerner, J. Climate sensitivity: Analysis of feedback mechanisms. *Climate processes and climate sensitivity*, pages 130–163, 1984.

Held, I. M. and Hou, A. Y. Nonlinear axially symmetric circulations in a nearly inviscid atmosphere. *Journal of the Atmospheric Sciences*, 37(3):515–533, 1980.

Johnson, R. and McClure, B. A model for northern hemisphere continental ice sheet variation. *Quaternary Research*, 6(3):325–353, 1976.

Kang, S. M. and Held, I. M. Tropical precipitation, ssts and the surface energy budget: a zonally symmetric perspective. *Climate dynamics*, 38(9-10):1917–1924, 2012.

Kang, S. M., Held, I. M., Frierson, D. M., and Zhao, M. The response of the itcz to extratropical thermal forcing: Idealized slab-ocean experiments with a gcm. *Journal of Climate*, 21(14):3521–3532, 2008.

Kiehl, J. T., Hack, J. J., Bonan, G. B., Boville, B. A., and Briegleb, B. P. Description of the ncar community climate model (ccm3). technical note. Technical report, National Center for Atmospheric Research, Boulder, CO (United States). Climate and Global Dynamics Div., 1996.

Knutson, T. R. Geophysical fluid dynamics laboratory - fms slab ocean model technical documentation, 2009. URL `http://www.gfdl.noaa.gov/fms-slab-ocean-model-technical-documentation`.

Lea, D. W., Pak, D. K., Peterson, L. C., and Hughen, K. A. Synchroneity of tropical and high-latitude atlantic temperatures over the last glacial termination. *Science*, 301(5638):1361–1364, 2003.

Licciardi, J. M., Teller, J. T., and Clark, P. U. Freshwater routing by the laurentide ice sheet during the last deglaciation. *Mechanisms of global climate change at millennial time scales*, pages 177–201, 1999.

Lindzen, R. S. and Nigam, S. On the role of sea surface temperature gradients in forcing low-level winds and convergence in the tropics. *Journal of the Atmospheric Sciences*, 44(17):2418–2436, 1987.

Oleson, K. W., Dai, Y., Bonan, G., Bosilovich, M., Dickinson, R., Dirmeyer, P., Hoffman, F., Houser, P., Levis, S., Niu, G.-Y., et al. Technical description of the community land model (clm). Technical report, NCAR Technical Note NCAR/TN-461+ STR, National Center for Atmospheric Research, Boulder, CO, 2004.

Peterson, L. C., Haug, G. H., Hughen, K. A., and Röhl, U. Rapid changes in the hydrologic cycle of the tropical atlantic during the last glacial. *Science*, 290(5498): 1947–1951, 2000.

Ritz, S. P., Stocker, T. F., Grimalt, J. O., Menviel, L., and Timmermann, A. Estimated strength of the atlantic overturning circulation during the last deglaciation. *Nature geoscience*, 6(3):208–212, 2013.

Schneider, E. K. Axially symmetric steady-state models of the basic state for instability and climate studies. part ii. nonlinear calculations. *Journal of the Atmospheric Sciences*, 34(2):280–296, 1977.

Schneider, E. K. and Lindzen, R. S. Axially symmetric steady-state models of the basic state for instability and climate studies. part i. linearized calculations. *Journal of the Atmospheric Sciences*, 34(2):263–279, 1977.

Smith, R. and Gent, P. Reference manual for the parallel ocean program (pop), ocean component of the community climate system model (ccsm2. 0 and 3.0). Technical report, Technical Report LA-UR-02-2484, Los Alamos National Laboratory, Los Alamos, NM, http://www. ccsm. ucar. edu/models/ccsm3. 0/pop, 2002.

Steele, M. and Ermold, W. Steric sea level change in the northern seas. *Journal of Climate*, 20(3):403–417, 2007.

Stevens, D. E. and Lindzen, R. S. Tropical wave-cisk with a moisture budget and cumulus friction. *Journal of the Atmospheric Sciences*, 35(6):940–961, 1978.

Stevens, D. E., Lindzen, R. S., and Shapiro, L. J. A new model of tropical waves incorporating momentum mixing by cumulus convection. *Dynamics of Atmospheres*

and Oceans, 1(5):365–425, 1977.

Stouffer, R. J., Yin, J., Gregory, J., Dixon, K., Spelman, M., Hurlin, W., Weaver, A., Eby, M., Flato, G., Hasumi, H., et al. Investigating the causes of the response of the thermohaline circulation to past and future climate changes. *Journal of Climate*, 19(8):1365–1387, 2006.

Voelker, A. H. et al. Global distribution of centennial-scale records for marine isotope stage (mis) 3: a database. *Quaternary Science Reviews*, 21(10):1185–1212, 2002.

Wan, X., Chang, P., Jackson, C. S., Ji, L., and Li, M. Plausible effect of climate model bias on abrupt climate change simulations in atlantic sector. *Deep Sea Research Part II: Topical Studies in Oceanography*, 58(17):1904–1913, 2011.

Wang, Y.-J., Cheng, H., Edwards, R. L., An, Z., Wu, J., Shen, C.-C., and Dorale, J. A. A high-resolution absolute-dated late pleistocene monsoon record from hulu cave, china. *Science*, 294(5550):2345–2348, 2001.

Wen, C. *A mechanistic study of Atlantic meridional overturning circulation changes on tropical Atlantic climate*. TEXAS A&M UNIVERSITY, 2009.

Xie, S.-P. A dynamic ocean-atmosphere model of the tropical atlantic decadal variability. *Journal of Climate*, 12(1):64–70, 1999.

Zhang, G. J. and Wang, H. Toward mitigating the double itcz problem in ncar ccsm3. *Geophysical research letters*, 33(6), 2006.